ANALYTICAL MODEL OF THE PROGRESSION OF CRACKING IN FIBER-REINFORCED COMPOSITES

A Dissertation

Submitted to the Graduate Faculty of the
Louisiana State University and
Agricultural and Mechanical College
in partial fulfillment of the
requirements for the degree of
Doctor of Philosophy

in

The Interdepartmental Programs in Engineering

by
Jane L. D. Runkle
B.S. in Engineering, Purdue University, 1985
M.S. in Engineering Science, Louisiana State University, 1991
December 1993

DEDICATION

Laurence Jacob Daugherty

ACKNOWLEDGEMENTS

The author wishes to express her sincere appreciation to her advisor and major professor, Dr. A. B. Doucet, for her helpful guidance, continuous support, encouragement, and valuable suggestions throughout the course of this study. Special thanks are also due to her advisory committee members, Dr. J. R. Collier, Dr. S. S. Pang, Dr. G. Z. Voyiadjis, Dr. S. Acharya, and Dr. J. Courtney for their time and comments.

The author acknowledges the support of her work by the National Science Foundation and by the Louisiana Space Consortium.

Thanks are also extended to Daniel Runkle, the author's husband, for his assistance with the photographic portion of the work. Without his support, encouragement, and love, this work would not have been possible. In addition, the author is greatly appreciative of the advice and encouragement given her by her parents, Jerrald and Kathryn Daugherty.

Finally, the author offers whole-hearted thanks and praise to her Lord and Savior, Jesus Christ, who has graciously provided her with all things - life, purpose, guidance, love, and peace beyond all understanding. All praise belongs to Him.

TABLE OF CONTENTS

LIST OF TABLES

LIST OF FIGURES

ABSTRACT

An analytical shear lag model has been developed for the progressive damage and final failure of glass-epoxy composites under biaxial loading. The amount of damage is determined for each layer at increasing static loads by comparing the strain energy released by the laminate assuming a crack occurs with the critical strain energy release rate found in the literature. When a layer cracks, the other layers must take additional load. Final failure occurs when the primary load carrying plies reach their ultimate strength. This model incorporates an algorithm for the effect of microdelamination on matrix cracking. The model has been experimentally verified by statically loading uniaxial glass-epoxy tension specimens and measuring damage accumulation in terms of crack density and the decrease of Young's modulus. The present study shows that the model developed can be used for predictions of damage and failure of glass-epoxy composites.

CHAPTER 1

INTRODUCTION

Fiber-reinforced composite materials have found widespread use in the aerospace and automotive industries, among others. They are used in such applications as solid rocket motor cases, aircraft fuselages and wing structures, boats, and automotive leaf springs. In none of these structures are they under uniaxial tension loading only. Since composites are generally used in the form of plates or shells, they typically see biaxial loading. Unfortunately, little analytical modeling has been performed for failure under biaxial loading.

The failure of composite materials is usually preceded by a substantial amount of damage. The first event is transverse matrix cracking in the 90° or low angle plies. As the transverse matrix cracks reach the interface between the 90° layer and the neighboring 0° or low angle layer, small delaminations tend to form. The thickness of the 90° layer determines whether delamination occurs. At first, these delaminations grow only a very small amount. Matrix cracks continue to form in the 90° ply layer until the "characteristic damage state" is reached. At this point, substantial delamination may occur. While delamination is occurring, the load carrying plies reach their ultimate strength and failure ensues.

Modeling the damage in composites enables industry to make more accurate decisions regarding the margins of safety of damaged hardware. Predictions can be made of the change in properties as a result of damage, and of the loading states which lead to unacceptable damage. For example, if a pressure vessel is overpressurized, the stress in the vessel can be determined. An estimation of the amount of damage and the probable degradation of properties can be made using models such as those proposed in this work.

While a number of models have been developed for predicting progressive damage in composites, very few are written for biaxial loading. None are written for transverse matrix cracking in composites with more than three layers. Finally, few make any attempt to incorporate the effects of delamination.

The models developed in this work incorporate transverse matrix cracking of fiber-reinforced composites under biaxial tension. The initial model is for composites of the type $[\pm\theta/90_n]_s$ under general biaxial tension. Transverse matrix cracking is modeled in the 90° plies and an algorithm for the effect of local delamination is included. In the final model, laminates of the type $[90_n/0_m/90_p]_s$ are studied. Transverse matrix cracking is modeled in all five layers. In-plane biaxial loading, except for in-plane shear, is modeled. In addition, the delamination algorithm is included.

Both models predict the stress and strain at the onset of matrix cracking, the progression of cracking, the effect of local delamination on transverse matrix cracking, and the change in Young's modulus as damage occurs. They are compared with experimental data.

CHAPTER 2

REVIEW OF LITERATURE

Microstructural Failure Mechanisms

In order to truly understand fracture of composite materials, one must begin by looking at the microstructural aspects. This section examines matrix microcracking, fiber breakage, matrix-fiber debonding, fiber pull-out, and the microstructural aspects of delamination. The microstructure of composites greatly affects their macroscopic behavior. The observations summarized in this section have led to the development of damage propagation models.

The Pseudoplastic Zone

For stable crack growth, the crack critical energy release rate, G_C, is equal to the fracture toughness or resistance to crack growth, R. G_C is defined as:

$$G_C = \frac{1}{2} P_C \left[\frac{dC}{da}\right] \tag{2.1}$$

where P_C is a critical force, C is the compliance and da is the crack extension [1]. Visconti [2] used G_I, the mode I elastic energy release rate, to describe composite fracture. Since the composites examined here are brittle, linear elastic fracture mechanics provides a reasonable measure of fracture toughness. Visconti used a stress intensity factor given by:

$$K_I = \frac{\sigma}{Pa} \tag{2.2}$$

where 2a is the length of the crack perpendicular to the direction of stress, σ. The propagation of the crack initiates when K_I reaches a critical value, K_{IC}, which depends on a critical stress, σ_C. Visconti proposes that the ability to withstand load in the presence of notches is due to the presence of a "pseudoplastic" zone ahead of the crack tip. In this zone, microcracking and microdelamination (really debonding) dissipate energy. His model is shown in Figure 2.1. Once the zone grows to a

certain size, given by a_o, cracking proceeds. Thus, K_{IC} can be defined for the case of no initial defects, or the case of initial defects:

$$K_{IC}=\sigma_C\sqrt{(a+a_o)\pi} \qquad \text{or} \qquad K_{IC}=\sigma^*\sqrt{a_o\pi} \tag{2.3}$$

where σ^* is the strength of the unnotched specimen, σ_C is critical stress, and a_o refers to a critical size of unavoidable defects present in the material. Finally, Visconti solves these equations for a_o and states that a_o is a characteristic constant of the material.

$$a_o=\frac{a}{\left[\frac{\sigma_C}{\sigma^*}\right]^2-1} \tag{2.4}$$

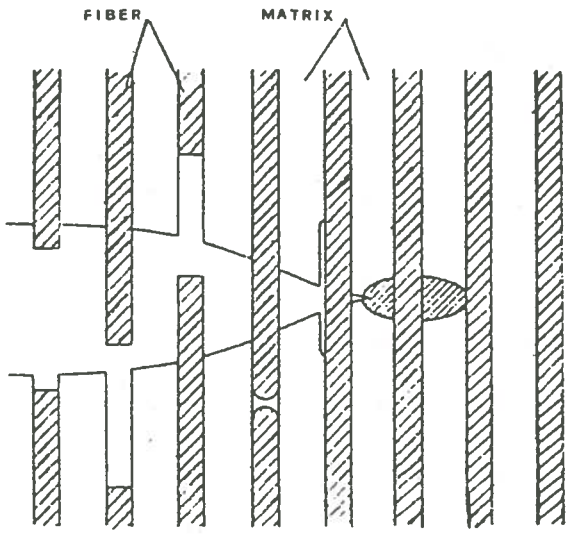

Figure 2.1. Model of the Mechanism Involved in Crack Propagation in a Composite [2]

For maximum fracture toughness, one must maximize the resistance to crack growth, R or G_C, since they are equal. Visconti realized that contributions to G_C arise from a number of physical processes, including matrix microcracking, fiber breakage, debonding, and fiber pull-out [1,2].

Matrix

The glass transition temperatures of epoxy matrices range from 300° F to 470° F, which means that they are glassy at their use temperatures [3]. In addition, since they are highly crosslinked, they cannot develop any significant degree of crystallinity [2]. They are, thus, brittle and linearly elastic. It is well known that glassy polymer fracture begins with the formation of low-density regions called crazes [4]. Crazes may initiate at interfaces or voids. They may be caused by post-cure shrinkage [5], straining, or development of pressure pockets due to moisture entering internal voids [3]. They can also be caused by chemical attack. Epoxy matrices, however, are generally quite resistant to chemicals and exhibit low shrinkage during curing [6]. Crazes absorb a certain amount of fracture energy, which helps the composite to fail incrementally rather than catastrophically. On the other hand, crazing reduces the strength of the matrix as shown by Pavan [7], who found the tensile craze yield strength, σ_{yc}, of a glassy polymer marix/particulate composite to be:

$$\sigma_{yc} = C\left\{2\left[1+\sqrt{1+4\frac{D}{C^2}}\right]\right\}^{-1} \tag{2.5}$$

Note that σ_{yc} depends on the material properties of the matrix, given by C and D, so this equation is true regardless of composite type. It also means that matrix cracking is governed by matrix strength, and that matrix properties strongly affect axial and transverse cracking and delamination resistance. In addition, as will be seen later, matrix microcracking usually precedes the other failure mechanisms. Before discussing the other failure modes, one must look at the fibers.

Fibers

Fibers, like graphite, are highly crystalline and oriented, giving them much higher strength and stiffness than epoxy matrices [4]. This is especially true at high rates of strain. Due to their high stiffness, Fibers typically strain less than do matrices, especially at high strain rates. In addition, fiber failure is generally defined at the fracture strain. Some fibers, however, like Kevlar (aramid), actually have a higher creep rate than epoxy at low stresses [5], which may contribute to

Kevlar-epoxy's relatively high fracture toughness. Graphite and glass fibers do not fall into this category. Individual fibers may break at less than 50% of the ultimate tensile load of the composite [8]. This is a random process due to randomly distributed defects in the fibers. Some researchers have modeled fiber failure due to such defects using a Weibull distribution. This idea is explained more fully in Chapter Two.

Agarwal and Broutman [8] discuss a rule of mixtures approach to define the energy required per unit area of the composite for fracture of fibers in tension, W_b, as well as energy release rate caused by fiber breakage during fracture, G:

$$W_b = G = \frac{V_f \sigma_f^2 \, l}{6E_f} \tag{2.6}$$

where V_f is the volume fraction of fibers, σ_f is the fiber ultimate strength, l is the fiber length, and E_f is the fiber Young's modulus. When a fiber fails, other fibers must take up the load, leading to additional fiber failures [6]. This may be an incremental process; however, if it occurs abruptly, it may result in catastrophic failure.

Fiber-Matrix Debonding

Matrix microcracking generally does not lead to catastrophic failure, but rather, dissipates energy. Matrix microcracks are, however, nuclei for further damage. When matrix microcracks reach fibers, debonding between the fiber and the matrix usually occurs. The purpose of the matrix is to transfer load to the fibers and it does this by a shear mechanism. Since the fibers are stiffer than the matrix, they prevent the matrix from elongating near the fiber. This results in a local strain at the fiber, which is higher than that in the bulk of the matrix [9]. If the corresponding local stress is greater than the local interfacial strength, debonding will occur. Although the matrix-fiber interface is often assumed to be perfect in analytical models, it actually has rough surfaces with corners, which act as stress concentrators. Thus the local stress is even higher than is usually predicted, resulting in premature debonding.

Cracking in a fiber-matrix composite can be modeled using a bimaterial plate, in which one phase is more brittle than the other. The crack propagates in the more ductile portion at, we assume, some constant velocity. As it approaches the second phase, it slows down and stops at the interface in what Theocaris [9] calls the crack-arrest phenomena. The crack then propagates along the interface until the strain energy necessary for it to propagate in phase two is reached. Now there are two independently propagating cracks. While this is a very interesting model, Theocaris, unfortunately, does not develop an equation for the energy of debonding. Kelly [1] does develop such a relation by equating the work of debonding with the strain energy appearing in the filament as a result of debonding. He finds that the work or energy of debonding is:

$$W_d = \frac{\pi r^2 \sigma_f^2 x}{6E_f} \tag{2.7}$$

where r is the fiber radius, E_f is the fiber modulus, σ_f is the fiber breaking strength, and x is the length of the debond. Debonding contributes less to the fracture toughness than does fiber pull-out, as shall be shown.

Fiber Pull-Out

Fiber pull-out generally occurs after a fiber has broken near, but not in the plane of, a matrix crack. The fiber will debond from the matrix and, since it can no longer carry a load, will pull away from the rest of the fiber, leaving a fiber-shaped hole in the matrix. This phenomen is shown in Figure 2.2, where the central fiber has broken at a distance, L, from the crack face. Fiber pull-out increases fracture toughness and is enabled by a low interfacial shear strength. Pull-out is most likely to occur when the fiber length is less than the critical fiber length, which is the fiber length needed for the in situ fiber stress to reach its maximum value at the fiber midpoint. However, Piggott [10] has shown that fiber pull-out can occur in continuous fiber composites provided that it is preceded by fiber breakage and/or debonding between fiber and matrix. In a continuous fiber composite, it is usually fiber breakage that precedes pull-out, since it is unlikely that

debonding will occur along the entire length of a fiber without fiber breakage occurring, as has been explained by Theocaris [9]. In addition, the fiber will probably break at the point of an inherent flaw.

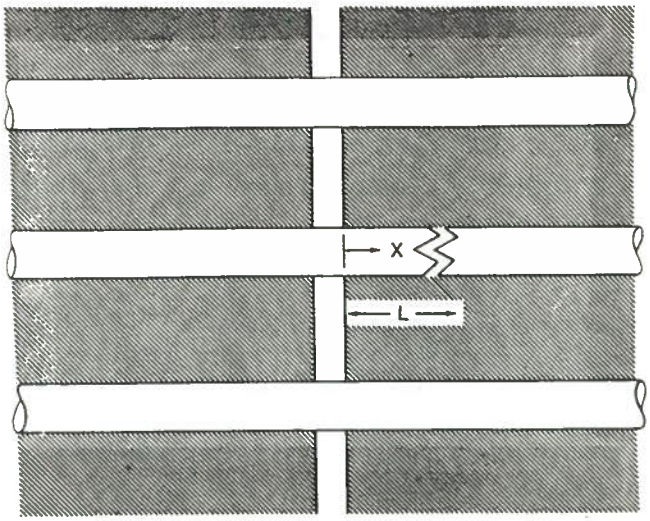

Figure 2.2. Fibers Bridging a Crack [10]

Kelly [1] defines the critical spacing of flaws as y_c,

$$y_c = \frac{\left[\sigma_f - \sigma_f^*\right] r}{\tau_i} = l_c \frac{\Delta\sigma_f}{\sigma_f}. \tag{2.8}$$

Here, σ_f is the fiber strength, σ_f^* is the strength at the flaws, $\Delta\sigma_f$ is $\sigma_f - \sigma_f^*$, r is the fiber radius, τ_i is the interfacial shear strength, and l_c is the critical fiber length, such that the in situ fiber strength reaches σf in the middle. If the actual spacing of flaws is y where $y < y_c$, then all fibers will break at flaws lying within a distance $\frac{1}{2} y_c$ from the crack. The average pull-out work per fiber is then:

$$W_p = \frac{\pi r \tau_i y^2}{12} \tag{2.9}$$

or for the composite per unit area,

$$W_p = \frac{V_f \tau_i y^2}{12r} \tag{2.10}$$

If, on the other hand, $y > y_c$, a fraction of fibers equal to $\frac{y_c}{y}$ will break at flaws and pull out, while a fraction of fibers equal to $1-\frac{y_c}{y}$ will not pull out but will break in the plane of the matrix crack. Then the work of fracture for the composite is:

$$W_p = \frac{V_f \tau_i y_c^3}{12ry} \tag{2.11}$$

By setting $y = y_c$, the dependence of W_p on τ_i and σ_f can be seen.

If $y = y_c$,

$$W_p = \frac{V_f \tau_i y_c^2}{12r} = \frac{V_f \tau_i \left[\frac{l_c \Delta\sigma_f}{\sigma_f}\right]^2}{12r} \tag{2.12}$$

Now,

$$l_c = \frac{\sigma_f r}{\tau_i} \tag{2.13}$$

so,

$$W_p = \frac{V_f r \Delta\sigma_f^2}{12\tau_i} \tag{2.14}$$

Since $\Delta\sigma_f$ is proportional to σ_f, W_p increases with increasing σ_f and decreasing τ_i. In addition, to increase fracture toughness, the fiber/matrix interfacial shear strength should be reduced relative to the fiber longitudinal tensile strength. In fact, Piggott [10] has shown experimentally that, when the residual interfacial cure shrinkage stress is decreased, the work of fracture increases. In addition, work of fracture decreases as fiber modulus increases. The fiber stress is small near the break and this loss of stress upon fracture causes the fiber to shrink longitudinally and expand radially. Thus, the fiber wants to pull out and does work during pull-out. If the fiber is brittle, it will exhibit less shrinkage and less expansion, lowering the work of fracture. Piggott also points out that, in order for fiber pull-out to occur, the crack must be very large. This means that even though fiber pull-out is a useful mechanism for increasing fracture toughness, the crack required is often so

large that the material is already in danger of certain failure. Fiber pull-out simply works to slow the failure process.

It can now be shown that the contribution of pull-out energy to fracture toughness is greater than that of debonding. Combining equations 2.8 and 2.10, we see that for a single fiber, the ratio of the pull-out work to the work of debonding, W_p/W_d, is proportional to E/σ_f, which is equal to the reciprocal of the maximum breaking strain. As stated earlier, fibers are very stiff, so the maximum breaking strain is always very small, on the order of a few percent. Therefore, Kelly states that E/σ_f is never less than 50 [1]. Hence, W_p, the energy associated with fiber pull-out, is substantially greater than W_d, the energy associated with debonding. In addition, since a small interfacial bond strength is required for both debonding and pull-out, a small interfacial shear strength will produce debonding followed by fiber pull-out. Therefore, it is worthwhile to look more closely at the interfacial bond strength.

The Interfacial Bond

The relationship between interfacial bond strength and fracture toughness can be illustrated by comparing graphite-epoxy and aramid-epoxy laminates. The interfacial bond strength in graphite-epoxy laminates is twice as high as the bond strength in aramid-epoxy composites, and this is likely the main reason that aramid-epoxy composites have a higher fracture toughness than graphite-epoxy materials. Penn, et al., [11] investigated the reasons for this phenomena by performing single filament pull-out tests. They suggest three possible reasons for the difference, namely, intermolecular interactions, chemical bonding, and mechanical interference.

Intermolecular interactions and chemical bonding were quickly ruled out, since graphite and aramid have similar forces acting at their surfaces, and they have nearly identical surface functionalities. The difference in modulus was also considered and was ruled out. Penn, et al., [11] found that the most likely cause for the difference in fracture toughness is the radial compression or

tension exerted by the matrix on the fiber because of thermal mismatch between matrix and fiber during cool-down after cure.

The coefficients of thermal expansion for fibers increase as temperature is raised, thus, fibers shrink in length and expand in diameter as the temperature is raised, and the opposite occurs upon cooling. Since graphite's transverse thermal expansion coefficient is less than that of a typical epoxy, the graphite fiber will not shrink upon cooling as much as will the annulus of matrix around it will decrease. Therefore, a high compressive stress will be exerted on the fiber by the matrix. Aramid's diameter decrases more upon cooling than does the diameter of graphite, giving a looser fit between matrix and fiber for Aramid. The difference in fit leads to a difference in interfacial shear strength. In fact, the interfacial shear strength between graphite fibers and epoxy is about three times greater than the shear strength between Aramid fibers and epoxy.

Delamination

Delamination is a result of failure of the matrix and of the fiber-matrix interface. Saghizadeh and Dharan [13] have made some interesting observations regarding delamination and the relative contributions of matrix cracking and fiber-matrix debonding to delamination fracture toughness. Since the delamination crack must work its way around fibers as it propagates, the local fracture mode is a mixture of Mode I and Mode III, even if the macroscopic fracture mode is Mode I delamination. This is shown in Figure 2.3. They found that delamination fracture toughness depends strongly on the fiber volume fraction; therefore, interfacial fracture toughness is more important than neat resin fracture toughness. Since fiber-matrix debonding, fiber pull-out, and fiber breakage energies also depend on fiber volume fraction and matrix failure does not, one may conclude that debonding, pull-out, and fiber breakage are greater contributors to delamination fracture toughness than is matrix fracture. Specifically, Saghizadeh and Dharan found that for graphite composites, the crack energy release rate decreases with fiber volume fraction. This is because increased fiber volume fraction increases the interfacial surface area, which lowers the crack

energy release rate, in effect, toughening the composite. Therefore, a fiber-reinforced epoxy laminate with a high fiber volume fraction should have a high resistance to delamination.

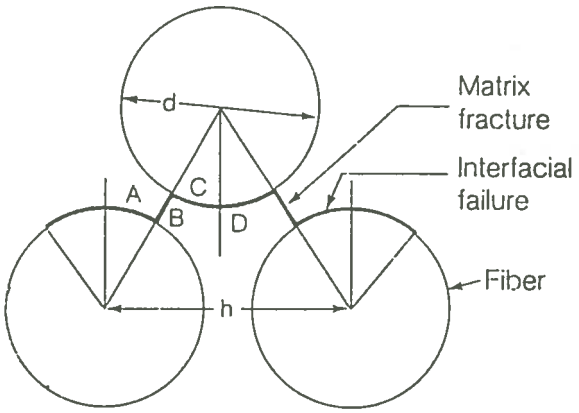

Figure 2.3. Crack Path Around Fibers During Delamination [13]

Relationship between Microstrucure and Fracture Toughness

We have seen that fracture toughness depends on matrix, fiber, and interface properties. In addition, it is evident that fiber pull-out is the greatest contributor to fracture toughness, but it cannot occur without being preceded by matrix microcracking, matrix-fiber debonding and fiber breakage. Often, as is shown in Figure 2.2, fibers will bridge a crack. Fiber bridging is another factor in preventing catastrophic failure, but it leads to complications in analyzing composite fracture. All of the mechanisms discussed are important to the development of fracture toughness in continuous fiber composites.

The fiber-matrix interface has been examined to see the effects of intermolecular and chemical bonds, as well as mechanical interactions between fibers and matrix [11,12]. For graphite- and aramid-epoxy composites, thermal mismatch between fibers and matrix is probably the most important factor in determining the strength of the interfacial bond. Penn, et al. [11] and Piggott [10] looked at aspects of this post-cure phenomenon. A tight fit increases interfacial shear strength and decreases fracture toughness, while a loose fit decreases shear strength and increases fracture

toughness. This helps explain the fact that aramid-epoxy has a higher fracture toughness than graphite-epoxy.

The ideas developed herein show relationships between various microscopic material characteristics and fracture toughness. Fracture toughness depends strongly on fiber pull-out energy, which in turn depends on the interfacial bond strength. Interfacial bond strengths have not been tabulated for many systems, making micromechanical models somewhat impractical at present. Although the models to be described in the next section are not micromechanical in nature, the behaviors they phenomenologically describe are micromechanical.

Progressive Failure Models

Progressive failure of a fiber reinforced composite usually begins with matrix microcracking transverse to the load. As a result of the matrix cracking in transverse or near transverse plies, there is a greater mismatch in local average strains between adjacent plies; therefore, delamination occurs. Final failure is usually preceded by or coincides with fiber failure in the 0° or nearly 0° plies. A critical literature survey is given of theories for transverse matrix cracking, edge and local delamination, and fiber failure.

Summary of Methods Used to Study Composite Fracture

Kanninen and Popelar [14] do an excellent job of summarizing composite fracture mechanics research and laying groundrules for such work. Two major types of analysis are those that take a continuum approach and those that use micromechanics. In addition, some researchers have used models that combine the two, using a continuum approach where possible, and integrating it with a micromechanics approach where it is needed to accurately describe the material behavior. Complications arise in any method, because crack growth is not likely to always be self-similar and K_{IC} depends on the crack path in composites. Obviously, the simple rule of mixtures is not adequate to describe composite fracture. Anisotropic fracture mechanics is a better macromechanical

approach, which becomes fairly straightforward, if the cracks are assumed to be aligned with the planes of material symmetry. In that case,

$$G_I = K_I^2 \sqrt{\frac{a_{11}a_{22}}{2}} \left[\sqrt{\frac{a_{22}}{a_{11}}} + \frac{2a_{12}+a_{66}}{2a_{11}} \right]^{\frac{1}{2}} \tag{2.15}$$

$$G_{II} = K_{II}^2 \frac{a_{11}}{\sqrt{2}} \left[\sqrt{\frac{a_{22}}{a_{11}}} + \frac{2a_{12}+a_{66}}{2a_{11}} \right]^{\frac{1}{2}} \tag{2.16}$$

where the a_{ij} are elements of the compliance matrix, and $K_I = \sigma\sqrt{\pi a}\,\sin^2\alpha$ and $K_{II} = \sigma\sqrt{\pi a}\,\sin\alpha\cos\alpha$ for an infinite sheet, 2a is the crack length and α is the angle between the stress direction and the crack plane. Sih and Liebowitz [14] have developed a relation for mixed-mode cracking in plane strain conditions:

$$G = \left[\sqrt{\frac{a_{22}}{a_{11}}} + \frac{2a_{12}+a_{66}}{2a_{11}} \right]^{\frac{1}{2}} \left[K_I^2 \sqrt{\frac{a_{11}a_{22}}{2}} + K_{II}^2 \frac{a_{11}}{\sqrt{2}} \right] + K_{III}^2 \frac{\sqrt{a_{44}a_{55}}}{2} \tag{2.17}$$

Kanninen and Popelar [14] have performed an in-depth review of a number of damage models. Their analysis was used to eliminate several models from consideration, as described here. Waddoups' model is semi-empirical with K_{IC} and l, a dimension of a characteristic intense energy region at the crack tip, to be found from experiment. Whitney and Nuismer's point stress criterion, which was written for laminates with holes, has been generalized to laminates with cracks, but is a poor predictor of cracking behavior [8]. Harrison's model allows for non-self similar crack growth by assigning two different strain energy release rates for growth in the plane of or normal to the crack, but it is only applicable to unidirectional composites. In addition G is hard to calculate for non-self similar crack growth. Poe's critical strain model is valid only for through-wall crack growth, and not delamination or splitting. Potter examines failure only in terms of fiber failure. As fibers fail in the loading direction for uniaxial tension, a damage zone develops. Potter's model is

useful because it differentiates between a large, blunt notch, which causes brittle failure governed by his initiation criterion and a small defect, which causes propagation of damage between fibers.

Kanninen and coworkers [14] have developed a hybrid model, in which a local heterogeneous region around the crack tip is embedded in an anisotropic elastic continuum. The heterogeneous region contains the fiber, the matrix, and the fiber/matrix interface region; therefore, the constitutive relations of each of these elements must be known up to the point of failure. The model is useful in that it can show the occurrence of fiber breakage, matrix microcracking, crack bridging, matrix/fiber debonding and axial splitting. In addition, it can be used to model any crack orientation. However, it is limited in that it cannot be accurately used for a real material, and, in fact, Kanninen has obtained qualitative results only. This is because the fiber/matrix interface is very difficult to study, so it's properties are unknown for most materials. The properties of an individual ply can be obtained readily and are available for many materials; therefore, a better approach is to use a mechanics model of a lamina in transverse tension and experiencing matrix cracking followed by delamination. This idea will be explored later.

Other models have been eliminated from consideration based on the advice of Reddy [15]. He compares several analytical and numerical methods for studying anisotropic materials with cracks, including classical, classical variational, such as Ritz and Galerkin, finite difference, finite element, and boundary element formulations. He recommends use of the finite element method. Some very useful work has been done using the finite element method; for example, Lee [16] has developed a three dimensional damage accumulation model, which vividly shows transverse matrix cracking followed by fiber breakage in the load-carrying plies. Failure of an element occurs in a certain mode when the stress appropriate for that failure mode reaches a critical value. Appropriate elements of the stiffness matrix for the failed finite element are then set to zero. Lee's model also accounts for delamination, but no delamination results are shown. Other finite element models include those of Sandhu, et al. [17], and Murray [18], which do not model delamination. The boundary element method, which is used by Tan and Bigelow [19] gives an approximation only on

the boundary of the domain, ignoring the interior of the material. Since damage in a composite often begins with transverse matrix cracking in the interior of the laminate, this method is not useful for development of a general damage propagation model. S. S. Wang's [20] edge delamination model is also not easily applied to interior cracking, although elements of it are useful as will be seen later.

The most interesting and useful models for transverse matrix cracking, edge delamination and local delamination are discussed in the following sections. None of the models are three-dimensional, but it will become clear that a three-dimensional or pseudo-three-dimensional model can be developed from them. In addition, it should be noted that none of these models have been used to predict biaxial behavior. Indeed, most of them are incapable of predicting it in their present form.

Shear Lag Theary and Transverse Matrix Cracking

The shear lag type of model was first proposed by Bailey and coworkers and expanded upon by Flaggs, Nuismer and coworkers, Lee and Daniel, Daniel and Tsai, and Laws and Dvorak [21-29]. In essence, a shear lag model states that the interlaminar shear stress is proportional to the difference in the average displacements of the two laminae under an applied load. One type uses an energy criterion for matrix cracking, while the other relies on a strength criterion. The constant of proportionality is called the shear lag parameter. Flaggs' paper, which will be discussed in more detail later, shows that, at least in some instances, 2-D shear lag theory predicts experimental behavior better than the finite element method [23]. Thus, the shear lag model is the type to be developed herein for transverse matrix cracking. There are essentially two kinds of shear lag models, those which use critical strain energy release rate as a criterion for cracking, and those which rely on laminate failure theories to determine the onset of cracking. They are typified by Lee and Daniel [25] and Laws and Dvorak [26]. Both are discussed in this section.

Laws and Dvorak [26] assume that a transverse crack propagates when it is energetically favorable to do so and use a probability density function to define the locations of cracks. Laws and Dvorak's model only considers a $[0_n/90_m]_s$ laminate (Figure 2.6). The model includes residual stresses after cure, which are defined as σ_t^R and σ_l^R for the residual stresses in the transverse or 90° plies and longitudinal or 0° plies, respectively. It assumes uniform displacements, u(x) and v(x), for the 0° and 90° laminae, respectively.

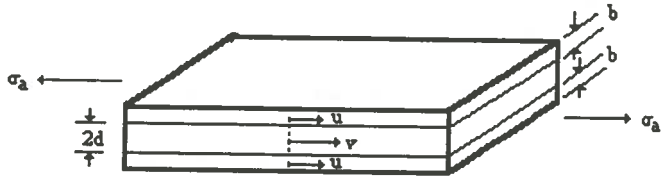

Figure 2.4. Symmetric Cross-Ply Laminate Under Axial Load [25]

The fundamental relationship in shear lag theory is:

$$\tau = K\,(v - u) \quad \text{or} \quad \frac{d\tau}{dx} = K\left[\frac{dv}{dx} - \frac{du}{dx}\right] \tag{2.18}$$

where τ is the interlaminar shear stress and the constant, K, is one form of the shear lag parameter. Thus, the differential equations for shear lag theory are:

$$\frac{d^2\sigma_t}{dx^2} - \frac{\xi^2}{d^2}\sigma_t = -\frac{\xi^2}{d^2}\left[\sigma_t^R + \frac{E_t}{E_o}\sigma_a\right] \quad \text{and} \quad \frac{d^2\sigma_l}{dx^2} + \frac{\xi^2}{d^2}\sigma_l = \frac{\xi^2}{d^2}\left[\sigma_l^R + \frac{E_l}{E_o}\sigma_a\right] \tag{2.19}$$

where ξ is the non-dimensional form of the shear lag parameter.

$$\xi^2 = \frac{Kd(bE_l + dE_t)}{bE_l E_t} \tag{2.20}$$

Solving the differential equations for σ_t and σ_l with the boundary condition, $\sigma_t = 0$ for $x = \pm h$ at each crack, gives:

$$\sigma_t = \left[\sigma_t^R + \frac{E_t}{E_o}\sigma_a\right]\left[1 - \frac{\cosh\frac{\xi x}{d}}{\cosh\frac{\xi h}{d}}\right] \tag{2.21}$$

$$\sigma_1 = \frac{E1}{E_o}\sigma_a\left[1+\frac{dE_t}{bE_1}\frac{\cosh\frac{\xi x}{d}}{\cosh\frac{\xi h}{d}}\right] + \sigma_1^R\left[1-\frac{\cosh\frac{\xi x}{d}}{\cosh\frac{\xi h}{d}}\right] \tag{2.22}$$

These are the stress distributions in each ply between two cracks a distance 2h apart. Neglecting the strain due to residual stress, one can calculate the average strain, ϵ_a, in the uncracked portion of the laminate in terms of σ_a, the applied stress. This leads to:

$$\frac{\sigma_a}{\epsilon_a} = E = E_o\left[1+\frac{\beta}{\xi}\frac{dE_t}{bE_1}\tanh\frac{\xi}{\beta}\right]^{-1} \tag{2.23}$$

where $\beta=\frac{d}{h}$ and is the crack density parameter. As $\beta \to 0$, $E \to E_o$ and as $\beta \to \infty$, $E \to bE_1/(b+d)$, which is the same as ply discount theory.

The change in strain energy when a third crack is introduced between the first two is given by:

$$\Delta W=\{(b+d)\sigma_a+b\sigma_1^R\}[u_2-u_1]_A^B+d\sigma_t^R\{[v_2-v_1]_A^C+[v_2-v_1]_C^B\} \tag{2.24}$$

where σ_a is the applied stress and the subscripts, 1 and 2, refer to the states before and after the introduction of the next crack. Incidentally, Laws and Dvorak postulate three probability density functions to predict the site of the next crack. The work done by the applied loads is:

$$W_{applied}=2(b+d)\sigma_a[u_2-u_1]_A^B \tag{2.25}$$

Knowing that $G=\mathcal{G}/2d$, since G is the energy released per unit area of the 90° ply, and using $\mathcal{G}=W_{applied}-\Delta W$ to get the energy released per unit width of composite, G can be found.

$$G=\frac{d(b+d)E_o}{\xi bE_1E_t}\left(\sigma_t^R+\frac{E_t}{E_o}\sigma_a\right)^2\left[\tanh\frac{\xi h_1}{2d}+\tanh\frac{\xi h_2}{2d}-\tanh\frac{\xi h}{d}\right] \tag{2.26}$$

First ply failure (fpf) occurs when $G=G_C$ and $\sigma_a=\sigma_a^{fpf}$. If G_C and σ_a^{fpf} are known, ξ can be found; however, G_C is difficult to measure accurately in composites, and the above equation requires an iterative solution. Laws and Dvorak circumvent the latter problem by assuming that the distances between cracks are still large at first ply failure, which causes the term containing tanh's to go to 1. Note that, under this definition, first ply failure in and of itself has a small effect on the stiffness of the laminate. After first ply failure, increasing crack density causes the laminate stiffness

to decrease rather rapidly, as will be shown in the chapter on results. Since G_C is difficult to measure in composites and has not been documented for many composite materials, many researchers believe it would be wise to develop a theory which does not require determination of G_C experimentally.

Lee and Daniel [25] have developed a theory without using G_C. It is almost identical to that of Laws and Dvorak with some important exceptions. Assuming a linear variation of the shear stress in the z direction, Lee and Daniel use general parabolic equations to determine the displacements in each layer as a function of z. Daniel corrected this problem in a more recent paper [27]. The shear stresses in each layer are given by:

$$\tau_{xzl} = G_{12}\frac{du}{dz} = G_{12}(2C_1z+C_2)$$
$$\tau_{xzt} = G_{23}\frac{dv}{dz} = G_{23}(2C_4z+C_5) \qquad (2.27)$$

where the subscript notation is the same as that of Laws and Dvorak [26]. The C_i are integration constants. Actually, τ_{xzl} is proportional to G_{13}. Lee and Daniel ignore the transverse deformation and assume $G_{13}=G_{12}$, but this author thinks this assumption, which amounts to saying the material is transversely isotropic with respect to the 2-3 plane, is poor, because the fibers are not necessarily uniformly distributed throughout the cross-section of a lamina. With these relations in mind, Lee and Daniel apply their boundary conditions of zero transverse stress at the crack faces, zero out of plane shear and z direction normal stress at z=0 and z=d+b, and equality of out of plane shear and z direction normal stress in the two plies at z=d. The displacements u and v are also assumed equal at z=d, which is a good assumption if bonding is perfect between the layers. Once delamination has occurred, this is not true. The resulting average displacements give:

$$\bar{u} - \bar{v} = \frac{\tau}{3G_{12}G_{23}}\left[bG_{23}+dG_{12}\right] \qquad (2.28)$$

Using the shear lag equation, $\tau=K(v-u)$, with equation (2.28), one finds:

$$K = \frac{3G_{12}G_{23}}{bG_{23}+dG_{12}} \qquad (2.29)$$

where K is the shear lag parameter. Since the shear stress distribution is assumed to be linear, τ_{xzl} and τ_{xzt} are related to τ by:

$$\tau_{xzl}=\tau\frac{b+d-z}{b},\ d\leq z\leq b+d \quad \text{and} \quad \tau_{xzt}=\tau\frac{z}{d},\ z\leq d \tag{2.30}$$

Using (2.33) and equilibrium, $\frac{\delta\sigma_z}{\delta z}+\frac{\delta\tau_{xz}}{\delta x}=0$, Lee and Daniel get the following through thickness normal stresses:

$$\sigma_{zl}=\frac{\xi^2 E_t}{dE_o}\frac{(b+d-z)^2}{2b}\frac{\cosh\left[\frac{\xi x}{d}\right]}{\cosh\left[\frac{\xi h}{d}\right]}\sigma_a$$

$$\sigma_{zt}=\frac{\xi^2 E_t}{dE_o}\left(\frac{b}{2}+\frac{d^2-z^2}{2d}\right)\frac{\cosh\left[\frac{\xi x}{d}\right]}{\cosh\left[\frac{\xi h}{d}\right]}\sigma_a \tag{2.31}$$

These are, of course, found using the appropriate boundary conditions. These two relations (2.34) are a significant contribution on the part of Lee and Daniel, since they can be used to define the onset of delamination. In addition, the σ_l and σ_t distributions are similar to those predicted by the three-dimensional elasticity results of Pagano and coworkers [30,31]. However, there is a discrepancy between Lee and Daniel's results for τ_{xzt} and those of Pagano. Because of the stress free condition at the crack face in the 90° layer, τ_{xz} should go to zero there for all $z<d$, as predicted by Pagano. In Lee and Daniel's model, τ_{xz} is only zero at $z=0$. In addition, the correct value for ξ in Lee and Daniel's model is open to question due to the use of G_{12} rather than G_{13}.

Lee and Daniel use Case I of Laws and Dvorak [26], which is that the next crack must occur exactly between the originally existing cracks. Rather than using energy considerations involving G_c, Lee and Daniel assume that a new crack forms when σ_t reaches the transverse tensile strength, F_{Tt}. While this assumption works adequately in Lee and Daniel's model, it is quite controversial. In fact, A.S.D. Wang [32] noted that: "It is the total strain energy trapped in the 90° layer that determines the onset of matrix cracking, not the in-situ tensile stress." The relationship between applied stress and crack density is found by substituting F_{Tt} for σ_t and 0 for x in equation

(2.22) to get:

$$\sigma_a = \frac{E_o}{E_t}\left(F_{Tt}\frac{\cosh\left[\frac{\xi h}{d}\right]}{\cosh\left[\frac{\xi h}{d}\right]-1} - \sigma_2^R\right) \tag{2.32}$$

This equation is much simpler than Laws and Dvorak's Case I equation for σ_a, which involves G_C in the expression for σ_a^{fpf}. Lee and Daniel's expression for decremented axial modulus is identical to that of Laws and Dvorak given in equation (2.24). The two methods thus give essentially the same result for the decremented stiffness due to cracking.

Nuismer and Tan [24] have developed a more general relationship between laminate properties and crack density. They used the orthotropic constitutive equations for each lamina, so they could model any laminate of type $[\pm\theta/90_n]_s$, where ply group 1 refers to the inner 90° plies and ply group 2 refers to the outer $\pm\theta$ plies. They also assumed general in-plane loading. Out of plane shear is given by:

$$\tau^* = A_{55}\left[\frac{\bar{u}^{(2)} - \bar{u}^{(1)}}{\bar{h}}\right] \tag{2.33}$$

where

$$A_{55} = \frac{3\bar{h}C_{55}^{(1)}C_{55}^{(2)}}{h^{(1)}C_{55}^{(2)} + h^{(2)}C_{55}^{(1)}} \tag{2.34}$$

and $C_{55}^{(i)}$ is from the i^{th} lamina's stiffness matrix, $h^{(i)}$ is the thickness of the i^{th} lamina, and $\bar{h} = h^{(1)}+h^{(2)}$. Note that this expression for A_{55} is similar to that given for the shear lag parameter, K. The notation used in this section and throughout this work is the standard notation used for laminates as defined by Jones [31]. The effective damaged laminate compliance relations are given by:

$$\bar{\epsilon}_x^{(1)} = \left[1+\left[\frac{\beta_1-\beta_2}{\beta_1}\right]\left[\frac{S_{11}^{(1)}S_{22}^{(1)}-S_{12}^{(1)}S_{12}^{(1)}}{S_{11}^{(1)}S_{22}^{(1)}}\right]\right]S_{11}^{(1)}\bar{\sigma}_x^{(1)} + S_{12}^{(1)}\bar{\sigma}_y^{(1)} + \epsilon_{xN}^{(1)} \tag{2.35}$$

$$\bar{\epsilon}_y^{(1)} = S_{12}^{(1)}\bar{\sigma}_x^{(1)} + S_{22}^{(1)}\bar{\sigma}_y^{(1)} + \epsilon_{yN}^{(1)} \tag{2.36}$$

$$\bar{\gamma}_{xy}^{(1)} = \left[\frac{\beta_4}{\beta_3}\right] S_{66}^{(1)} \bar{\tau}_{xy}^{(1)} \tag{2.37}$$

where $S_{ij}^{(1)}$ are elements of the compliance matrix for ply group 1, e_{xN} and e_{yN} are nonmechanical strains, $\bar{\epsilon}$ and $\bar{\sigma}$ are averaged strains and stresses, and

$$\beta_1 = 1 - \frac{\tanh(\alpha_1 L)}{\alpha_1 L} \qquad \beta_2 = 1 + \frac{h^{(1)} Q_{11}^{(1)} \tanh(\alpha_1 L)}{h^{(2)} Q_{11}^{(2)} \alpha_1 L} \tag{2.38}$$

$$\beta_3 = 1 - \frac{\tanh(\alpha_2 L)}{\alpha_2 L} \qquad \beta_2 = 1 + \frac{h^{(1)} Q_{66}^{(1)} \tanh(\alpha_2 L)}{h^{(2)} Q_{66}^{(2)} \alpha_2 L}$$

Now Q_{ij} are elements of the lamina stiffness matrix, 2L is the distance between matrix cracks, and

$$\alpha_1^2 = \frac{3 C_{55}^{(1)} C_{55}^{(2)}}{h^{(1)} C_{55}^{(2)} + h^{(2)} C_{55}^{(1)}} \left(\frac{h^{(1)} Q_{11}^{(1)} + h^{(2)} Q_{11}^{(2)}}{h^{(2)} Q_{11}^{(2)} h^{(1)} Q_{11}^{(1)}} \right) \tag{2.39}$$

$$\alpha_2^2 = \frac{3 C_{44}^{(1)} C_{44}^{(2)}}{h^{(1)} C_{44}^{(2)} + h^{(2)} C_{44}^{(1)}} \left(\frac{h^{(1)} Q_{66}^{(1)} + h^{(2)} Q_{66}^{(2)}}{h^{(2)} Q_{66}^{(2)} h^{(1)} Q_{66}^{(1)}} \right)$$

In addition, Nuismer and Tan [27] use strain, rather than stress, to define first ply failure.

Flaggs [23] uses a two dimensional shear lag model, similar to the one dimensional models described above to study laminates of the type $[\pm\theta, 90_n]_s$ where θ refers to a relatively low angle ply, and $[0_2, \pm\phi]_s$, where ϕ refers to a high angle ply. Instead of applying the shear lag idea to τ_{xz} or τ_{13} only, Flaggs has applied it to τ_{23}, as well. This greatly complicates the model, but it may enhance its accuracy. In addition, Flaggs' model incorporates in-plane shear loading. The derivation is not given here, since it follows a similar line of reasoning to Laws and Dvorak's model [26]. Figure 5 shows a comparison of Flaggs' shear lag model with finite element predictions and experimental data.

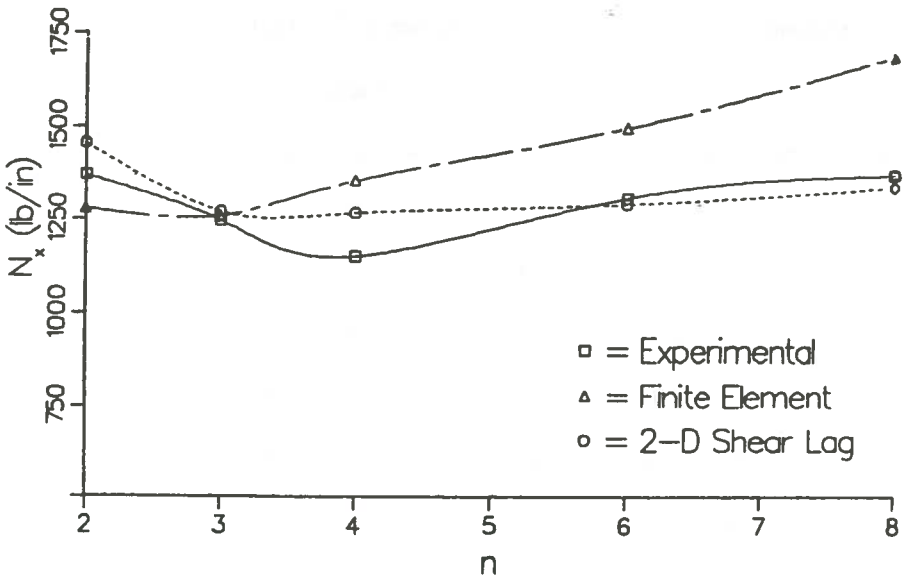

Figure 2.5. Comparison of Laminate Load at Onset of Matrix Cracking to Finite Element and 2-D Shear Lag Predictions for $[\pm 25/90_n]_s$ T300/934 Laminate Family [23]

Daniel and Tsai [28] have also written a model for transverse matrix cracking in the 90° plies of laminates of the type $[0_n/90_m]_s$. It can accomodate general in-plane biaxial loading but is otherwise quite similar to Lee and Daniel's model. Of course, strain energy release rate is not used. Results were shown for 10° off-axis loading only.

Longitudinal splitting is another form of matrix cracking, which is due to the Poisson effect. The strains produced by differential Poisson contractions of the laminae are increased when transverse cracking occurs. Interestingly, Bailey and coworkers [21, 22], did not see longitudinal splitting in carbon/epoxy, but only in glass/epoxy, even though the Poisson's ratio mismatch is much greater in carbon/epoxy. They believe that the reason for this is that the particular CFRP studied had small ultimate failure strains. Bader, et al. [21] have developed an expression for the minimum composite strain at which longitudinal splitting is energetically favored for a crossply laminate.

$$\epsilon_{lc}(\min)=\frac{1}{\nu_l}\left\{\frac{E_c^*(b+d)}{E_l\, d}\left[-\frac{3}{4}\epsilon^{th}+\left[\frac{1}{16}(\epsilon^{th})^2+\frac{\gamma_t\, d\, E_l\sqrt{\phi}}{(b+d)E_c^*E_t}\right]^{\frac{1}{2}}\right]+\nu_t\epsilon_c\right\} \tag{2.40}$$

where E_c^* is the Young's modulus in the transverse direction, b, d, E_l, and E_t are the same as defined by Laws and Dvorak [26], ϵ^{th} is the tensile thermal strain in the transverse ply, ϵ_c is the strain at the first transverse crack, ν_l and ν_t are the Poisson's ratio of the longitudinal and transverse plies, respectively, γ_t is the fracture surface energy per unit area of the inner ply, and ϕ is given by

$$\phi = \frac{E_c G_t}{E_l E_t} \frac{(b+d)}{b d^2} \tag{2.41}$$

According to Swanson [33], matrix cracking reduces strength, and this reduction is more pronounced in tough matrices than in brittle matrices. This is because longitudinal splitting along the fiber/matrix interface in the more brittle matrices is a toughening mechanism. As was seen in Chapter One, debonding between the fiber and matrix contributes to fracture toughness. The contribution of debonding to fracture toughness is greater in brittle matrices, because the matrix has little intrinsic toughness. In composites with tough matrices, however, the loss of toughness due to matrix cracking probably overshadows any toughening effect due to debonding. This toughening effect should ideally be accounted for in a model of transverse cracking in fiber-reinforced epoxy composites.

Tsai, Daniel, and Lee [29] account for longitudinal cracking in their shear lag model. This model encompasses $[0_m/90_n]_s$ laminates under biaxial loading; however, like Daniel's previous models, it depends on transverse strength and not on strain energy release rate. It is important to note that shear loading is not included in this model. Tsai, et al., showed that it is impossible under shear lag theory, to incorporate cracking in both directions and shear loading effects. Finally, while the model was written for biaxial loading, it is compared with experimental results for loading in one direction only.

Delamination

Delaminations tend to start at free edges, like holes and cutouts, internal flaws, ply drop-offs, or joints. In fiber-reinforced epoxy systems, delamination follows matrix cracking. In a ply with 90° laminae, matrix cracking begins in the 90° plies, followed by delamination at the

interfaces bounded by at least one 90° ply. A complete model must include both edge and local delamination. With biaxial testing, local delamination is significantly more important than edge delamination.

Models for Transverse Cracking and Edge Delamination

Two edge delamination models will be examined, but first the observations of A.S.D. Wang [32,34] will be discussed. In composite fracture, the properties of the composite are, of course, very important. Less obvious is the influence of ply thickness on cracking. From a statistical point of view, one assumes that a thicker lamina contains more defects than a thin lamina, so it is likely to fail at a lower stress or strain level. The laminate's stress field and the distribution of defects are then very important in determining cracking of the material. On the other hand, one may employ a fracture mechanics approach, which uses the strain energy release rate.

A. S. D. Wang [32, 34] used a fracture mechanics approach. Wang assumes that the strain energy trapped in the laminae depends on thickness. He uses finite element calculations to find the strain energy release rate, G(a), for transverse cracking and edge delamination under thermal and transverse uniaxial mechanical loading, and compares his predictions with uniaxial test results on each layup examined. Assumptions made in his Monte Carlo simulation include self-similar cracking, mode I transverse cracking, and mixed mode edge delamination. He finds that the strain energy release rate for delamination increases as the number of 90° plies increases in a $[\pm 25/90_n]_s$ laminate, where $n=1/2,1,2,3,$and 4. Transverse cracking in the 90° plies occurs at a very high strain for small n ($n=1/2$ and $n=1$), and it is preceded by edge delamination between the 90° plies.

Wang's results also show that final failure occurs after delaminations from both sides of the specimen grow until 70-80% of the width is delaminated. On the other hand, if n is greater than 1, transverse cracking precedes edge delamination and occurs at a much smaller strain. In fact, the transverse cracking onset strain in $[\pm 25/90_n]_s$ laminates with $1<n\leq 4$ is less than that for a $[90_8]$ laminate, which proves Wang's assertion that the strain energy in the 90° layer must be used to

determine the onset of transverse matrix cracking. The results are somewhat different for crossply laminates [32]. For example, while edge delamination does occur in the $[\pm 25/90_2]_s$ laminates, $[0_2/90_2]_s$ laminates exhibit no edge delamination after matrix cracking. Edge delaminations occur between the central 90° plies for n=1/2, 1 and 2, while for n=3 and 4, local and edge delaminations are predicted to occur between the -25° and 90° plies. For n=3, the prediction is correct: delamination is mixed mode and the onset strain is close to the predicted value.

Failure occurs very rapidly after the onset of edge delamination. For n=4, on the other hand, delamination is predicted to be mostly mode II, but in experiments, no noticeable delamination occurs before final failure [32]. In a later paper [34], however, Wang shows that the predicted delamination does occur, and, in addition, finds that the same failure modes occur for n=6 and 8, as well. As n increases above 4, the onset loads for delamination decrease to approach those for transverse matrix cracking, and for n=8, they are approximately equal to each other and to the failure load.

Wang uses a simple discount method to account for multiple transverse cracks. He assumes that the properties of the 90° layers are decreased by 10% when transverse cracking occurs prior to delamination. In addition, his method does not account for delamination occurring at the tips of transverse cracks. He does, however, note that delamination between the 90° plies is due primarily to normal stress, delamination between +25° and -25° plies is dominated by shear (Mode II), and delamination between 90° and 25° plies is mixed mode. These observations are useful for prediction of delamination at matrix crack tips.

Poursartip [35] studied transverse cracking and delamination under static and cyclic tensile loading. He showed that the crack density in the 90° plies of an unnotched $[45/0/-45/90]_s$ graphite epoxy laminate was 0.9 cracks/mm. Delamination then occurred first at either the 90/90 interface or the 90/-45 interfaces. These delaminations progressed rapidly in the axial direction and more slowly in the transverse direction, jogging between interfaces by means of matrix cracks in the 90° layers. During delamination, transverse crack density grew to 1.8 cracks/mm as the size of the

delaminations grew. Transverse cracking occurred to a lesser extent in the -45° plies, where it was initiated at the laminate free edge and was densest in the delaminated region. On the other hand, transverse cracks in the 90° plies extended to the area in front of the delamination. Cracks appeared later and crack density was much less in the 45° plies than in the -45° plies; however, 45° cracks were also found mostly in the delaminated area.

Poursartip [34] has proposed that the matrix cracking required less energy than delamination; therefore, transverse matrix cracking helped to prevent delamination. In other words, as energy is made available for the formation of new surfaces, it is used for additional matrix cracking, rather than for delamination. He has found that the delamination crack resistance, G_R, increases as delamination progresses, partly due to the diminishing supply of weaker crack paths, but also due to an increasing use of energy for matrix cracking. This is supported by the observation of a great deal of matrix cracking during delamination. Poursartip's observations are very useful, and he has achieved good results with a rather simple model.

Poursartip used O'Brien's [36,37] stiffness reduction equation for edge delamination:

$$E=(E^*-E_{LAM})\frac{A}{A^*}+E_{LAM} \tag{2.42}$$

where E_{LAM} is the laminate longitudinal tangent modulus before delamination, A/A* is the ratio of delaminated area to total interfacial area, and E* is the modulus of the laminate completely delaminated along one or more interfaces. This delaminated modulus can be found from:

$$E^*=\frac{\sum_{i=1}^{m} E_i t_i}{t} \tag{2.43}$$

where t_i and E_i are the thickness and modulus of the i^{th} sublaminate and m is the total number of sublaminates. O'Brien has verified these relations by experiments using graphite-epoxy laminates.

Transverse matrix cracking combined with edge delamination has been studied for $[0/90]_s$ and $[\pm 45/0/90]_s$ glass/epoxy laminates by Caslini, Zanotti and O'Brien [38], who used shear lag analysis and fracture mechanics to characterize damage in a manner similar to that of Laws and Dvorak [26]. They extended the cross ply results to laminates where the 90° ply is constrained by

0° plies, but may have other plies surrounding the 0/90 combination. They did not, however, study cracking in the outer off-angle plies. They base their model on the experimental observations of glass/epoxy under fatigue loading. The number of matrix cracks reaches a saturation value, which is a function of laminate characteristics, and matrix cracking in the 90° plies precedes all other damage. They also mention that damage accumulation behavior depends on test and load levels. The fact that matrix crack density reaches a saturation value is somewhat problematical in their model, since the closed form solution gives G as a function of dE/dA, which continually increases as stress increases, and never goes to zero as it should.

Caslini et al., like Poursartip, used O'Brien's [36] sublaminate method for modeling free edge delamination. (See equations 2.42 and 2.43 above). The strain energy release rate for a body of volume, V, under a constant strain, ϵ, is:

$$G=-V\frac{\epsilon^2}{2}\frac{dE}{dA}=\frac{\epsilon^2 t}{2}(E_{LAM}-E^*) \tag{2.44}$$

O'Brien used edge delamination experiments to find the strain at which delamination was first detected. He then used equation (2.44) to determine G_C, which was subsequently used to predict delamination in other laminates.

O'Brien's approach for edge delamination works well for graphite-epoxy, but not for glass-epoxy, because glass epoxy is more likely to experience extensive matrix cracking before the onset of delamination, and because edge delaminations grow only a small amount in quasi-static conditions before final failure due to a lower Poisson's ratio mismatch in glass-epoxy. Thus, Caslini, et al., are forced to use a linear regression analysis of experimental data to model stiffness loss due to cracking in glass/epoxy laminates.

Valisetty and Rehfield [39] also used a sublaminate method to model edge delamination, but, unlike Caslini, et al., they found the interlaminar stresses. They used homogeneous plate theory to solve the finite-width free edge delamination problem. They applied the theory on a ply-by-ply basis and were able to satisfy equilibrium and compatibility. They did this for uniaxial tension only and compared their results with a finite element analysis and not with experimental data.

Although some elements of S. S. Wang's [20] approach are not useful in the type of model proposed here, one useful concept is his evaluation of G using Irwin's virtual crack extension concept.

$$G=G_I+G_{II}+G_{III} \tag{2.45}$$

$$=\lim_{\delta\beta\to 0}\frac{1}{2\delta\beta}\int_0^{\delta\beta}\Big\{\sigma_z\Big[r,0\Big]\Big[w^{(k)}\Big[\delta\beta-r,\pi\Big]-w^{(k+1)}\Big[\delta\beta-r,-\pi\Big]\Big] + \tau_{yz}\Big[r,0\Big]\Big[v^{(k)}\Big[\delta\beta-r,\pi\Big]-v^{(k+1)}\Big[\delta\beta-r,-\pi\Big]\Big] + \tau_{xz}\Big[r,0\Big]\Big[u^{(k)}\Big[\delta\beta-r,\pi\Big]-u^{(k+1)}\Big[\delta\beta-r,-\pi\Big]\Big]\Big\}dr$$

where polar coordinates (r,φ) are used, $\delta\beta$ is the length of the virtual crack extension; σ_z, τ_{xz}, and τ_{yz} are the interlaminar stresses; and u, v, and w are the displacements of the k^{th} lamina in the x, y, and z directions. Notice that G_I is proportional to σ_z, G_{II} is proportional to τ_{yz}, and G_{III} is proportional to τ_{xz} in Wang's formulation, which is solved for a general symmetric laminate subjected to a uniform axial strain, ϵ_x. Note that this author has rotated Wang's axes to make this equation correspond to the other equations given here.

Models of Transverse Matrix Cracking and Local Delamination

Armanios [40] has developed a model similar to that of Caslini, et al., but Armanios' model is for local delamination rather than edge delamination. Talreja [41] has proposed a very different model, in which he describes interlaminar and intralaminar failure modes according to associated damage vectors. In addition, O'Brien [37] has developed a sublaminate approach to local delamination.

Armanios [40] has developed a shear deformation model with the sublaminate approach similar to that described above, along with fracture mechanics, to predict local delamination at transverse crack tips. Transverse cracks terminate where the ply orientation changes, and, at the crack tips, local or transverse crack tip delaminations grow in a direction normal to that of the

transverse crack. For the purpose of modeling local delaminations, Armanios treats the transverse cracks as free edges. He assumes plane strain conditions in the x-z plane, neglecting through thickness strain, ϵ_{zz}. This assumption means that, with his method, one cannot correctly estimate the interlaminar normal stress. Thus, Armanios calculates G_{II} as

$$G_{II}=\lim_{\delta\to 0}\frac{1}{2\delta}\int_0^{\delta} T_1(x-\delta)\Delta u(x)dx \tag{2.46}$$

where T_1 is the interlaminar shear along sublaminate 1 (Figure 2.6), Δu is the relative sliding displacement, and taking the limit as $\delta\to 0$ gives G_{II} at the delamination crack tip. Note the similarity between this equation and equation (2.45). In fact, S.S. Wang's equation can be adapted for transverse crack tip delamination by showing that G_{II} is proportional to τ_{xz} and G_{III} is proportional to τ_{yz}.

In Armanios' model, taking $\delta=0$ in equation (2.46) gives a trivial result, so the limit is actually calculated as δ approaches an appropriate decay length, or length within which the presence of the crack significantly alters the response of the material in comparison with the corresponding far

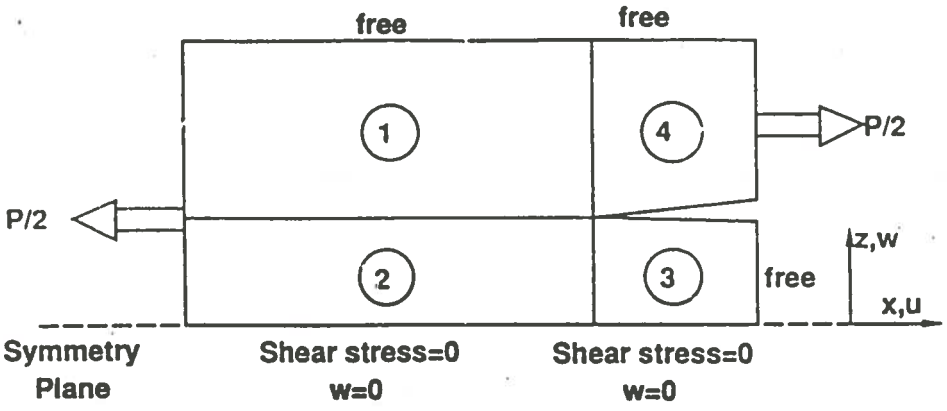

Figure 2.6. Modeled Region and Sublaminate Scheme [39]

field response. Armanios estimates the total strain energy release rate from the equation,

$$G_T=\frac{P^2}{2b}\frac{dC}{da}=\frac{P^2}{2b^2}\left[\frac{1}{A_{11(1)}}-\frac{1}{A_{11(1)}+A_{11(2)}}+I_1-I_2\right] \tag{2.47}$$

where P is the uniform axial force applied to the specimen, b is the specimen width, and dC/da is

the change in compliance with crack growth. A_{11} is the classical laminate theory axial stiffness in the 11 direction, (i) refers to the sublaminate, and I_1 and I_2 are associated with delamination length.

Armanios has fully predicted critical delamination growth stresses for $[\pm 25/90_n]_s$ laminates with some success and his results are reasonably correlated with experimental values of critical strain for large numbers of 90° plies ($n \geq 4$).

O'Brien [37] has developed a sublaminate approach for local delamination, as well as for edge delamination. The difference between the two is that in local delamination, the 90° ply becomes totally isolated. O'Brien assumes that the delamination starts at the matrix crack tips and progresses down the length of the laminate. Thus, the equation for the modulus of a locally delaminated laminate, E^*_{LD} is:

$$E^*_{LD} = \frac{\sum_{i=1}^{m} E_i t_i}{t} \tag{2.48}$$

where i refers to plies with $\theta \neq 90$ only and the other variables have the same meaning as given above. Now the modulus of the locally delaminated cross-section, E_{LD}, is simply the modulus of the remaining plies, and is given by:

$$E_{LD} = E^*_{LD}\left[\frac{t}{t_{LD}}\right] \tag{2.49}$$

where t_{LD} is the thickness of the laminate less the thickness of the 90° plies that have been isolated. Finally, the strain at which local delamination occurs is:

$$\epsilon_c = \frac{1}{E_{LAM} t}\sqrt{\frac{2mG_C}{\left[\frac{1}{E_{LD} t_{LD}} - \frac{1}{E_{LAM} t}\right]}} \tag{2.50}$$

where E_{LAM} is the modulus of the laminate before delamination and G_C is the critical strain energy release rate of the laminate. Equations 2.50 and 2.47 are essentially the same, except for the term I_1-I_2 in Armanios' equation. This term indicates that the applied load for additional delamination depends on delamination size, but it is not highly significant. Armanios compares his model with O'Brien's and the predicted delamination onset strains are the same.

Talreja [41] takes a different, albeit no less interesting, approach to the study of transverse matrix cracking and local delamination growth. He looks at a general orientation of matrix cracks in an initially orthotropic laminate of the type $[0/\pm\theta_n]_s$. Specifically, he studies laminates with $\theta=90°$ and n=1/2 and 3 and laminates with $\theta=45°$ and n=1. A major difference between Talreja's model and the others is that he assumes a general crack orientation and shows that, after cracking, the laminate loses its orthotropy if the crack is not oriented along the material axes. He groups what he calls "failure entities" into two damage modes, according to their orientation and growth characteristics. The first is the intralaminar damage mode, which is matrix cracking, and the second is the interlaminar damage mode, which is local delamination. His model, based on experimental observations, begins with matrix cracking in plies not oriented along the principal tensile loading direction. These cracks increase monotonically in number until a saturation level is reached, whereupon cracks initiate in adjacent plies transverse to these primary matrix cracks. Obviously, this scenario is correct for a laminate with $\theta=45°$, but if $\theta=90$, the transverse cracks will simply extend through the 90° plies with the same orientation in all of them. Talreja asserts that these intralaminar cracks initiate interlaminar cracks, which appear initially as isolated delamination regions, but grow and merge into strip-like delamination zones. Eventually, crack interactions increase to a point where fiber failures begin, followed rapidly by final failure of the material.

By assuming that damage modes do not interact substantially, which only holds until delamination begins, Talreja used a form of superposition of damage modes to develop his polynomial expression for the elastic potential which must be invariant to transformations expressing the orthotropic symmetry initially present in the laminate. Unfortunately, the polynomial expression for the elastic potential also contains phenomenological constants, which must be determined experimentally. Talreja has obtained a good comparison of his model with the results of fatigue testing.

Yang and Boehler [42] developed a model for matrix cracking and local delamination, which describes in detail the interaction between the two damage modes. Their observations echo those of

Talreja. They observed that a small amount of local delamiatnion occurs as soon as transverse matrix cracks reach the bounding region. Theoretically, this is due to a singularity in the interlaminar shear stress at the transverse crack tip. This initial delamination soon arests due to its stable nature. The size of the initial delamination depends on material properties and ply thickness. A greater 90° ply thickness implies a larger initial delamination. In addition, the likelihood of such initial delaminations decreases as crack spacing decreases. As the crack spacing approaches the shear lag distance, which is related to the thickness of the 90° layer, no further delamination occurs until the characteristic damage state is reached. This characteristic damage state refers to the final matrix crack density. After the characteristic damage state is reached, delamination begins again, because no further energy can be dissipated by the formation of matrix cracks.

Models for transverse matrix cracking, edge delamination, and local delamination have been examined. Before final failure can occur, one additional fracture process must occur. That process is fiber failure in the primary load-carrying plies.

Fiber Failure

Fiber failure in load carrying plies precedes or coincides with final failure, but random fiber breaks can also lead to matrix cracks transverse to and along the direction of the fibers [18]. The rule of mixtures has been used to define the strength of the plies with fibers oriented in the direction of the load, but it overestimates the strength of composites with poor fiber/matrix interface strength [14]. On the other hand, statistical methods have been used, which say that longer fibers have more flaws than shorter fibers, so they tend to break at lower stresses. A commonly used statistical model is the Weibull distribution, which will be discussed in more detail.

Once a fiber breaks, the load is transferred by shear in the matrix back to the fiber a short distance along its length from the break. The distance between the fiber break and the location where load can again be transferred from matrix to fiber is termed the ineffective length, since the fiber does not carry the applied load over that distance. Fiber failure propagates through a ply as

fibers must take additional load due to previous fiber failures. In addition, ineffective or debonded fibers aligned at the boundary of voids have a strong effect on transverse tensile strength.

Since the rule of mixtures approach is inaccurate and the statistical approach is difficult to use, many researchers use the experimentally determined failure stress or strain of a unidirectional lamina as the criterion for failure in the fiber direction. For example, fiber failure has been defined by Lee [16] and by Murray [18] to occur at the unidirectional lamina tensile strength in the fiber direction. Approaches of this nature rely on experimental measurement of the unidirectional tensile strength, but the value obtained will include all fiber-related failure micromechanisms, fiber-matrix debonding, pull-out, and breakage, since all of these contribute to unidirectional tensile failure. Poe [14] used an interesting approach based on fiber failure strain. While his model was written for the laminate as a whole, it may be useful for examination of the fiber-dominated failure modes only. He found that

$$K_{IC}=\frac{E_y \epsilon_{1C}\sqrt{2\pi x}}{1-\nu_{xy}\left[\frac{E_x}{E_y}\right]^{\frac{1}{2}}\cos^2\alpha+\left[\frac{E_y}{E_x}\right]^{\frac{1}{2}}\sin^2\alpha} \tag{2.51}$$

where ϵ_{1C} is the critical fiber strain, x is the distance from the crack tip, E_x, E_y, and ν_{xy} are the elastic constants of the ply containing the crack with x parallel to the crack and y normal to the crack, and α is the fiber orientation angle of the load-carrying ply with respect to the y-axis. The problem with this theory is that it will not hold if extensive delamination or longitudinal splitting occurs. It remains to be seen if it will hold if it is used only for fiber failure, rather than laminate failure.

Other interesting approaches are those of Rosen [43] and Phoenix and Wu [44]. Rosen uses the idea of fiber ineffective length to represent the stress field in a unidirectional fiber composite with distributed fractures. By neglecting the stress concentrations at the fiber breaks, the tensile strength can be expressed as a statistical function of ineffective length. Phoenix and Wu use a

Weibull distribution function,

$$F(\sigma)=1\text{-}\exp\left\{-\left[\frac{\sigma}{\sigma_1(R)}\right]^{\beta(\rho+1)}\right\} \tag{2.52}$$

where $\beta(\rho+1)$ is the shape parameter and $\sigma_1(R)$ is the scale parameter with R equal to the rate of stress increase. Rosen's distribution is probably a Weibull distribution, but his equation is unclear. It turns out that use of the unidirectional tensile strength or critical fiber strain is adequate for a shear lag model [25, 28].

The approximate analytical models discussed have primarily been developed for and compared with uniaxial tension data only. Obviously, there is a need for a model capable of predicting damage and failure under biaxial loading conditions, since few actual structures see uniaxial loading only.

Failure Theories

The only methods commonly used to predict failure are failure theories and curve fits [45-51] including maximum strain, maximum stress, Tsai-Wu, and curve fits in the form of Tsai-Wu.

Maximum strain is the most commonly used failure criterion and is useful, because the mode of failure is predicted. This criterion says that failure occurs when the strain component in any one of the principal material directions of the lamina exceeds its corresponding ultimate strain. This is similar to the maximum stress criterion, which also can predict failure mode. Both criteria take the following form, which is the explicit form of the maximum stress criterion [45].

$$\begin{aligned} &\sigma_{11} \geq X_T \text{ for } \sigma_{11}>0 && \sigma_{22} \geq Y_T \text{ for } \sigma_{22}>0 \\ &|\sigma_{11}| \geq X_C \text{ for } \sigma_{11}<0 && |\sigma_{22}| \geq Y_C \text{ for } \sigma_{22}<0 \\ &|\sigma_{12}| \geq S \text{ for all } \sigma_{12} \end{aligned} \tag{2.53}$$

where X_T and X_C are the tensile and compressive strengths, respectively, in the longitudinal fiber direction, Y_T and Y_C are the tensile and compressive strengths, respectively, in the transverse fiber direction, and S is the in-plane shear strength.

The Tsai-Wu and Tsai-Hill theories are similar, but Tsai-Wu predicts fiber-reinforced composite failure more accurately than does Tsai-Hill [30]. The Tsai-Wu [46] criterion is:

$$F_i\sigma_i+F_{ij}\sigma_i\sigma_j\geq 1 \tag{2.54}$$

or, for specially orthotropic materials in two dimensions,

$$F_1\sigma_{11}+F_2\sigma_{22}+F_{11}\sigma_{22}^2+F_{22}\sigma_{22}^2+2F_{12}\sigma_{11}\sigma_{22}+F_{66}\sigma_{12}^2 \geq 1 \tag{2.55}$$

where:

$$\begin{aligned} F_1&=\frac{1}{X_T}-\frac{1}{X_C} & F_{11}&=\frac{1}{X_TX_C} & F_{66}&=\frac{1}{S_TS_C} \\ F_2&=\frac{1}{Y_T}-\frac{1}{Y_C} & F_{22}&=\frac{1}{Y_TY_C} & & \\ F_{12}&=\frac{1}{2P^2}\left[1-P\left[\frac{1}{X_T}-\frac{1}{X_C}+\frac{1}{Y_T}-\frac{1}{Y_C}\right]-P^2\left[\frac{1}{X_TX_C}+\frac{1}{Y_TY_C}\right]\right] & & & \end{aligned} \tag{2.56}$$

where S_T and S_C are positive and negative shear strengths, respectively, and P is the strength determined from a biaxial test with $\sigma_1=\sigma_2=P$ and $\sigma_{12}=0$.

Hashin's [18] failure theory is three-dimensional in nature, and takes the form:

$$A_1I_1+B_1I_1^2+A_2I_2+B_2I_2^2+C_{12}I_1I_2+A_3I_3+A_4I_4\geq 1 \tag{2.57}$$

where I_i are the stress invariants,

$$\begin{aligned} I_1&=\sigma_{11} & I_3&=\sigma_{22}^2-\sigma_{22}\sigma_{33} \\ I_2&=\sigma_{22}+\sigma_{33} & I_4&=\sigma_{12}^2+\sigma_{13}^2 \end{aligned} \tag{2.58}$$

Hashin correctly argues that failure is due to normal and shear stresses acting on the failure plane. He points out that σ_{22} does not contribute to fiber failure and σ_{11} does not contribute to matrix failure. Additionally, he stated that σ_{11} and σ_{12} acting on the 2-3 plane are responsible for fiber failure, while σ_{22} and σ_{12} acting on the 1-3 plane cause matrix failure.

Chang's [18] model is simply a modified form of the Hashin model, incorporating nonlinear shear behavior, and it will not be reproduced here.

Feng's [47] model is also very similar to that of Hashin, but he allows large deformations to occur by using Cauchy strain invariants. The Feng criterion, decoupled for fiber and matrix dominated failure is:

$$A_1(I_1-3)+A_{11}(I_1-3)^2+A_2(I_2-3)-1=0 \quad (2.59)$$

for matrix dominated failure and

$$A_5(I_5-3)+A_{55}(I_5-3)^2+A_4(I_4-3)-1=0 \quad (2.60)$$

for fiber dominated failure, where the I_i are the Cauchy strain invariants and the A_i are constants determined empirically for a given material.

Many people have tried to develop failure theories for composites, however simple curve fitting of biaxial test data is still used to create failure surfaces, because the data do not correlate well with any common failure theories [48]. Methods for predicting failure include Tsai-Wu failure theory, linear laminated plate theory with maximum strain criteria, and progessive failure modelling with a maximum strain criterion. These theories have been used to try to predict failure of tubular and cruciform specimens made of several different composite materials.

Modeling of Biaxial Failure

Swanson and Christoforou [49] used tubular specimens to test AS4/3501-6 carbon epoxy quasi-isotropic $[90/\pm45/0]_s$ laminates. Their stress-strain data shows good agreement with linear laminated plate theory (LPT) until the stress reaches about 90 ksi, when the stiffness of the samples decreases. This is due partly to a nonlinear shear response in the 45 degree plies and partly to matrix microcracking. The reduction in slope would be greater were it not for the increased stiffness at strains greater than 1% noticed in tests of uniaxial tensile coupons. These effects seem to cancel one another to some extent, giving a small net reduction in slope. The data were compared with three failure models. They used both LPT and a progressive failure model with a maximum fiber strain failure criterion and Tsai-Wu. The progressive failure model includes a criterion for matrix cracking, a model of stiffness changes with further straining after matrix cracking, a criterion for ultimate fiber failure, and a nonlinear matrix shear response. The two maximum fiber strain criteria compare well with the experimental data, but the Tsai-Wu method does not correlate well at all, presumably because it predicts failure in laminates in which matrix failure coincides with or leads to

laminate failure. Fiber dominated failure, in which the matrix simply redistributes stresses as the fibers fail, is not well modelled by the quadratic Tsai-Wu equation [43].

Zimmerman and Adams [50], have used cruciform specimens for biaxial testing and a least squares curve fit of the data to plot an elliptical failure surface for Rynite, which is an injection molded glass reinforced polyethylene terephthalate. The failure surface curve fit is similar in form to the Tsai-Wu equation, as described by Owen [51]. The Tsai-Wu equation is:

$$F_{xx}\sigma_x^2+2F_{xy}\sigma_x\sigma_y+F_{yy}\sigma_y^2+F_{ss}\sigma_s^2+F_x\sigma_x+F_y\sigma_y=1 \tag{2.61}$$

and the curve fit is

$$A\sigma_x^2+C\sigma_x\sigma_y+B\sigma_y^2+D\sigma_x+E\sigma_y=1 \tag{2.62}$$

Although the curve fit equation does not contain an $F_{ss}\sigma_s^2$ term, the values given for A, B, D, and E are approximately equal to their corresponding Tsai-Wu parameters, F_{xx}, F_{yy}, F_x, and F_y, as calculated from the curve fit data. The value for C is of the same order of magnitude as, but is not equal to F_{xy}.

Zimmerman, Walrath and Adams [52] have also studied unidirectional, continuous fiber graphite/aluminum composites. Again, they used cruciform biaxial specimens to study the failure modes of the composite and calculated the elliptical failure surface using a least squares fit. The curve fit parameters corresponded with the Tsai-Wu equation in the same way as the Rynite parameters did. Of course, since one term is missing, neither comparison of curve-fits with Tsai-Wu theory tells us anything more than that there is some similarity. It is hard to tell whether Tsai-Wu would be too conservative, as it was for the tubular samples discussed above. However, failure is more matrix-dependent in the materials used by Adams' group, than it is in epoxy matrix composites.

Failure models are useful predictors of failure, and one can use them to ascertain some information about material behavior. However, the present failure theories cannot, in and of themselves, predict progressive cracking or the change in stiffness that accompanies such cracking. They do not account for delamination. Therefore, it is important to use a progressive failure model

like those already described. This researcher feels that the shear lag model is the best candidate for further exploration, since it is relatively straightforward and has given good results as shown above.

CHAPTER 3

DEVELOPMENT OF MODEL

Initial Model

The initial model incorporates transverse matrix cracking in the 90° plies of fiber reinforced composites of the type $[\pm\theta/90_n]_s$ under biaxial tension. It also includes an estimation of local delamination effects. Transverse matrix cracking typically occurs first in the more constrained or thicker 90° plies when a load is applied transverse to the ply fiber direction. The matrix cracking in the 90° plies is modeled using a two-dimensional shear lag theory along with the Griffith energy criterion for crack propagation. By changing Flaggs' [23] boundary conditions to allow for more than one crack, progressive cracking can be modeled more generally than has previously been done. Before describing the progressive failure model, the governing equation must be solved for the appropriate boundary conditions. The expressions obtained from the solution of the governing equation allow the formation of an algorithm to predict transverse matrix cracking as static loading is increased.

Explanation and Solution of the Governing Equation

The governing equation is developed using linear laminated plate theory constitutive equations for each lamina group ($\pm\theta$ and 90°), equilibrium relations which incorporate transverse shear stress continuity, and shear lag theory. It is assumed that ply group 1 ($\pm\theta$) takes the entire applied load at the points of 90° ply cracking. See Figure 3.1. The details are given by Flaggs [23]. The coordinate system is defined by the material coordinate system of ply group 2; that is, direction 1 is in the direction of the 90° ply fibers. The governing equation for cracking in ply group 2, the 90° ply group, is from Flaggs [23]. It is derived for half of the laminate, since the

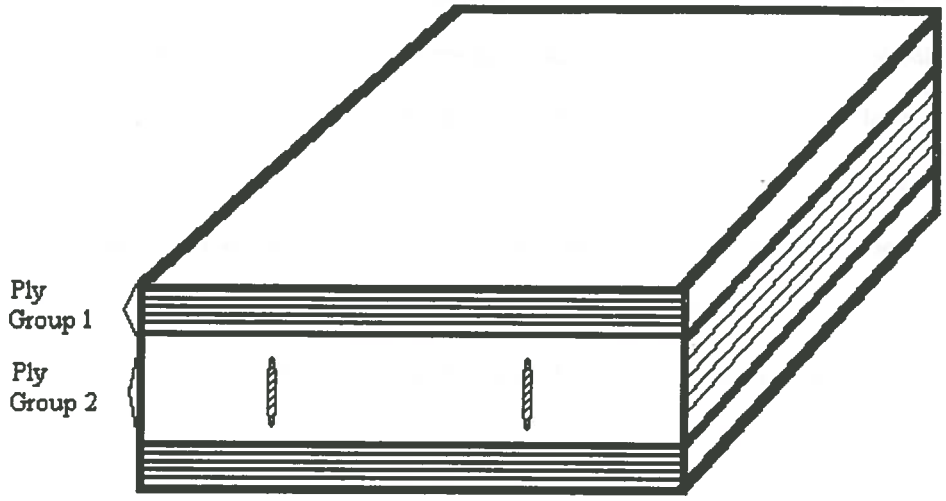

Figure 3.1. The Onset of Transverse Matrix Cracking

laminate is symmetric. The governing equation is given by:

$$\begin{Bmatrix} \frac{d^2\Delta n_2}{dx_2^2} \\ \frac{d^2\Delta n_6}{dx_2^2} \end{Bmatrix}^{(1)} - \begin{bmatrix} L_{22} & L_{26} \\ L_{62} & L_{66} \end{bmatrix} \begin{Bmatrix} \Delta n_2 \\ \Delta n_6 \end{Bmatrix}^{(1)} = \begin{Bmatrix} 0 \\ 0 \end{Bmatrix} \tag{3.1}$$

where Δn_2 and Δn_6 are the changes in the integrated transverse tensile and in-plane shear loads in ply group 1 due to the presence of cracks in ply group 2, and the L matrix is adopted from Flaggs [23] and modified slightly. It is defined by:

$$\begin{bmatrix} L_{22} & L_{26} \\ L_{62} & L_{66} \end{bmatrix} = \frac{2}{H_2^2} \begin{bmatrix} t_{44} & t_{45} \\ t_{54} & t_{55} \end{bmatrix}^{-1} \begin{bmatrix} A_{44}^{(2)} & 0 \\ 0 & A_{55}^{(2)} \end{bmatrix} \begin{bmatrix} F_{12}^{(1)} & F_{22}^{(1)} + \frac{1}{A_{22}^{(2)}} & F_{26}^{(1)} \\ F_{16}^{(1)} & F_{26}^{(1)} & F_{66}^{(1)} + F_{66}^{(2)} \end{bmatrix}$$
$$\cdot \begin{bmatrix} a_2 & -a_6 \\ 1 & 0 \\ 0 & 1 \end{bmatrix}^{(1)} \tag{3.2}$$

where the Aij are elements of the laminated plate theory ABD matrix for ply group (1) or (2) as shown, the Fij terms are elements of the inverse A matrix, H_2 is half of the thickness of the 90° ply group and the t and a terms are taken directly from Flaggs [23]. The reader should note that this governing equation is defined for ply group 1 symmetric or nonsymmetric. Flaggs [23] solved this equation for a single crack; thus, his boundary conditions were defined at $x_2 = 0$ and $x_2 = \infty$. The boundary conditions used in the present solution are for cracks at $x_2 = \pm c/2$, where c is the distance between two adjacent cracks and the origin of the x_2 axis is exactly between the two cracks. See Figure 3.2. At the cracks, the change in ply group 1 loads are Δn_2° and Δn_6°, which are the

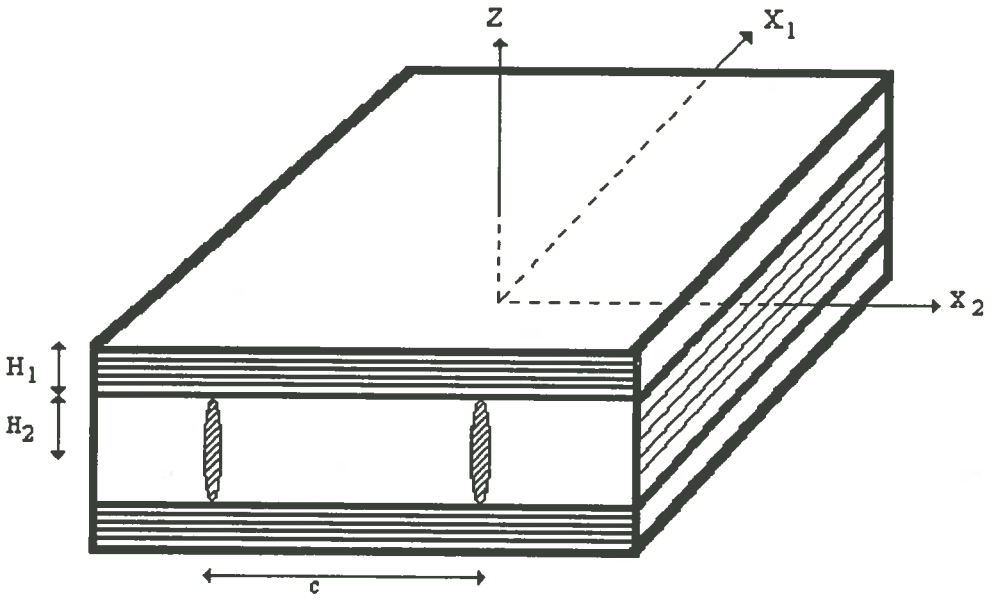

Figure 3.2. Transverse Matrix Cracking

loads in ply group 2 at the crack locations before cracking. The solution to the governing equation is:

$$\Delta n_2 = \left[\frac{\frac{1}{2}(L_{66}-L_{22}+\lambda_3^2-\lambda_1^2)\Delta n_2^\circ - L_{26}\Delta n_6^\circ}{(\lambda_3^2-\lambda_1^2)}\right]\left[\frac{\cosh(\lambda_1 x_2)}{\cosh(\lambda_1 c/2)}\right] + \left[\frac{\frac{1}{2}(L_{22}-L_{66}+\lambda_3^2-\lambda_1^2)\Delta n_2^\circ + L_{26}\Delta n_6^\circ}{(\lambda_3^2-\lambda_1^2)}\right]\left[\frac{\cosh(\lambda_3 x_2)}{\cosh(\lambda_3 c/2)}\right] \quad (3.3)$$

$$\Delta n_6 = \left[\frac{\frac{1}{2}(L_{22}-L_{66}+\lambda_3{}^2-\lambda_1{}^2)\Delta n_6{}^\circ - L_{62}\Delta n_2{}^\circ}{(\lambda_3{}^2-\lambda_1{}^2)}\right]\left[\frac{\cosh(\lambda_1 x_2)}{\cosh(\lambda_1 c/2)}\right] + \left[\frac{\frac{1}{2}(L_{66}-L_{22}+\lambda_3{}^2-\lambda_1{}^2)\Delta n_6{}^\circ + L_{62}\Delta n_2{}^\circ}{(\lambda_3{}^2-\lambda_1{}^2)}\right]\left[\frac{\cosh(\lambda_3 x_2)}{\cosh(\lambda_3 c/2)}\right] \tag{3.4}$$

where the λ_i are the roots of the auxiliary equation, and are:

$$\lambda_{1,3} = \sqrt{\frac{1}{2}(L_{22}+L_{66}) \pm \frac{1}{2}\sqrt{(L_{22}-L_{66})^2+4L_{26}L_{62}}} \tag{3.5}$$

Now, the $\Delta n_i{}^\circ$ are initially given by the $n_i^{(2)}$ and:

$$\begin{Bmatrix} n_1 \\ n_2 \\ n_6 \end{Bmatrix}^{(2)} = \begin{bmatrix} A_{11} & A_{12} & 0 \\ A_{12} & A_{22} & 0 \\ 0 & 0 & A_{66} \end{bmatrix}^{(2)} \begin{Bmatrix} \epsilon_1 \\ \epsilon_2 \\ \epsilon_6 \end{Bmatrix}^{(2)} - \begin{Bmatrix} n_{1_t} \\ n_{2_t} \\ n_6{}^t \end{Bmatrix}^{(2)} \tag{3.6}$$

where the n_i^t are the residual integrated thermal loads due to curing. Likewise,

$$\begin{Bmatrix} n_1 \\ n_2 \\ n_6 \end{Bmatrix}^{(1)} = \begin{bmatrix} A_{11} & A_{12} & A_{16} \\ A_{12} & A_{22} & A_{26} \\ A_{16} & A_{26} & A_{66} \end{bmatrix}^{(1)} \begin{Bmatrix} \epsilon_1 \\ \epsilon_2 \\ \epsilon_6 \end{Bmatrix}^{(1)} - \begin{Bmatrix} n_{1_t} \\ n_{2_t} \\ n_6{}^t \end{Bmatrix}^{(1)} \tag{3.7}$$

and the ϵ_i are equal for ply groups 1 and 2. The change in load in the 1 direction is proportional to the change in the 2 direction load, and the proportion is (A_{12}/A_{22}).

Progressive Cracking Model

The Griffith energy criterion for cracking is $d(\Delta W_{ext}-\Delta W_{int})/da \geq G_c$ where ΔW_{ext} is the external work done on the laminate and ΔW_{int} is the change in strain energy of the laminate. In the current state there are two cracks, as discussed above. In the new damage state, there will be an additional crack located somewhere between the first two. If probability density based on the stress distribution between the two cracks is used, one finds that the expected average location of the third

crack is halfway between the first two. However, flaws in the material are randomly distributed, and the probability density function for the location of the new crack should ideally take that into account. Therefore, the location of the new crack is unknown at present.

In order to get from crack state one to crack state two, one assumes that the applied load must be increased. This is because crack state one is assumed to be the equilibrium crack state for the applied loads which caused it. The strain energy density for state j is, including both in-plane and transverse shear terms:

$$dW_{intj} = \sum_{k=1}^{n} \int_{hk-1}^{hk} \int_{\{\epsilon\}}^{\{\epsilon\}_j} {}^{(k)}\sigma_{mn}\, d{}^{(k)}\epsilon_{mn}\, dz\, dx_2 \qquad (3.8)$$

$$= \frac{1}{2}\sum_{k=1}^{n} \left\{\Delta n\right\}_j^T \left[[F]\{\Delta n\}_j + 2\{\epsilon\} - 2[F]\{n^t\}\right] dx_2 + \frac{1}{2}\sum_{k=1}^{n} \left[\frac{H_k^2}{4}\right] \left\{\begin{matrix}\tau_{23}\\ \tau_{13}\end{matrix}\right\}_j^T [F_s]^{(k)} \left\{\begin{matrix}\tau_{23}\\ \tau_{13}\end{matrix}\right\}_j dx_2$$

where T refers to transpose, k indicates the ply group, and F_s is the inverse shear matrix. Both matrix cracking states are referred to the initial strain at the onset of cracking. Integrating this equation between $x_2 = -c/2$ and $x_2 = c/2$ gives ΔW_{int} for state j. Then, ΔW_{int} is $\Delta W_{int_2} - \Delta W_{int_1}$. The work done on the total laminate by external loads during crack formation is found from the applied loads and the ply group 1 mechanical strains. The quantity dW_{ext} is integrated from -c /2 to c /2, and is given by:

$$dW_{ext} = 2N_{2j}\left(\Delta {}^{(1)}\epsilon_{2j} - \Delta {}^{(1)}\epsilon_{2j-1}\right)dx_2 + 2N_{6j}\left(\Delta {}^{(1)}\epsilon_{6j} - \Delta {}^{(1)}\epsilon_{6j-1}\right)dx_2 \qquad (3.9)$$

where the one direction term is zero due to the assumption that strain in the one direction does not change, and the coefficient of 2 is used because N_2 and N_6 are defined as the loads applied to half of the laminate only.

For a laminate in which ply group one is symmetric, the resulting equation for total energy released by the introduction of the first two cracks is:

$$\Delta W_{ext}-\Delta W_{int}=4\left\{\left[\frac{N_2}{A_{22}^{(1)}}+\left[\frac{A_{12}^{(2)}}{A_{22}^{(2)}}-\frac{A_{12}^{(1)}}{A_{22}^{(1)}}\right]\epsilon_1+\frac{n_2^{t(1)}}{A_{22}^{(1)}}-\frac{n_2^{t(2)}}{A_{22}^{(2)}}\right]\left[\frac{A}{\lambda_1}\tanh\frac{\lambda_1 c}{2}+\frac{B}{\lambda_3}\tanh\frac{\lambda_3 c}{2}\right]\right.$$

$$\left.+\left[\frac{N_6}{A_{66}^{(1)}}+\frac{n_6^{t(1)}}{A_{66}^{(1)}}-\frac{n_6^{t(2)}}{A_{66}^{(2)}}\right]\left[\frac{C}{\lambda_1}\tanh\frac{\lambda_1 c}{2}+\frac{D}{\lambda_3}\tanh\frac{\lambda_3 c}{2}\right]\right\}$$

$$-\left[\frac{1}{A_{22}^{(1)}}+\frac{1}{A_{22}^{(2)}}\right]\left[A^2\left[\frac{1}{\lambda_1}\tanh\frac{\lambda_1 c}{2}+\frac{1}{2\cosh^2(\lambda_1 c/2)}\right]+B^2\left[\frac{1}{\lambda_3}\tanh\frac{\lambda_3 c}{2}+\frac{1}{2\cosh^2(\lambda_3 c/2)}\right]\right.$$

$$\left.+4AB\left[\frac{\lambda_1\tanh(\lambda_1 c/2)-\lambda_3\tanh(\lambda_3 c/2)}{\lambda_1^2-\lambda_3^2}\right]\right]-\left[\frac{1}{A_{66}^{(1)}}+\frac{1}{A_{66}^{(2)}}\right]\left[C^2\left[\frac{1}{\lambda_1}\tanh\frac{\lambda_1 c}{2}+\frac{1}{2\cosh^2(\lambda_1 c/2)}\right]\right.$$

$$\left.+D^2\left[\frac{1}{\lambda_3}\tanh\frac{\lambda_3 c}{2}+\frac{1}{2\cosh^2(\lambda_3 c/2)}\right]+4CD\left[\frac{\lambda_1\tanh(\lambda_1 c/2)-\lambda_3\tanh(\lambda_3 c/2)}{\lambda_1^2-\lambda_3^2}\right]\right] \tag{3.10}$$

$$+\sum_{k=1}^{n}\left\{\left[\frac{H_k^2\lambda_1^2}{4}(F_{44}^{(k)}A^2+2F_{45}^{(k)}AC+F_{55}^{(k)}C^2)\right]\left[\frac{1}{\lambda_1}\tanh\frac{\lambda_1 c}{2}-\frac{1}{2\cosh^2(\lambda_1 c/2)}\right]\right.$$

$$-\left[\frac{H_k^2\lambda_1^2}{4}(F_{44}^{(k)}B^2+2F_{45}^{(k)}BD+F_{55}^{(k)}D^2)\right]\left[\frac{1}{\lambda_3}\tanh\frac{\lambda_3 c}{2}-\frac{1}{2\cosh^2(\lambda_3 c/2)}\right]$$

$$\left.-\left[\frac{H_k^2\lambda_1\lambda_3}{2(\lambda_1^2-\lambda_3^2)}[F_{44}^{(k)}AB+2F_{45}^{(k)}(AD+BC)+F_{55}^{(k)}CD]\right]\left[\lambda_1\tanh\frac{\lambda_3 c}{2}-\lambda_3\tanh\frac{\lambda_1 c}{2}\right]\right\}$$

where

$$A=\left[\frac{\frac{1}{2}(L_{66}-L_{22}+\lambda_3^2-\lambda_1^2)\Delta n_2^0-L_{26}\Delta n_6^0}{(\lambda_3^2-\lambda_1^2)}\right]$$

$$B=\left[\frac{\frac{1}{2}(L_{22}-L_{66}+\lambda_3^2-\lambda_1^2)\Delta n_2^0+L_{26}\Delta n_6^0}{(\lambda_3^2-\lambda_1^2)}\right] \qquad (3.11)$$

$$C=\left[\frac{\frac{1}{2}(L_{22}-L_{66}+\lambda_3^2-\lambda_1^2)\Delta n_6^0-L_{62}\Delta n_2^0}{(\lambda_3^2-\lambda_1^2)}\right]$$

$$D=\left[\frac{\frac{1}{2}(L_{66}-L_{22}+\lambda_3^2-\lambda_1^2)\Delta n_6^0+L_{62}\Delta n_2^0}{(\lambda_3^2-\lambda_1^2)}\right]$$

When this energy term is divided by a characteristic crack size, the result can be compared with G_c and the applied load required to cause cracking can be iteratively determined. The characteristic crack size used is $2H_2$ for H_2 less than 2 1/2 times the ply thickness, and it is equal to 2 1/2 times the ply thickness if H_2 is greater than that amount [23]. This is the appropriate size for edge notch flaws, which are more likely than internal flaws in tensile test coupons. Such tensile coupons were used in the experiments, which were done for verification of the current work. In addition, this author has chosen to use the same method as Flaggs [23] for estimating G_c under biaxial loading conditions. Both Mode I and Mode III cracking are present under combined in-plane tension and shear; therefore, G_c for each mode must be combined. The equations are not reproduced here. For the laminate and test modeled in this paper, the inclusion of mode III cracking in the evaluation of G_c had little effect on the results.

At this point, the loads at which subsequent cracks are formed can be determined. The current model assumes incremental increases in load at constant crack density, then checks for cracking at the next crack density by comparing G with G_c. The increase of load in each ply must

be determined in the present model, because Δn_2° and Δn_6° change as the load changes. As a first approximation for the initial model, these quantities are based on the fraction of the load carried by each ply group after the previous cracks have formed. These average ply group loads are multiplied by the total load increment to get the load increment in each ply group. The location of the next crack must also be determined and is not straightforward. As mentioned in Chapter 2, Wang [32] assumes the randomly located flaws follow a normal distribution, Laws and Dvorak [26] assume a probability density function based on the stress in ply group 2, and Lee and Daniel [25] and Tsai, Daniel, and Lee [29] assume that the next crack must occur exactly half-way between the previous two cracks. The last assumption is used in the present model for simplicity, since both Wang's [32] and Laws and Dvorak's [26] probability functions predict that, on the average, the next crack will indeed occur halfway between the previous two.

Effect of Local Delamination

Local delamination occurs as a result of transverse matrix cracking. When the transverse matrix cracks reach the boundary between the layers, the interlaminar shear stress at the crack tip becomes singular, and delamination occurs. See Figure 3.3. In this model, the λi terms fill the function of the shear lag parameter defined in similar models [21-28]. Since the shear lag parameter is used to describe the interaction between the ply groups, and this interaction will change should damage develop between plies, the shear lag parameter must be sensitive to this change [25,26].

When local delamination occurs, the through thickness shear stiffness change, G_{23}, can be approximated, using the rule of mixtures, by $G_{23}(1\text{-}4\beta H_2)$ where G_{23} is the value of the through thickness shear modulus before delamination, β is the crack density and is equal to 1/c, and c is the distance between two adjacent cracks. This expression is obtained by assuming that the average shear modulus varies linearly down the length of the specimen. In addition, it is assumed that the shear lag distance, the distance from the transverse crack over which the transverse shear stress decays to zero, is the distance over which the transverse shear stiffness is zero or very small. The

distance between the cracks is divided into segments equal in length to the shear lag distance, which is assumed to be approximately one-half the thickness of the cracked ply group, and the shear stiffness returns to its original value at the midpoint between the two cracks.

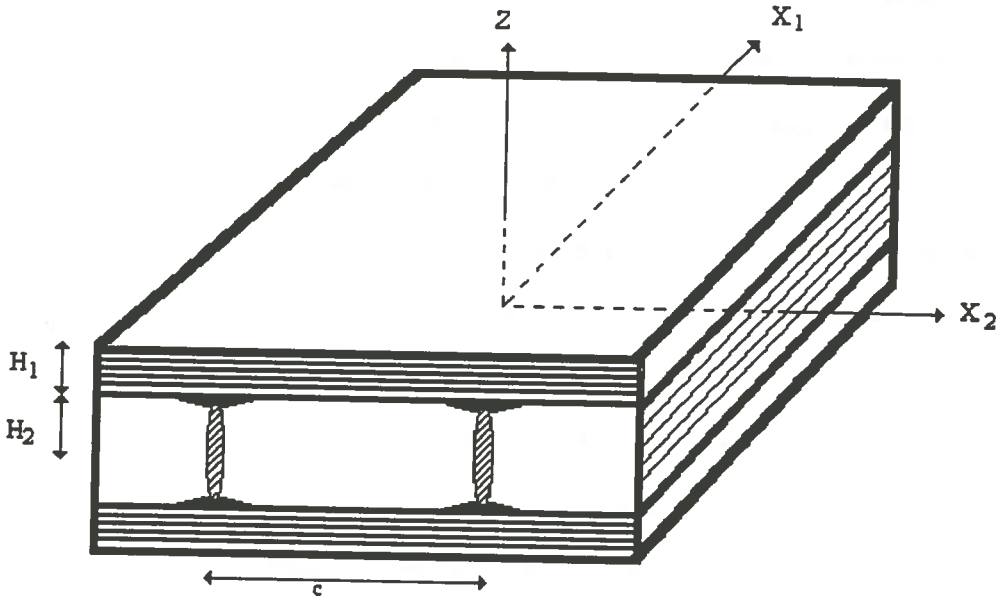

Figure 3.3. Local Transverse Crack Tip Delamination

The expression developed in this work is similar to the one proposed by Yang and Boehler [42] for the reduced through-thickness shear modulus, G_{23}^{*}:

$$G_{23}^{*} = G_{23}\,[1 - h(\beta, H_2)] \tag{3.12}$$

where h is a function of crack density and delamination size and is equal to $2\beta H_2$ plus an additional term involving β and H_2. The notation used in the equation has been changed to be consistent with that used in this work. When the distance between two cracks approaches a value of a little over four times the shear lag distance, the modification factor approaches a limiting value. This distance is approximately the same as the distance developed rigorously by Yang and Boehler.

The reason behind the limit on the modification factor has been explained by Yang and Boehler [42]. For the first several transverse matrix cracks, the strain energy release rate for local delamination is greater than G for the next matrix crack, but, as the local delamination grows, the resistance to crack growth increases; that is, G becomes smaller. (Refer to equation 2.1). Thus, the delamination only grows a short distance from the matrix crack tip, which, according to Yang and Boehler's [42] analysis, is approximately equal to the shear lag distance. Once the delamination has been arrested, additional matrix cracks may form, since the strain energy release rate for matrix cracking would now be larger than that for continued delamination.

As the distance between matrix cracks approaches the shear lag distance, delamination no longer occurs at each matrix crack. Yang and Boehler [42] show that γ_4 is proportional to h, so τ_i is proportional to h(1-h), and, using equation 2.1, it can then be shown that the strain energy release rate for delaminations of constant size increases and then decreases as G_{23} decreases. Thus, after the first few matrix cracks, local delamination is no longer energetically favorable and matrix cracking occurs without associated local delaminations. At this point, the decrease in modulus for local delamination has reached its limiting value.

The point at which the modulus decrease reaches the limiting value can be estimated using O'Brien's [37] equation for local delamination. A more general form of equation (2.50) is:

$$P = \sqrt{\frac{2mG}{\left[\frac{1}{E_{LD}t_{LD}}\right] - \left[\frac{1}{E_{LAM}t}\right]}} \qquad (3.13)$$

where P is the applied load, G is the strain energy release rate for delamination, E_{LD} and t_{LD} are the modulus and thickness, respectively, of the delaminated cross-section, and E_{LAM} and t are the modulus and thickness, respectively, of the laminate before delamination. At the transition between matrix cracking plus delamination and matrix cracking only, the strain energy release rate for delamination must be equal to that of matrix cracking. By using the strain energy release rate for matrix cracking in O'Brien's [37] equation, the load at which the transition occurs can be

determined, and this prediction correlates very well with the point at which the shear lag distance between cracks is reached. O'Brien's equation is used as a rule, then, for the limit on the decrease in shear modulus as small delaminations occur.

As a first approximation, this author has hypothesized that, since the shear lag parameter given in equation (3.5) is proportional to the square root of the transverse shear modulus, that it should be modified as follows:

$$\lambda_{1,3}=\sqrt{\frac{1}{2}(L_{22}+L_{66}) \pm \frac{1}{2}\sqrt{(L_{22}-L_{66})^2+4L_{26}L_{62}}}\left[\sqrt{1-4\beta H_2}\right] \tag{3.14}$$

This shear lag modification term is similar to the interlaminar damage vector developed by Talreja [41]. Under biaxial loading, the change in transverse stiffness will be greater due to the presence of forces in both in-plane directions, causing the delamination to propagate rapidly in both directions. Thus, the modification term is now defined for two dimensions, rather than just one. Thus, for biaxial loading, the following approximation has been found to produce good results:

$$\lambda_{1,3}=\sqrt{\frac{1}{2}(L_{22}+L_{66})\pm\frac{1}{2}\sqrt{(L_{22}-L_{66})^2+4L_{26}L_{62}}}\left[\frac{1}{2}(1-4\beta H_2)\right] \tag{3.15}$$

Note that these equations are only for delamination between ply groups 1 and 2. Edge delamination between the 90° plies cannot be modeled in this manner.

Final Model

The major difference between the initial model and the final model is that the final model incorporates an additional 90° layer. The eventual goal of this researcher is to develop a model for laminates of the type $[\pm\theta/90_n]_s$. The system of equations for this laminate type cannot be solved directly using the method outlined here; therefore, this researcher has decided to model laminates of

the type $[90_n/0_m/90_p]_s$ as a first step toward the final goal. This seemingly small step actually complicates the model significantly. The laminate type is shown in Figure 3.4.

Explanation and Solution of the Governing Equations

The approach to modeling progressive cracking is essentially the same as was shown in the initial model section with some exceptions. The outermost 90° layer will be designated the top layer, the 0° layer is the middle, and the innermost 90° layer will be called the bottom layer. This makes sense, since only half of the laminate is modeled due to the inherent laminate symmetry.

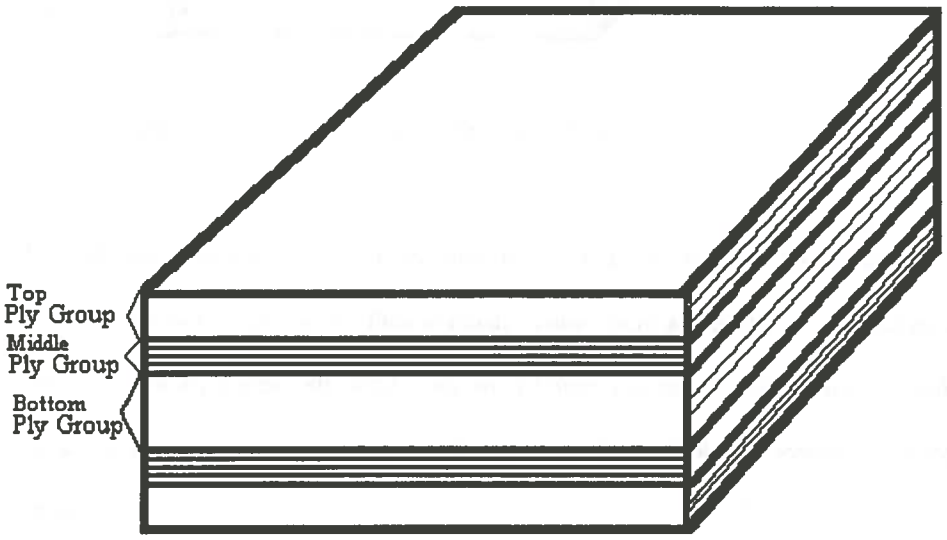

Figure 3.4. Laminate Type Used in the Final Model

Since there are three layers to consider, the load lost at the point of cracking of one layer must now be taken by the two layers, which are not cracked at that point. The development of the governing equations is discussed in detail in Appendix A. Figure 3.5 shows the coordinate system and some of the parameters used in the derivation.

The solution of the governing equations with the appropriate boundary conditions is shown in Appendix B. Using the solutions for ply group loads from the initial model, the forms for the changes in ply group loads due to cracking can be assumed for the final model. These loads are

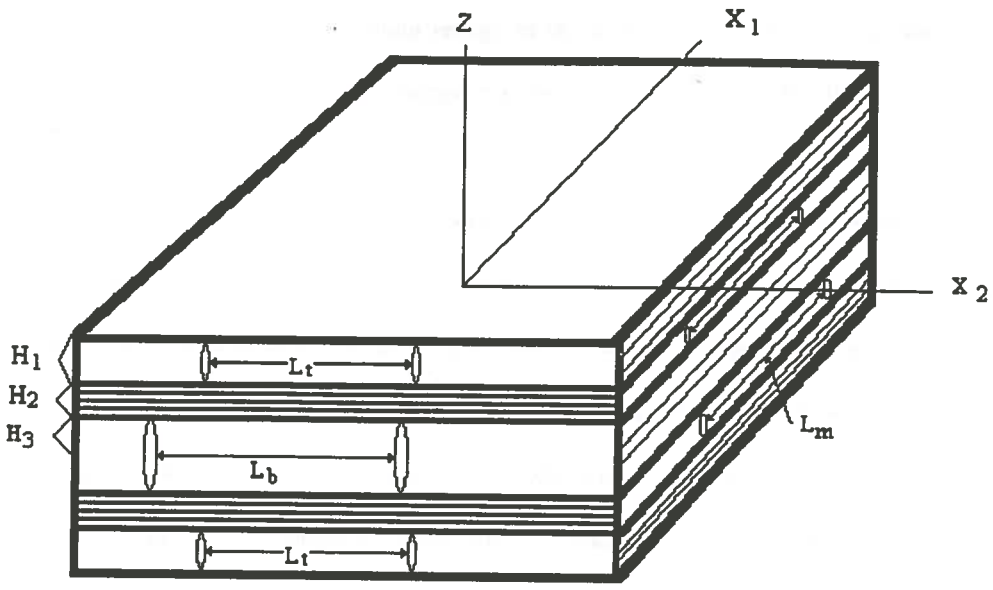

Figure 3.5. Transverse Matrix Cracking in the Final Model

substituted into the governing equations to solve for the constant terms. The boundary conditions of zero stress at the crack locations are then applied. Thus, there are twelve governing equations, three boundary condition equations, six total load equilibrium equations and twenty-one unknowns. In order to solve the equations more efficiently, the Maple symbolic processor in Mathcad 4.0 by Mathsoft was used.

The form of the change in ply group load terms does not allow for the boundary conditions to be satisfied everywhere, so they are satisfied by an averaging scheme. This is similar to the method used by Tsai, Daniel, and Lee [29]. In addition, the coordinate systems of the top and bottom ply groups are assumed to be independent, since the coordinate systems are based on the crack locations in the individual ply groups.

Modeling of Progressive Cracking in the Laminate

Progressive cracking is again modeled using basic fracture mechanics principles, and a FORTRAN program has been written for ease of calculation. The development of the equations for

work done by external loads and strain energy in the individual ply groups is given in Appendix C. Once again, the change in strain energy for each ply group includes the in-plane and through thickness shear terms.

A FORTRAN program has been written to perform all calculations, since many of them are iterative. For example, the load at which cracking starts is found by assuming a single crack separated from any other crack by an infinite distance occurs in a given ply group. The load in the laminate is increased until the strain energy release rate for the laminate is equal to the critical strain energy release rate for cracking to occur. This procedure is repeated for each ply group. Cracking begins in the ply group in which the strain energy release rate is reached at the smallest applied load. The actual crack densities of the three ply groups are then fed into the progressive cracking portion of the model. In this section, additional cracking is assumed to occur in each ply group respectively. The applied load is increased until the critical strain energy release rate is reached by the laminate for cracking in one of the ply groups. The crack densities are then updated. Thus, the program returns crack density versus applied load. In addition, strains and moduli at each crack density are calculated. Finally, local delamination is modeled in the same manner as in the initial model, except that the shear lag modification term is applied to the shear lag parameters of the top and bottom ply groups. This is necessary, because the through thickness shear stiffness of the bottom layer is included in both shear lag parameters.

The initial and final models are compared with data in the literature and with in-house experimental data in Chapter 5.

CHAPTER 4

EXPERIMENTAL METHODS

Four E-glass epoxy laminates were tested under monotonic tensile loading and the progression of damage was measured. The results were compared with the progressive cracking model previously described.

Specimen Preparation

The materials tested in this research were symmetrical lay-ups of 3M Scotchply 1003 pre-impregnated glass epoxy laminae. Table 4.1 gives the material properties of the cured Scotchply 1003 samples used. The layup used to verify the initial model was $[0/90_2]_s$. The layups used to verify the final model were $[90/0/90_3]_s$ and $[90_2/0_2/90]_s$. The layups used were chosen to

Table 4.1. Material Properties of Cured Scotchply 1003

Tensile Modulus (Msi)		Shear Modulus (Msi)	
0°, E_1	5.7	G_{12}	1.4
90°, E_2	1.4	G_{13}	1.4
E_3	1.4	G_{23}	.63
Tensile Strength (ksi)		**Coefficients of Thermal Expansion**	
0°, σ_{ult1}	108	α_1	3.5
90°, σ_{ult2}	2.9	α_2	11.4
Poisson's Ratios		**Critical Strain Energy Release Rate (in-lb/ib)**	
ν_{12}	0.3	G_C	.227
ν_{13}	0.3		
ν_{23}	0.49		

test modeling extremes, as well as to investigate the effect of relative thicknesses of constrained and unconstrained 90° plies.

Referring to Table 4.1, the 0° tensile modulus, the in-plane Poisson's ratio, and the 0° tensile strength were verified experimentally. The critical strain energy release rate was estimated using equation 4.1 [32].

$$G_C = \frac{\pi \ \sigma_{ult2}^2 \ a_c}{2E_2} \tag{4.1}$$

where $2a_c$ is the critical or effective flaw size and is equal to 5.0 times the total thickness of the 90° ply group [23]. This method correlates well with the estimates of other researchers [21-23, 25]. The other values were taken from the manufacturer or were found using the assumption of transverse isotropy. The only significant variation from the manufacturer's data was in tensile strength. The manufacturer's value was 140 ksi. The discrepancy is probably due to flaws in the specimens manufactured in-house. A flaw can initiate a local crack or debond that may lead to premature failure. The other material properties would not be substantially affected by such flaws.

The composite laminate specimens were manufactured as 10 x 10 inch lay-ups in a 12-ton simple heated (maximum of 500° F), vacuum bag press. Pre-impregnated Scotchply 1003 was cut into 10 x 10 in squares and stacked in layers of appropriate orientation. After the tacky laminate was layed up and smoothed out, it was placed between two sheets of Airtech Release Ease 234TFP-1 teflon coated, woven glass fiber release film. Three 11 x 11 inch sheets of Richmond, E-5555 #116 high temperature release fabric were placed on top of the sandwich and three layers of courser high temperature woven fiberglass were placed underneath the sandwich. These fabrics act as bleeder cloths for the curing process. They act to facilitate outgassing and resin pull off during the manufacturing process.

Once the laminate sandwich is laid on the bottom plate of the press, Schnee-Morehead vacuum bag one inch (S-M 5126-2) sealing tape is placed around the perimeter of the sandwich. This is to act as a sealant between the base of the press and the vacuum bag. Once in position, the

backing of the sealing tape is removed and a 14 x 14 inch layer of Richmond, Vac-Pak UHT-750 ultra high temperature bagging film is placed over the top of the composite sandwich and smoothed against the sealing tape. A vacuum is then drawn through a hole in the base plate at the edge of the laminate.

The press is then closed and brought to a jack pressure of 1,000 psi. At this pressure, the laminate is cured for 20 min at a stabilized 250° F temperature. At the end of this cycle, the jack is pumped up to 1,500 psi and the thermostat is increased to 330° F. Once the temperature reaches 330°, the laminate is cured for 25 minutes. At this point, the laminate is removed from the press, peeled away from the release film and left to cool.

After the laminate has been prepared, the 10 x 10 inch specimen is cut into nine, 1 x 8 inch samples. The top and bottom 1 inch is cut off and discarded, to remove any edge tapering, and the same is done to sample 1 and sample 9. All of the testing in this research involved the use of the best three samples from the center of the 10 x 10 specimen. The machining of the samples was performed using an Everett 3450 rpm cutting machine with an Everett #1410, 10 inch abrasive cut-off wheel.

Experimental Setup and Procedures

An Instron 8500 Series Servohydraulic Testing System with a 50,000 lb load cell and standard tension grips was used to apply a uniaxial tensile load to each specimen. For most experiments, strain was measured using Measurements Group CEA-06-125UW-350 350 Ω strain gages, which all had a gage factor of 2.12. A Measurements Group Model 2160 strain amplifier was used to amplify and condition the signal from the strain gages. An amplification of 400 was used. For the experiments done to verify the initial model, an Instron Dynamic Extensometer with a 0.5 inch gage length and a ± 0.2 inch travel was used. The output from the strain amplifier or extensometer and the output from the 50,000 lb Instron load cell were fed into a Hewlett Packard 8090A Measurement

Plotting System. Damage progression was measured via both the decrease in Young's modulus and by the density of transverse cracks formed.

The samples were loaded in increments of 400 to 1000 lbs, depending on the expected failure load. The idea was to obtain at least six measurements. Loading was done at a rate of 500 lbs/min. This relatively slow rate was chosen to allow the damage state in the laminate to reach equilibrium for each measurement.

In order to obtain stress information from the load data, the average cross sectional area was measured for each specimen. Five measurements were taken of the width and thickness of the specimen in the region where the strain gage was to be placed. Using the information described, Young's modulus was calculated for each loading step.

In order to measure the progression of cracking, a laminate edge was dyed and photographed at each load increment to reveal cracks. The load increments varied according to the specimen being tested, with the goal being to obtain about eight data points per specimen. Thus, the load increments used varied from 250 to 1000 lbs. The specimen cross-sectional edge was inked using stamp pad ink according to a procedure developed by Doucet [53]. The ink was allowed to soak into the cracks for approximately 5 minutes; whereupon, the excess ink was wiped off, and the sample was carefully and lightly polished with 400 grit sandpaper to remove surface ink. A Konica 35mm camera with Izumanon Close-up lens attachment and black and white film was positioned approximately 4 inches from the inked side of the laminate. Good contrast was obtained for most pictures. The photographs were viewed at 8x magnification with a Hama Lupe, and cracks were counted over at least three different inch-long segments. The three measurements were averaged to get the crack density at a given load. This procedure minimized error due to localized flaws. As a result, a photographic history of the damage was recorded from 0 lbs to failure via this dye penetration technique.

CHAPTER 5

RESULTS AND DISCUSSION

The progressive cracking model is compared with the results of several experiments and with a model and experimental data from Laws and Dvorak. A note on the use of the FORTRAN program is in order. When delamination is incorporated into the model, i.e. for laminates where the central 90° ply has four or more layers, the strain energy release rate is higher than G_C during the delamination portion. This is expected, since delamination increases the strain energy dissipated due to cracking. Ideally, G should be required to be equal to G_C for matrix cracking plus G_C for local delamination as a criterion for their occurrence. However, since the delamination size for each crack or load increment as well as the modulus decrease associated with delamination have been determined a priori, the conditions for delamination would be overconstrained were G_C to be specified as well. Thus, the strain energy release rate increases to a value of almost twice the G_C for matrix cracking and then decreases to the G_C for matrix cracking as delamination ends. Modeling delamination in this manner is not entirely certain, so the model stress versus crack density curves for samples with a large amount of delamination are plotted using the initiation of cracking and the crack state at the end of the initial local delamination as the first two data points. The results that follow are thus based on engineering judgment and not just a blind usage of the progressive cracking model.

Initial Model

The initial model is compared with the results of one set of published experiment and with another shear lag model in the literature. It is then compared with the results of in-house experimentation.

$[0/90_3]_s$ E-Glass Epoxy

The model is first compared with the uniaxial tensile testing results of $[0/90_3]_s$ E-glass epoxy reported by Laws and Dvorak [26]. The experimental results, their model, and the present model are shown in Figure 5.1. Since transverse crack tip delamination is expected to occur

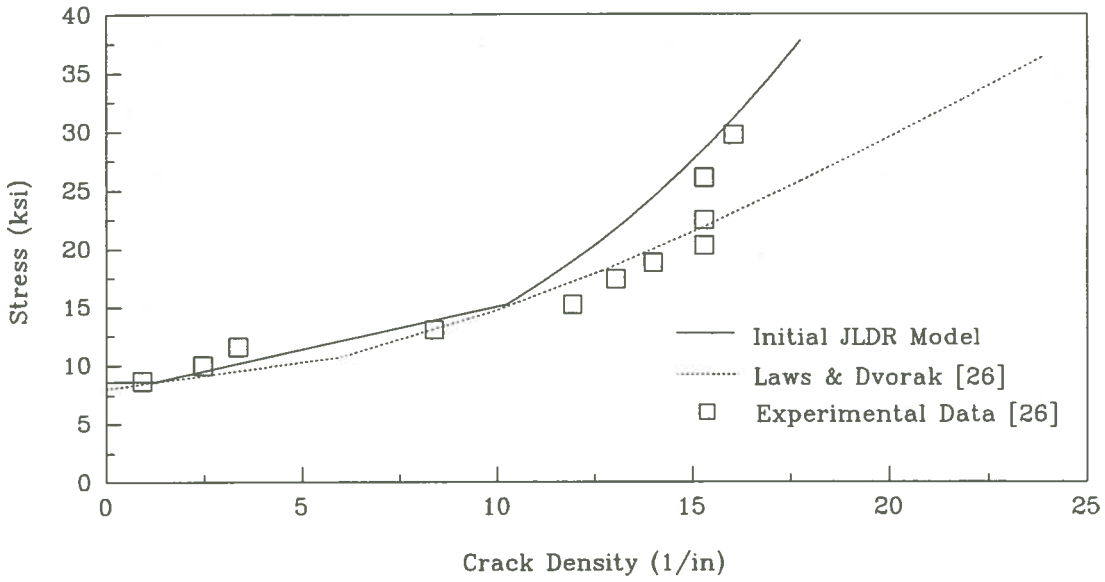

Figure 5.1. Comparison of Model Predictions with Experimental Data for Matrix Cracking in $[0/90_3]_s$ E-Glass Epoxy

between the 0° and 90° plies, the factor described in equation (3.14) was included in the evaluation of the λ_i. The present model shows excellent agreement with the experimental data in the region of higher crack densities. Laws and Dvorak's model shows better agreement in the middle crack density range, but their model does not predict transverse matrix crack saturation as well as does the present model.

$[0/90_2]_s$ E-Glass Epoxy Scotchply

Next the initial model is compared with experimental results of $[0/90_2]_s$ E-glass epoxy Scotchply. A small amount of delamination is expected in this laminate and is taken into account by

the model. Observations verified that prediction, since small delaminations were noticed emanating from the transverse crack tips at one of the interfaces, but not at both interfaces. There is a discrepancy between the experimental results and the model predictions of final failure, which is due primarily to the fact that both specimens tested failed at the tabs, indicating a stress concentration not accounted for in the model. The predicted failure stress is based on the stress in the 0° plies of the crossply laminate reaching the ultimate tensile strength found experimentally and is 37.6 ksi. The experimental failure stress was 24.4 ksi for one sample and 25.0 ksi for the other. The modulus predicted using the material properties given in Chapter 4 is 3.16 Msi and the actual moduli measured were 3.14 Msi and 2.80 Msi. This difference is not great, thus, the true composite laminate failure stress probably matches that used in the prediction. The results are as shown in Figures 5.2 and 5.3. Figure 5.3 shows that the model accurately predicts the modulus decrease.

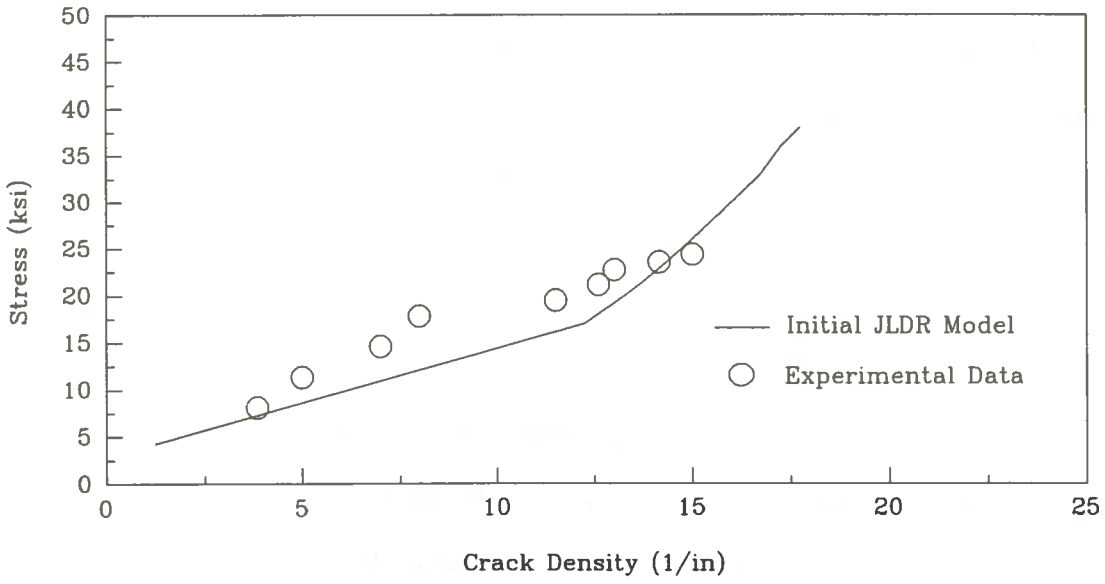

Figure 5.2. Comparison of Model Predictions with Experimental Data for Matrix Cracking in $[0/90_2]_s$ E-Glass Epoxy

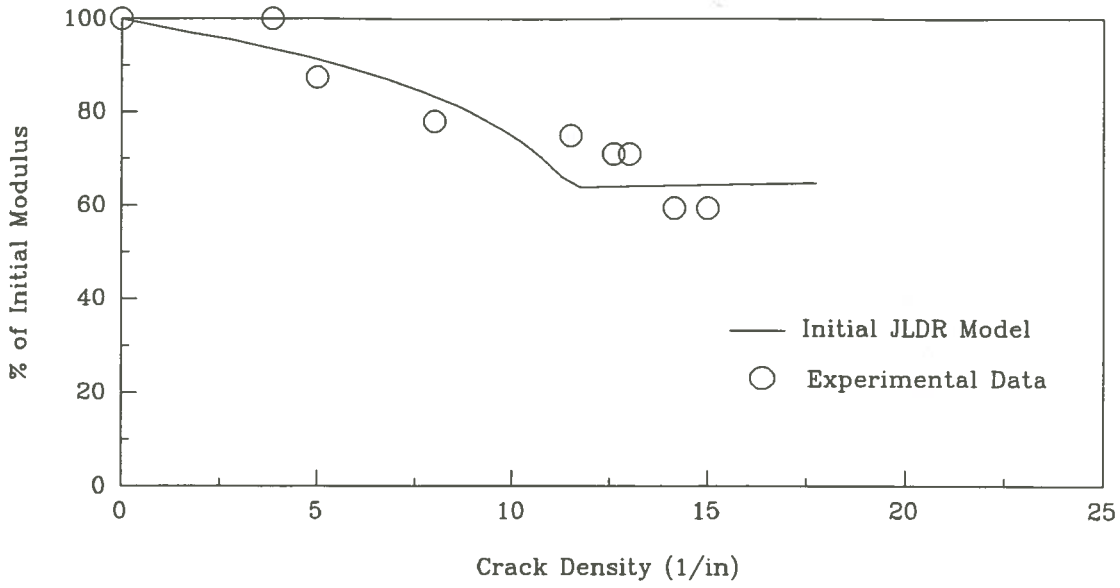

Figure 5.3. Comparison of Model Predictions with Experimental Data for Modulus Decrease in $[0/90_2]_s$ E-Glass Epoxy

Final Model

The final model is compared with the experimental results for $[90_2/0_2/90]_S$ and $[90/0/90_3]_S$ laminates under loading in the x direction, where x is the longitudinal material direction of the 0° plies. The experimental data of three different specimens is averaged in the Case 3 plots. The Case 1 plots include averaging of data from three specimens at failure. Data from two specimens are averaged for crack progression due to poor photographic quality of one of the specimens.

Case 1: $[90_2/0_2/90]_s$ E-Glass Epoxy Scotchply Under N_x

Agreement between the model and the experimental data is quite good, as is shown in Figures 5.4 and 5.5. The modulus prediction was good, with the model predicting a Young's modulus of 3.48 Msi and the samples having moduli of 3.44 Msi and 3.61 Msi. Recall that, according to Wang [34], a central ply group must have at least four total plies for delamination to occur. Since the ply groups subject to cracking are thin, no delamination is expected; therefore, the

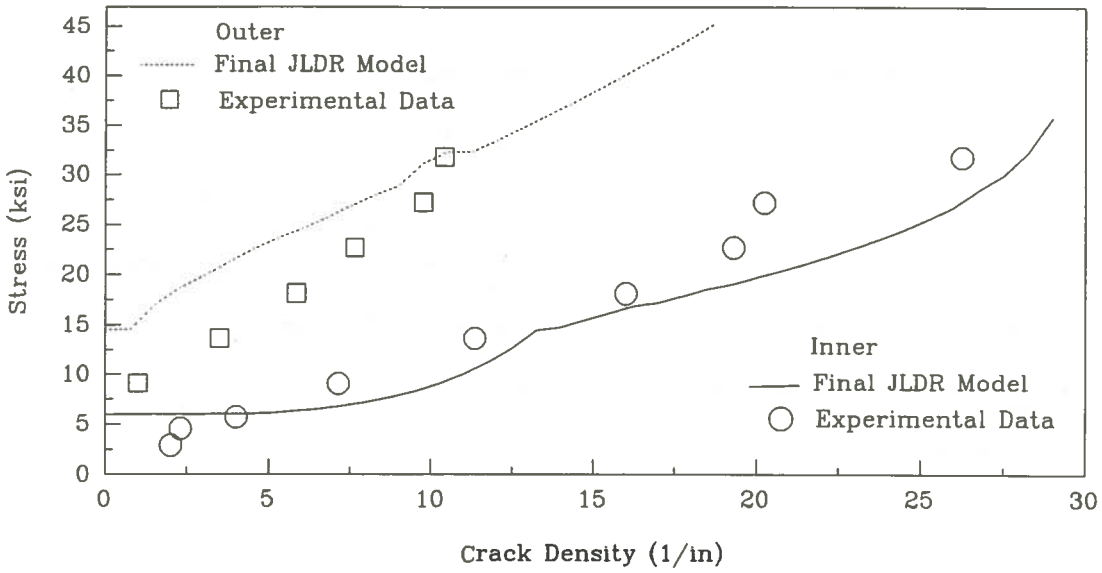

Figure 5.4. Comparison of Model Predictions with Experimental Data for Matrix Cracking in $[90_2/0_2/90]_s$ E-Glass Epoxy Under N_x

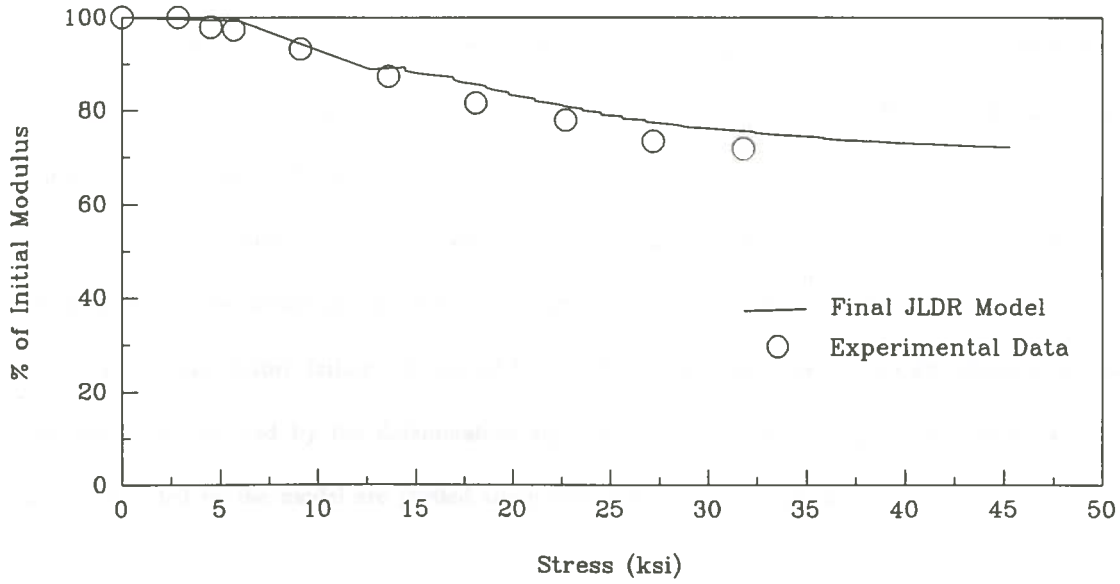

Figure 5.5. Comparison of Model Predictions with Experimental Data for Modulus Decrease in $[90_2/0_2/90]_s$ E-Glass Epoxy Under N_x

model is assumed accurate throughout the progression of cracking. The change in slope in the inner ply group stress vs. crack density curve corresponds approximately with the onset of additional matrix cracking in the outer ply group.

Once again, the failure strength is overestimated by the maximum stress criterion used in the model. The model predicted failure at 45 ksi, while the experimental failure occurred at 32 ksi for both samples. Both of the samples reported, like the ones discussed above, failed at the tabs. One sample showed no delamination, while the other showed only a thin three inch long edge delamination along the back side between the top and middle ply groups. Since edge delamination does not interact with matrix cracking to the extent that local delamination interacts with it, edge delamination was not incorporated into the model. The samples failed with no longitudinal splitting.

Case 3: $[90/0/90_3]_s$ E-Glass Epoxy Scotchply Under N_x

Again, we see a very good agreement between prediction and experiment in Figures 5.6 and 5.7. In addition, the prediction of failure stress was excellent. The predicted failure stress was 21.4 ksi and the three samples tested failed at 21.7 ksi, 19.3 ksi and 18.3 ksi. The excellent agreement is likely due to the fact that all samples failed away from the tabs. One sample failed nicely in the gage section with substantial local delamination between the middle and bottom ply groups and no splitting. The other two failed near, but not at, the tabs, and they also showed substantial local delamination with no splitting.

Local delamination was included in the model for this case and, indeed, small local delaminations were observed for the first four cracks, as predicted. No further delamination occurred until just before failure. It should be noted that the model predictions for modulus decrease were obviously skewed by the delamination algorithm in this case; therefore, the initial and final values predicted by the model are plotted along with the experimental data.

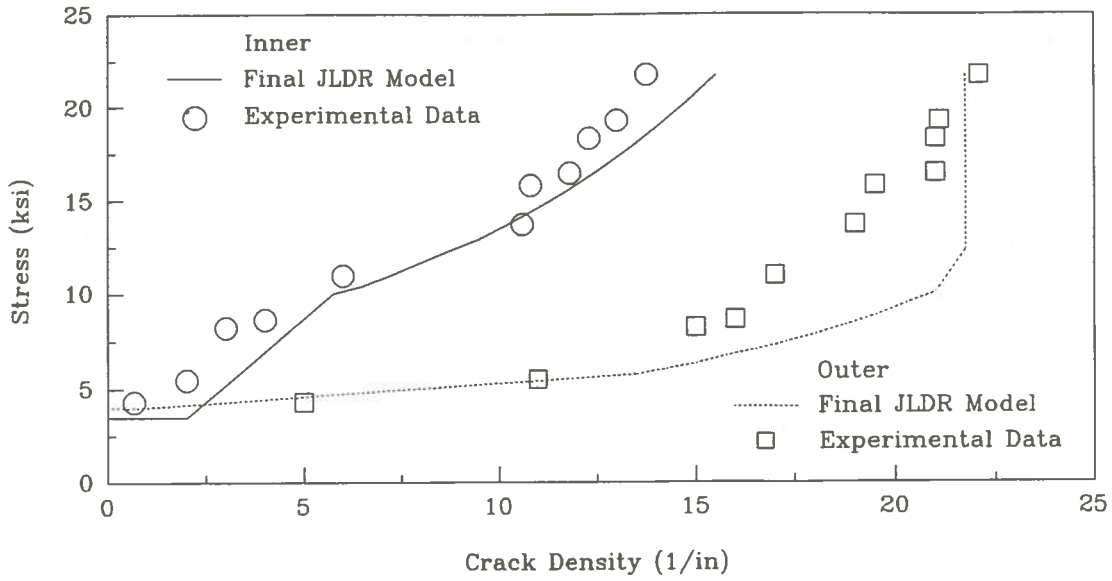

Figure 5.6. Comparison of Model Predictions with Experimental Data for Matrix Cracking in $[90/0/90_3]_s$ E-Glass Epoxy Under N_x

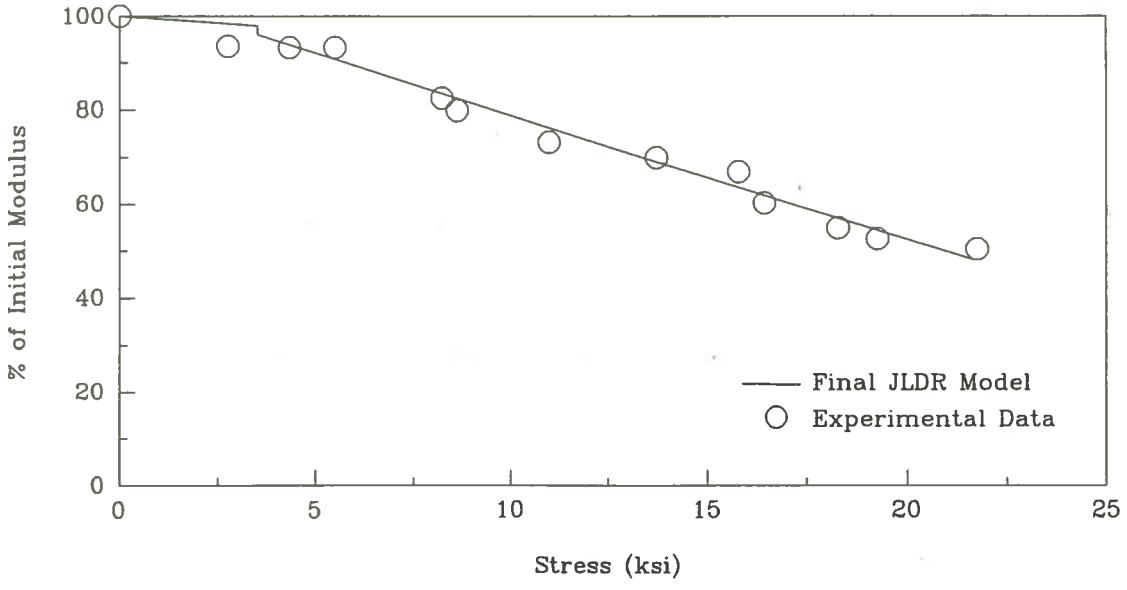

Figure 5.7. Comparison of Model Predictions with Experimental Data for Modulus Decrease in $[90/0/90_3]_s$ E-Glass Epoxy Under N_x

Cases 2 and 4: Loading Under N_y

The model was designed to predict progressive cracking in the 0° plies of the above laminates under loading in the y direction; however, the results were poor. This is most likely due to the additional complication of two different interlaminar shear stresses. As modeled, the outer and central layers of these laminates experience interlaminar shear stress due to cracking on one surface only. The interlaminar shear stress is zero on the outside surface and at the midplane of the laminate. The complex asymmetry of the through thickness boundary conditions on the 0° plies is a likely explanation for the problem. The experimental results are shown in Figures 5.8 through 5.11 for future reference, since this is an area to be explored in future work.

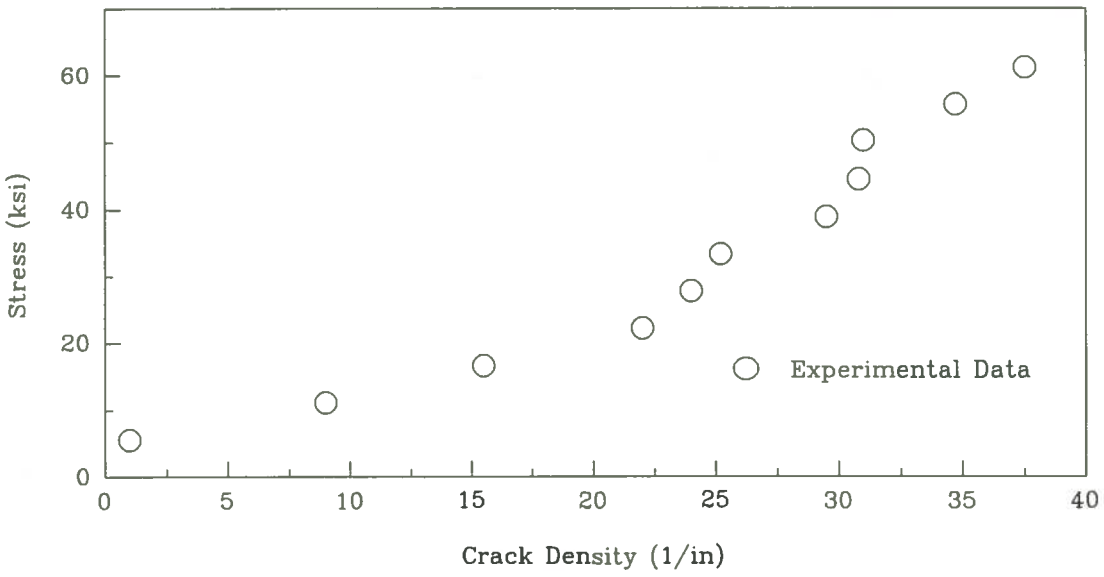

Figure 5.8. Experimental Results for Matrix Cracking in $[90_2/0_2/90]_s$ E-Glass Epoxy Under N_y

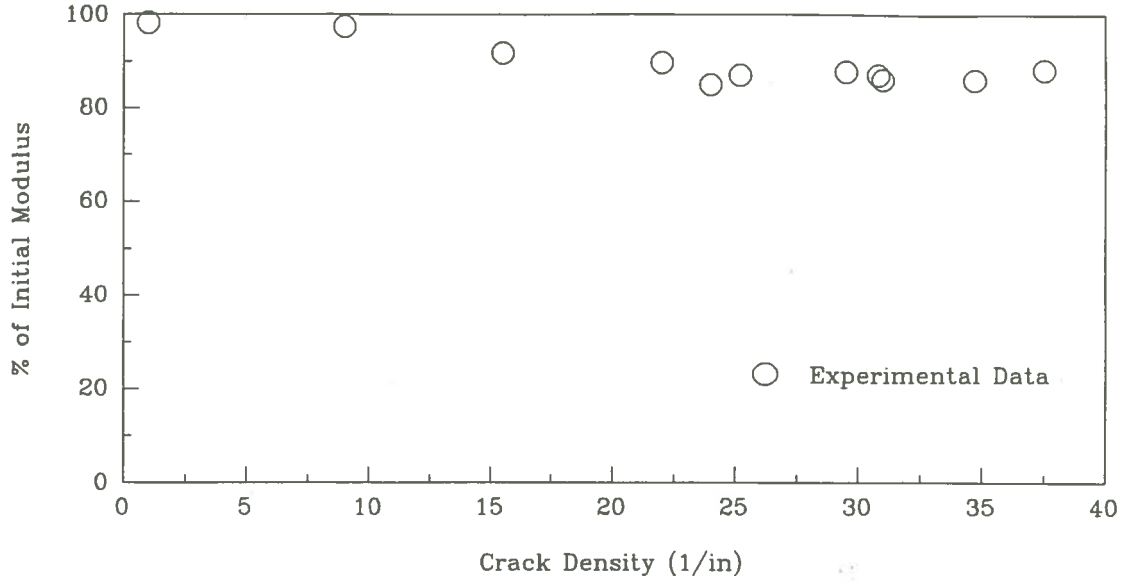

Figure 5.9. Experimental Results for Modulus Decrease in $[90_2/0_2/90]_s$ E-Glass Epoxy Under N_y

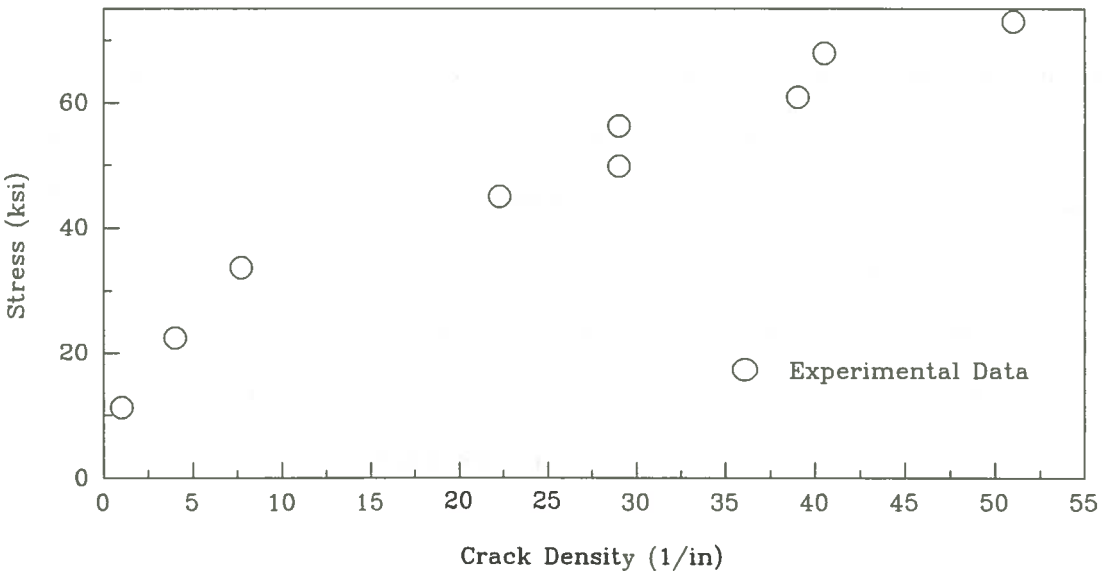

Figure 5.10. Experimental Results for Matrix Cracking in $[90/0/90_3]_s$ E-Glass Epoxy Under N_y

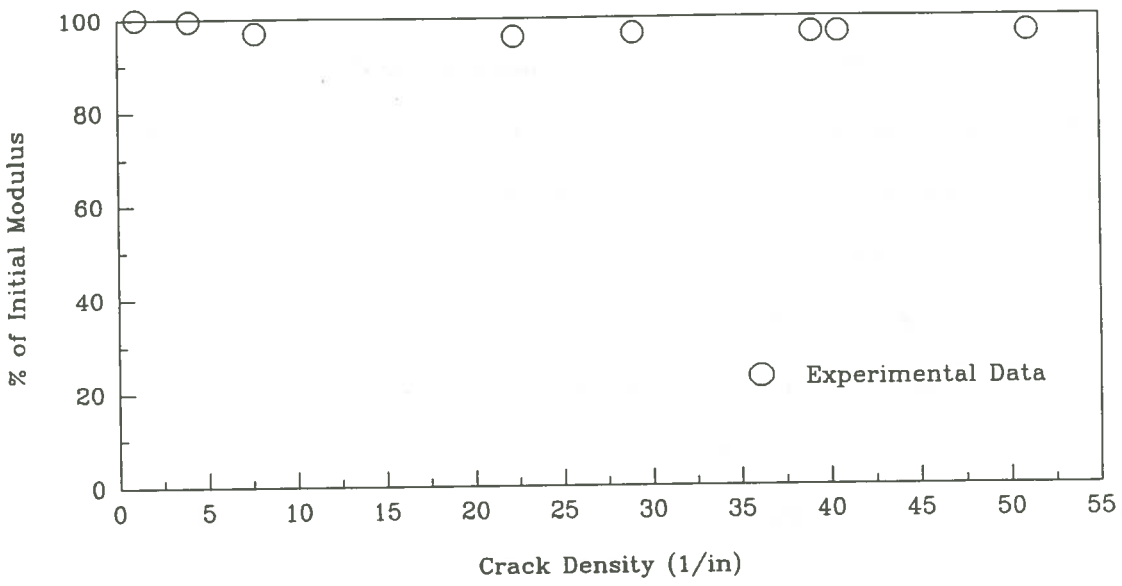

Figure 5.11. Experimental Results for Modulus Decrease in $[90/0/90_3]_s$ E-Glass Epoxy Under N_y

Error Analysis

In reducing the data, several sources of error were taken into account and steps were taken to minimize such error. The sources of experimental error included misalignment of the extensometer and strain gages, extensometer blade slip, strain gage transverse sensitivity, Wheatstone bridge nonlinearity, load cell error, measurement of specimen cross-section, measurement of the slope of the load versus strain plots, and measurement of the crack density from the photographs. The instrumental error was calculated and found to be negligible. The possible human error was limited by taking multiple measurements where possible.

CHAPTER 6

SUMMARY AND CONCLUSIONS

Two models have been developed which predict transverse matrix cracking in fiber-reinforced composites under static biaxial loading. They utilize fundamental fracture mechanics principles and include the effects of local delamination. The initial model predicts transverse matrix cracking in the 90° ply group of laminates of the type [$\pm\theta$/90m]s or [0n/90m]s under in-plane biaxial loading, including in-plane shear. The final model is written to predict transverse matrix cracking in all ply groups of laminates of the type [90n/0m/90p]s under in-plane biaxial loading but not including in-plane shear. The inputs to the model are material properties including critical strain energy release rate. In addition, the degree of delamination expected, in terms of delamination at one or both transverse matrix crack tips, must be supplied. The model gives stress and strain at the onset of transverse matrix cracking, a prediction of progressive cracking as load is increased, and the decrease in modulus as cracking occurs. It also shows the effect of transverse crack tip delamination on transverse matrix cracking. In addition, the laminate ultimate failure stress is predicted. Specific conclusions and contributions are summarized here.

1. The initial model is the only shear lag model developed to date to predict progressive matrix cracking under biaxial loading using fundamental fracture mechanics principles. In addition, it is the first shear lag model to incorporate the interaction between ply groups in terms of local delamination.

2. The final model is the only shear lag model, which is written for cracking in all ply groups of laminates with five ply groups. It is also written for in-plane biaxial loading and it also incorporates the effect of local delamination on matrix cracking.

3. Models were compared with experimental data for E-glass epoxy composites and excellent agreement was obtained in most cases. In cases where agreement was not perfect

throughout the progression of cracking, excellent agreement with the initial and final damage states was still obtained.

The current model lays the foundation for a more rigorous predictive method for transverse matrix cracking and local delamination in all ply groups of laminates with angle plies; however, additional work remains. First the problem with loading in the N_y direction (Cases 2 and 4) must be solved. Then, the model should be expanded to include transverse matrix cracking in angle plies. A more rigorous method for evaluating the effects of local delamination should be developed. A statistical method for predicting the site of each new crack would enhance accuracy of the model, particularly for the initial damage development, since crack spacing becomes more uniform as cracking progresses. Verification under biaxial loading should also be done.

The success of the model predictions and the experimental observations lead to some important generalizations. Small delaminations occur at transverse crack tips and they account for a decrease in the shear modulus of the laminate. Local delamination depends strongly on the thickness of the central 90° layer, and, when it occurs, it has a substantial effect on transverse matrix cracking. Final failure is accurately predicted by applying the maximum stress criterion to the uncracked plies, provided the samples fail in the gage section.

REFERENCES

[1] Kelly, A., "Interface Effects and the Work of Fracture of a Fibrous Composite," *Proceedings of the Royal Society of London*, **A319**, 1970, pp. 95-116.

[2] Visconti, I. Crivelli, "Design of Continuous Fiber Composite Structures" in *The Role of the Polymeric Matrix in the Processing and Structural Properties of Composite Materials* (ed. by James C. Seferis and Luigi Nicolais), New York, Plenum Press, 1983.

[3] Halpin, J. C., "The Role of the Matrix in Fibrous Composite Structures" in *The Role of the Polymeric Matrix in the Processing and Structural Properties of Composite Materials* (ed. by James C. Seferis and Luigi Nicolais), New York, Plenum Press, 1983.

[4] Billmeyer, Fred W., Jr., *Textbook of Polymer Science*, New York, John Wiley & Sons, 1984.

[5] Jansson, J. F. and H. Sundstrom, "Creep and Fracture Initiation in Fiber Reinforced Plastics" in *The Role of the Polymeric Matrix in the Processing and Structural Properties of Composite Materials* (ed. by James C. Seferis and Luigi Nicolais), New York, Plenum Press, 1983.

[6] Mallick, P. K., *Fiber Reinforced Composites*, New York, Marcel Dekker, Inc., 1988.

[7] Pavan, A., "Stress and Strength Analysis In and Around Composite Inclusions in Polymer Matrices," in *The Role of the Polymeric Matrix in the Processing and Structural Properties of Composite Materials* (ed. by James C. Seferis and Luigi Nicolais), New York, Plenum Press, 1983.

[8] Agarwal, Bhagwan D. and Lawrence J. Broutman, *Analysis and Performance of Fiber Composites*, New York, John Wiley & Sons, 1980.

[9] Theocaris, P. S., "Definition of Interphase in Composites," in *The Role of the Polymeric Matrix in the Processing and Structural Properties of Composite Materials* (ed. by James C. Seferis and Luigi Nicolais), New York, Plenum Press, 1983.

[10] Piggott, M. R., "Fibre Length-Strength Relationships and the Fracture of Composites," in *Advances in Fracture Research: Volume I* (ed. by D. Francois), Pergamon Press, 1982.

[11] Penn, L., F. Bystry, W. Karp, and S. Lee, "Aramid/Epoxy vs. Graphite/Epoxy: Origin of the Difference in Strength at the Interface," in *Molecular Characterization of Composite Interfaces* (ed. by Hatsuo Ishida and Ganesh Kumar), New York, Plenum Press, 1985.

[12] Allred, Ronald E., Edward W. Merrill, and David K. Roylance, "Surface Chemistry and Bonding of Plasma-Aminated Polyaramid Filaments," in *Molecular Characterization of Composite Interfaces* (ed. by Hatsuo Ishida and Ganesh Kumar), New York, Plenum Press, 1985.

[13] Saghizadeh, H. and C. K. H. Dharan, "Delamination Fracture Toughness of Graphite and Aramid Epoxy Composites", *Transactions of the ASME*, **108**, 1986, pp. 290-295.

[14] Kanninen Melvin F. and Carl H. Popelar, *Advanced Fracture Mechanics*, Oxford University Press, New York, 1985.

[15] Reddy, J. N., "On Computational Schemes for Global-Local Stress Analysis," *Computational Methods for Structural Mechanics and Mechanics*, ed. by W. Jefferson Stroud, Jerrold M. Housner, John A. Tanner, and Robert J. Hayduk, NASA Conference Publication 3034, NASA Langley, Hampton, VA, pp. 123-134, 1985.

[16] Lee, James D., "Three Dimensional Finite Element Analysis of Damage Accumulation in Composite Laminate," *Computers and Structures*, **15**, 1982, pp. 335-350.

[17] Sandhu, R. S., G. P. Sendeckyj, and R. L. Gallo, "Modeling of the Failure Process in Notched Laminates," in *Mechanics of Composite Materials*, ed. by Zvi Hashin and Carl T. Herakovich, New York, Pergamon Press, 1983, pp. 437-448.

[18] Murray, Y. D., "Theory and Verification of the Fiber Composite Damage Model Implemented in DYNA3D," DNA-TR-89-132, Defense Nuclear Agency, 1989.

[19] Tan, P.W. and C. A. Bigelow, "Analysis of Cracked Laminates with Holes Using the Boundary Force Method", *AIAA Journal*, **26**, 1988, pp. 1094-1099.

[20] Wang, S. S., "Fracture Mechanics for Delamination Problems in Composite Materials," *Journal of Composite Materials*, **17**, 1983, pp. 210-223.

[21] Bader, M. G., J. E. Bailey, P. T. Curtis, and A. Parvizi, "The Mechanisms of Initiation and Development of Damage in Multi-Axial Fibre-Reinforced Plastics Laminates," *Mechanical Behavior of Materials*, ICM3, ed. by K. J. Miller and R. F. Smith, Pergamon Press, New York, 1979, pp. 227-239.

[22] Bailey, J. E., P. T. Curtis, and A. Parvizi, "On the Transverse Cracking and Longitudinal Splitting Behaviour of Glass and Carbon Fibre Reinforced Epoxy Cross Ply Laminates and the Effect of Poisson and Thermally Generated Strain," *Proceedings of the Royal Society of London A*, **366**, 1979, pp. 599-623.

[23] Flaggs, D. L., "Prediction of Tensile Matrix Failure in Composite Laminates," *Journal of Composite Materials*, **19**, 1985, pp. 29-50.

[24] Nuismer, R. J., and S. C. Tan, "Constitutive Relations of a Cracked Composite Laminate," *Journal of Composite Materials*, **22**, 1988, pp. 306-321.

[25] Lee, J. W., and I. M. Daniel, "Progressive Transverse Cracking of Crossply Composite Laminates," *Journal of Composite Materials*, **24**, 1990, pp. 1225-1243.

[26] Laws, Norman, and George J. Dvorak, "Progressive Transverse Cracking in Composite Laminates," *Journal of Composite Materials*, **22**, 1988, pp. 900-916.

[27] Nuismer, R. J. and S. C. Tan, "The Role of Matrix Cracking in the Continuum Constitutive Behavior of a Damaged Composite Ply," in *Mechanics of Composite Materials*, ed. by Zvi Hashin and Carl T. Herakovich, New York, Pergamon Press, 1983, pp. 437-448.

[28] Daniel, I. M. and C. L. Tsai, "Analytical/Experimental Study of Cracking in Composite Laminates Under Biaxial Loading," *Composites Design, Manufacture, and Application*, ICCM/8, ed. by S. W. Tsai and G. S. Springer, SAMPE, Covina, CA, 1991, pp. 37:C1-C10.

[29] Tsai, C. L., I. M. Daniel, and J. W. Lee, "Progressive Matrix Cracking of Crossply Composite Laminates under Biaxial Loading," *Microcracking-Induced Damage in Composites*, AMD-Vol. 111, ed. by George J. Dvorak and Dimitris C. Lagoudas, American Society of Mechanical Engineers, New York, 1990, pp. 9-18.

[30] Soni, S. R. and N. J. Pagano, "Elastic Response of Composite Laminates," in *Mechanics of Composite Materials*, ed. by Zvi Hashin and Carl T. Herakovich, New York, Pergamon Press, 1983, pp. 437-448.

[31] Jones, R. M., *Mechanics of Composite Materials*, New York, McGraw-Hill, 1975.

[32] Wang, A. S. D., "Fracture Mechanics of Sublaminate Cracks in Composite Materials," *Composites Technology Review*, **6**, 1984, pp. 45-62.

[33] Swanson, in "Report on Workshop on Multiaxial Evaluation of Fiber Composite Materials," Volume I, ed. by Rembert F. Jones, Jr., David Taylor Research Center, Bethesda, MD, November, 1990.

[34] Wang, A. S. D., "Growth Mechanisms of Transverse Cracks and Ply Delamination in Composite Laminates," *Advances in Composite Materials, Proceedings of the Third International Conference on Composite Materials*, ed. by A. R. Bunsell, C. Bathias, A. Martrenchar, D. Menkes, and G. Verchery, Pergamon Press, 1980, pp. 170-185.

[35] Poursartip, Anoush, "The Characterization of Edge Delamination Growth in Laminates Under Fatigue Loading," *ASTM STP* 937, ed. by Norman J. Johnston, American Society for Testing and Materials, Philadelphia, 1987, pp. 222-241.

[36] O'Brien, T. K., "Characterization of Delamination Onset and Growth in a Composite Laminate", *Damage in Composite Materials, ASTM STP 775*, ed. by K. L. Reifsnider, American Society for Testing and Materials, Philadelphia, 1982, pp. 140-167.

[37] O'Brien, T. K., "Analysis of Local Delaminations and Their Influence on Composite Laminate Behavior," *Delamination and Debonding of Materials, ASTM STP 876*, ed. by W. S. Johnson, American Society for Testing and Materials, Philadelphia, 1985, pp. 282-297.

[38] Caslini, M., C. Zanotti, and T. K. O'Brien, "Fracture Mechanics of Matrix Cracking and Delamination in Glass/Epoxy Laminates," NASA-TM-89007, NASA Langley, Hampton, VA, 1986.

[39] Valisetty, R. Rao and Lawrence W. Rehfield, "A New Ply Model for Interlaminar Stress Analysis," *Delamination and Debonding of Materials, ASTM STP 876*, ed. by W. S. Johnson, American Society for Testing and Materials, Philadelphia, 1985, pp. 52-68.

[40] Armanios, Erian A., "Analysis of Interlaminar Fracture in Composites Under Combined Loading," NASA-CR-185055, NASA Langley, Hampton, VA, 1988.

[41] Talreja, Ramesh, "Stiffness Properties of Composite Laminates with Matrix Cracking and Interior Delamination," *Engineering Fracture Mechanics*, **25**, 1986, pp. 751-762.

[42] Yang, W. and J. P. Boehler, "Micromechanics Modelling of Anisotropic Damage in Cross-Ply Laminated," *International Journal of Solids and Structures*, **29**, 1992, pp. 1303-1328.

[43] Rosen, B. Walter, "Failure of Fiber Composite Laminates," in *Mechanics of Composite Materials*, ed. by Zvi Hashin and Carl T. Herakovich, New York, Pergamon Press, 1983, pp. 437-448.

[44] Phoenix, S. L. and E. M. Wu, "Statistics for the Time Dependent Failure of Kevlar-49/Epoxy Composites: Micromechanical Modeling and Data Interpretation," in *Mechanics of Composite Materials*, ed. by Zvi Hashin and Carl T. Herakovich, New York, Pergamon Press, 1983, pp. 437-448.

[45] Vinson, J. R. and R. L. Sierakowski, *The Behavior of Structures Composed of Composite Materials*, Boston, Martinus Nijhoff Publishers, 1987.

[46] Tsai, Stephen W. and Edward M. Wu, "A General Theory of Strength for Anisotropic Materials," *Journal of Composite Materials*, **5**, 1971, pp. 58-80.

[47] Feng, William W., "A Failure Criterion for Composite Materials,"*Journal of Composites Materials*, **25**, 1991, pp. 88-99.

[48] Daniel, I. M., "Experimental Mechanics of Composite Materials", in *Mechanics of Composite Materials, Recent Advances, Proceedings of IUTAM Symposium on Mechanics of Composite Materials*, New York, Pergamon Press, 1983, pp. 473-496.

[49] Swanson, S. R. and A. P.Christoforou, "Response of Quasi- Isotropic Carbon/Epoxy Laminates to Biaxial Stress", *Journal of Composite Materials*, 20, 1986, pp. 457-471.

[50] Zimmerman, Richard S. and Donald F. Adams, "Biaxial Loading Characterization of Dupont Rynite 545 E-Glass Reinforced Thermoplastic Resin", Report No. UWME-DR-301-105-1, Department of Mechanical Engineering, University of Wyoming, Laramie, Wyoming, 1983.

[51] Owen, M. J., "Biaxial Failure of GRP - Mechanisms, Modes and Theories", in *Composite Structures 2, Proceedings of Second International Conference on Composites Structures*, Marshall, I. H. (ed), Elsevier Applied Science Publisher, 1983, pp. 21-39.

[52] Zimmerman, Richard S., David E. Walrath, and Donald F. Adams, "Biaxial Loading Characterization, Failure Mode Study and Micromechanical Predictions and Correlations for Graphite/Aluminum Composites", Report No. UWME-DR-501-104-1, Department of Mechanical Engineering, University of Wyoming, Laramie, Wyoming, 1985.

[53] Runkle, D. B. and A. B. Doucet, "Effect of Stacking Sequence on Damage Accumulation," *Proceedings of the American Society for Composites 7th Technical Conference*, Lancaster, PA, Technomic, 1992, pp. 735-742.

APPENDIX A

DEVELOPMENT OF THE GOVERNING EQUATIONS FOR THE FINAL MODEL

In this appendix, the governing equations are derived. Table A.1. gives symbol definitions for reference, and the coordinate system is shown in Figure 3.5.

Table A.1. Symbols Used in the Model Equations

Symbol	Meaning
N_j	Integrated laminate force resultant in the j direction
A_{ij}	Element of extensional stiffness matrix defined by linear laminated plate theory
ϵ_j	Laminate midplane strain in j direction
N_j^T	Integrated laminate thermal force resultant in the j direction
Q_i	Integrated laminate through-thickness shear resultant in the i direction
γ_i	Laminate through-thickness shear strain
$n_j^{(k)}$	Integrated stress resultant in the j direction for the k^{th} ply group
$n_j^{t(k)}$	Integrated thermal force resultant for the k^{th} ply group
$q_i^{(k)}$	Integrated through-thickness shear resultant for the k^{th} ply group
U_i	Total displacement in the i direction
u_i	Laminate midplane displacement in the i direction
$\epsilon_j^{(k)}$	Midplane strain in k^{th} ply group
$\tau_{ij}^{(k)}$	Shear stress in the ij direction for the k^{th} ply group
τ_{ij}^{i}	Interlaminar shear stress between ply groups 1 and 2

Table A.1. Symbols Used in the Model Equations (continued)

τ_{ij}^{th}	Interlaminar shear stress between ply groups 2 and 3
$\Delta n_i^{(k)}$	Change in integrated force resultant due to cracking
H_k	Thickness of k^{th} ply group
L_t	Distance between two cracks in ply group 1
L_m	Distance between two cracks in ply group 2
L_b	Distance between two cracks in ply group 3

For a crossply laminate with no applied in-plane shear force, the constitutive relations can be written as:

$$\begin{Bmatrix} N_1 \\ N_2 \end{Bmatrix} = \begin{bmatrix} A_{11} & A_{12} \\ A_{12} & A_{22} \end{bmatrix} \begin{Bmatrix} \epsilon_1 \\ \epsilon_2 \end{Bmatrix} - \begin{Bmatrix} N_1^T \\ N_2^T \end{Bmatrix}$$

and (A.1)

$$\begin{Bmatrix} Q_4 \\ Q_5 \end{Bmatrix} = \begin{bmatrix} A_{44} & 0 \\ 0 & A_{55} \end{bmatrix} \begin{Bmatrix} \gamma_4 \\ \gamma_5 \end{Bmatrix}$$

Each lamina group or layer is treated as a Mindlin plate element. This approach was taken by Flaggs [23]. The constitutive relations for each ply group take the form:

$$\begin{Bmatrix} n_1 \\ n_2 \end{Bmatrix}^{(k)} = \begin{bmatrix} A_{11} & A_{12} \\ A_{12} & A_{22} \end{bmatrix}^{(k)} \begin{Bmatrix} \epsilon_1 \\ \epsilon_2 \end{Bmatrix}^{(k)} - \begin{Bmatrix} n_1 \\ n_2 \end{Bmatrix}^{(k)} \quad \text{(A.2)}$$

and

$$\begin{Bmatrix} q_4 \\ q_5 \end{Bmatrix}^{(k)} = \begin{bmatrix} A_{44} & 0 \\ 0 & A_{55} \end{bmatrix}^{(k)} \begin{Bmatrix} \gamma_4 \\ \gamma_5 \end{Bmatrix}^{(k)} \quad \text{(A.3)}$$

where the $A_{ij}^{(k)}$ are the elements of the stiffness matrices for each ply group. Note that for simplicity, we assume that in-plane shear is zero throughout the laminate. Tsai, Daniel and Lee [29] have made this assumption with little loss of accuracy. The displacements are assumed to be:

$$U_1=u_1(x_1,x_2)+z\gamma_5(x_1,x_2)$$

$$U_2=u_2(x_1,x_2)+z\gamma_4(x_1,x_2) \tag{A.4}$$

$$U_3=0$$

The strain in the laminate when the first crack occurs is given by:

$$\hat{\epsilon} = \begin{Bmatrix} \hat{\epsilon}_1 \\ \hat{\epsilon}_2 \end{Bmatrix} \tag{A.5}$$

For in-plane loading, the strain is equal in all lamina groups prior to cracking. The strain state for each lamina group before or after cracking is defined as follows:

$$\epsilon_1^{(k)} = \frac{\delta U_1^{(k)}}{\delta x_1} = \frac{\delta u_1^{(k)}}{\delta x_1} + z\frac{\delta \gamma_5^{(k)}}{\delta x_1}$$

$$\epsilon_2^{(k)} = \frac{\delta U_2^{(k)}}{\delta x_2} = \frac{\delta u_2^{(k)}}{\delta x_2} + z\frac{\delta \gamma_4^{(k)}}{\delta x_2} \tag{A.6}$$

$$\gamma_4^{(k)} = \frac{\delta U_2^{(k)}}{\delta z}$$

$$\gamma_5^{(k)} = \frac{\delta U_1^{(k)}}{\delta z}$$

The equations of equilibrium are:

$$\frac{\delta n_1^{(k)}}{\delta x_1} + \tau_{13}^{(k)}\left[\frac{Hk}{2}\right] - \tau_{13}^{(k)}\left[\frac{-Hk}{2}\right] = 0$$

$$\frac{\delta n_2^{(k)}}{\delta x_2} + \tau_{23}^{(k)}\left[\frac{Hk}{2}\right] - \tau_{23}^{(k)}\left[\frac{-Hk}{2}\right] = 0 \qquad \text{(A.7)}$$

$$q_5^{(k)} - \frac{Hk}{2}\left[\tau_{13}^{(k)}\left[\frac{Hk}{2}\right] + \tau_{13}^{(k)}\left[\frac{-Hk}{2}\right]\right] = 0$$

$$q_4^{(k)} - \frac{Hk}{2}\left[\tau_{23}^{(k)}\left[\frac{Hk}{2}\right] + \tau_{23}^{(k)}\left[\frac{-Hk}{2}\right]\right] = 0$$

Now, symmetry and the sample configuration dictate that the through-thickness shear stresses are zero at the laminate midplane and at the surface of the laminate. In addition, continuity implies that $\tau_{23}^{(k)}$ and $\tau_{13}^{(k)}$ are equal at the interfaces between lamina groups. The interlaminar shear stresses are called τ_{ij}^{th} between ply groups 1 and 2 and τ_{ij}^{i} between ply groups 2 and 3.

After cracking occurs in a ply group, the load taken by that ply group changes according to the following relation:

$$\begin{Bmatrix}\Delta n_1\\ \Delta n_2\end{Bmatrix}^{(k)} = \begin{Bmatrix}n_1\\ n_2\end{Bmatrix}^{(k)} - \begin{bmatrix}A_{11} & A_{12}\\ A_{12} & A_{22}\end{bmatrix}^{(k)} \begin{Bmatrix}\hat{\epsilon}_1\\ \hat{\epsilon}_2\end{Bmatrix}^{(k)} + \begin{Bmatrix}n_1^t\\ n_2^t\end{Bmatrix}^{(k)} \qquad \text{(A.8)}$$

$$= \begin{bmatrix}A_{11} & A_{12}\\ A_{12} & A_{22}\end{bmatrix}^{(k)} \begin{Bmatrix}\epsilon_1-\hat{\epsilon}_1\\ \epsilon_2-\hat{\epsilon}_2\end{Bmatrix}^{(k)}$$

Substituting equation (A.8) and the through thickness boundary conditions discussed above into equations (A.7), one finds for ply group one:

$$\frac{\delta}{\delta x_1}\left[\Delta n_1^{(1)} + A_{11}\,\hat{\epsilon}_1^{(1)} + A_{12}\,\hat{\epsilon}_2^{(1)} - n_1^{t(1)}\right] - \tau_{13}^{th} = 0$$

$$\frac{\delta}{\delta x_2}\left[\Delta n_2^{(1)} + A_{12}\,\hat{\epsilon}_1^{(1)} + A_{22}\,\hat{\epsilon}_2^{(1)} - n_2^{t(1)}\right] - \tau_{23}^{th} = 0 \qquad \text{(A.9)}$$

Differentiating with respect to x_1 or x_2 as appropriate gives:

$$\frac{\delta^2 \Delta n_1^{(1)}}{\delta x_1^{\,2}} - \frac{\delta \tau_{13}^{th}}{\delta x_1} = 0$$

$$\frac{\delta^2 \Delta n_2^{(1)}}{\delta x_2^{\,2}} - \frac{\delta \tau_{23}^{th}}{\delta x_2} = 0 \qquad \text{(A.10)}$$

Likewise, for group 2,

$$\frac{\delta^2 \Delta n_1^{(2)}}{\delta x_1^{\,2}} + \frac{\delta \tau_{13}^{th}}{\delta x_1} - \frac{\delta \tau_{13}^{i}}{\delta x_1} = 0$$

$$\frac{\delta^2 \Delta n_2^{(2)}}{\delta x_2^{\,2}} + \frac{\delta \tau_{23}^{th}}{\delta x_2} - \frac{\delta \tau_{23}^{i}}{\delta x_2} = 0 \qquad \text{(A.11)}$$

and, for group 3,

$$\frac{\delta^2 \Delta n_1^{(3)}}{\delta x_1^{\,2}} + \frac{\delta \tau_{13}^{i}}{\delta x_1} = 0$$

$$\frac{\delta^2 \Delta n_2^{(3)}}{\delta x_2^{\,2}} + \frac{\delta \tau_{23}^{i}}{\delta x_2} = 0 \qquad \text{(A.12)}$$

The basis of shear lag theory is that

$$\gamma = \frac{\delta u}{\delta z} \text{ and } \bar{\gamma} = \frac{\Delta u}{\Delta z} = \frac{\text{u(top of layer) - u(bottom of layer)}}{\text{thickness of layer}} \tag{A.13}$$

so,

$$\begin{aligned}
\bar{\gamma}_5^{(1)} &= \frac{1}{H_1}\left[u_1^{(1)}\left[\frac{H_1}{2}\right] - u_1^{(2)}\left[\frac{H_2}{2}\right]\right] \\
\bar{\gamma}_4^{(1)} &= \frac{1}{H_1}\left[u_2^{(1)}\left[\frac{H_1}{2}\right] - u_2^{(2)}\left[\frac{H_2}{2}\right]\right] \\
\bar{\gamma}_5^{(2)} &= \frac{1}{H_2}\left[u_1^{(1)}\left[\frac{-H_1}{2}\right] - u_1^{(2)}\left[\frac{-H_2}{2}\right]\right] \\
\bar{\gamma}_4^{(2)} &= \frac{1}{H_2}\left[u_2^{(1)}\left[\frac{-H_1}{2}\right] - u_2^{(2)}\left[\frac{-H_2}{2}\right]\right] \\
\bar{\gamma}_5^{(3)} &= \frac{1}{H_3}\left[u_1^{(2)}\left[\frac{-H_2}{2}\right] - u_1^{(3)}\left[\frac{-H_3}{2}\right]\right] \\
\bar{\gamma}_4^{(3)} &= \frac{1}{H_3}\left[u_2^{(2)}\left[\frac{-H_2}{2}\right] - u_2^{(3)}\left[\frac{-H_3}{2}\right]\right]
\end{aligned} \tag{A.14}$$

Substituting equations (A.14) into the moment equilibrium equations (A.7),

$$\begin{aligned}
&\frac{A_{55}^{(1)}}{H_1}\left[u_1^{(1)}\left[\frac{H_1}{2}\right] - u_1^{(2)}\left[\frac{H_2}{2}\right]\right] - \frac{H_1}{2}\tau_{13}^{th} = 0 \\
&\frac{A_{44}^{(1)}}{H_1}\left[u_2^{(1)}\left[\frac{H_1}{2}\right] - u_2^{(2)}\left[\frac{H_2}{2}\right]\right] - \frac{H_1}{2}\tau_{23}^{th} = 0
\end{aligned} \tag{A.15}$$

$$\frac{A_{55}^{(2)}}{H_2}\left[u_1^{(1)}\left[\frac{-H_1}{2}\right]-u_1^{(2)}\left[\frac{-H_2}{2}\right]\right]-\frac{H_2}{2}\left[\tau_{13}^{th}+\tau_{13}^{i}\right]=0 \qquad (A.16)$$

$$\frac{A_{44}^{(2)}}{H_2}\left[u_2^{(1)}\left[\frac{-H_1}{2}\right]-u_2^{(2)}\left[\frac{-H_2}{2}\right]\right]-\frac{H_2}{2}\left[\tau_{23}^{th}+\tau_{13}^{i}\right]=0$$

$$\frac{A_{55}^{(3)}}{H_3}\left[u_1^{(2)}\left[\frac{-H_2}{2}\right]-u_1^{(3)}\left[\frac{-H_3}{2}\right]\right]-\frac{H_3}{2}\tau_{13}^{i}=0 \qquad (A.17)$$

$$\frac{A_{44}^{(3)}}{H_3}\left[u_2^{(2)}\left[\frac{-H_2}{2}\right]-u_2^{(3)}\left[\frac{-H_3}{2}\right]\right]-\frac{H_3}{2}\tau_{23}^{i}=0$$

Differentiating (A.15)

$$\frac{A_{55}^{(1)}}{H_1}\left[\frac{\delta u_1^{(1)}}{\delta x_1}-\frac{\delta u_1^{(2)}}{\delta x_1}\right]-\frac{H_1}{2}\frac{\delta \tau_{13}^{th}}{\delta x_1}=0 \qquad (A.18)$$

$$\frac{A_{44}^{(1)}}{H_1}\left[\frac{\delta u_2^{(1)}}{\delta x_2}-\frac{\delta u_2^{(2)}}{\delta x_2}\right]-\frac{H_1}{2}\frac{\delta \tau_{23}^{th}}{\delta x_2}=0$$

The midplane lamina strains, $\bar{\epsilon}_i^{(k)}$ are determined at z=0, so equations (A.6) become:

$$\bar{\epsilon}_1^{(k)}=\frac{\delta u_1^{(k)}}{\delta x_1} \quad \text{and} \quad \bar{\epsilon}_2^{(k)}=\frac{\delta u_2^{(k)}}{\delta x_2} \qquad (A.19)$$

Equations (A.16) are then

$$\frac{A_{55}^{(1)}}{H_1}\left[\bar{\epsilon}_1^{(1)} + \frac{H_1}{2\,\delta x_1}\delta\gamma_5^{(1)}\;\bar{\epsilon}_1^{(2)} - \frac{H_2}{2\,\delta x_1}\delta\gamma_5^{(2)}\right] - \frac{H_1}{2\,\delta x_1}\delta\tau_{13}^{th} = 0$$

$$\frac{A_{44}^{(1)}}{H_1}\left[\bar{\epsilon}_2^{(1)} + \frac{H_1}{2\,\delta x_2}\delta\gamma_4^{(1)}\;\bar{\epsilon}_2^{(2)} - \frac{H_2}{2\,\delta x_2}\delta\gamma_4^{(2)}\right] - \frac{H_1}{2\,\delta x_2}\delta\tau_{23}^{th} = 0 \qquad \text{(A.20)}$$

Likewise, for ply group 2,

$$\frac{A_{55}^{(2)}}{H_2}\left[\bar{\epsilon}_1^{(1)} - \frac{H_1}{2\,\delta x_1}\delta\gamma_5^{(1)}\;\bar{\epsilon}_1^{(2)} + \frac{H_2}{2\,\delta x_1}\delta\gamma_5^{(2)}\right] - \frac{H_2}{2}\left[\frac{\delta\tau_{13}^{th}}{\delta x_1} + \frac{\delta\tau_{13}^{i}}{\delta x_1}\right] = 0$$

$$\frac{A_{44}^{(2)}}{H_2}\left[\bar{\epsilon}_2^{(1)} - \frac{H_1}{2\,\delta x_2}\delta\gamma_4^{(1)}\;\bar{\epsilon}_2^{(2)} + \frac{H_2}{2\,\delta x_2}\delta\gamma_4^{(2)}\right] - \frac{H_2}{2}\left[\frac{\delta\tau_{23}^{th}}{\delta x_2} + \frac{\delta\tau_{23}^{i}}{\delta x_2}\right] = 0 \qquad \text{(A.21)}$$

and, for ply group 3,

$$\frac{A_{55}^{(3)}}{H_3}\left[\bar{\epsilon}_1^{(2)} - \frac{H_2}{2\,\delta x_1}\delta\gamma_5^{(2)}\;\bar{\epsilon}_1^{(3)} + \frac{H_2}{2\,\delta x_1}\delta\gamma_5^{(3)}\right] - \frac{H_3}{2\,\delta x_1}\delta\tau_{13}^{i} = 0$$

$$\frac{A_{44}^{(3)}}{H_3}\left[\bar{\epsilon}_2^{(2)} - \frac{H_1}{2\,\delta x_2}\delta\gamma_4^{(2)}\;\bar{\epsilon}_2^{(3)} + \frac{H_2}{2\,\delta x_2}\delta\gamma_4^{(3)}\right] - \frac{H_3}{2\,\delta x_2}\delta\tau_{23}^{i} = 0 \qquad \text{(A.22)}$$

Substituting for γ_4 and γ_5,

$$\frac{A_{55}^{(1)}}{H_1}\left[\bar{\epsilon}_1^{(1)} + \frac{H_1^2}{4}F_{55}^{(1)}\frac{\delta\tau_{13}^{th}}{\delta x_1}\;\bar{\epsilon}_1^{(2)} - \frac{H_2^2}{4}F_{55}^{(2)}\left[\frac{\delta\tau_{13}^{th}}{\delta x_1} + \frac{\delta\tau_{13}^{i}}{\delta x_1}\right]\right] - \frac{H_1}{2\,\delta x_1}\delta\tau_{13}^{th} = 0$$

$$\frac{A_{44}^{(1)}}{H_1}\left[\bar{\epsilon}_2^{(1)} + \frac{H_1^2}{4}F_{44}^{(1)}\frac{\delta\tau_{23}^{th}}{\delta x_2}\;\bar{\epsilon}_2^{(2)} - \frac{H_2^2}{4}F_{44}^{(2)}\left[\frac{\delta\tau_{23}^{th}}{\delta x_2} + \frac{\delta\tau_{23}^{i}}{\delta x_2}\right]\right] - \frac{H_1}{2\,\delta x_2}\delta\tau_{23}^{th} = 0 \qquad \text{(A.23)}$$

$$\frac{A_{55}^{(2)}}{H_2}\left[\bar{\epsilon}_1^{(1)} - \frac{H_1^2}{4}F_{55}^{(1)}\frac{\delta\tau_{13}^{th}}{\delta x_1} - \bar{\epsilon}_1^{(2)} + \frac{H_2^2}{4}F_{55}^{(2)}\left[\frac{\delta\tau_{13}^{th}}{\delta x_1} + \frac{\delta\tau_{13}^{i}}{\delta x_1}\right]\right] - \frac{H_2}{2}\left[\frac{\delta\tau_{13}^{th}}{\delta x_1} + \frac{\delta\tau_{13}^{i}}{\delta x_1}\right] = 0$$

$$\frac{A_{44}^{(2)}}{H_2}\left[\bar{\epsilon}_2^{(1)} + \frac{H_1^2}{4}F_{44}^{(1)}\frac{\delta\tau_{23}^{th}}{\delta x_2} - \bar{\epsilon}_2^{(2)} - \frac{H_2^2}{4}F_{44}^{(2)}\left[\frac{\delta\tau_{23}^{th}}{\delta x_2} + \frac{\delta\tau_{23}^{i}}{\delta x_2}\right]\right] - \frac{H_2}{2}\left[\frac{\delta\tau_{23}^{th}}{\delta x_2} + \frac{\delta\tau_{23}^{i}}{\delta x_2}\right] = 0 \qquad \text{(A.24)}$$

$$\frac{A_{55}^{(3)}}{H_3}\left[\bar{\epsilon}_1^{(2)} - \frac{H_2^2}{4}F_{55}^{(2)}\left[\frac{\delta\tau_{13}^{th}}{\delta x_1} + \frac{\delta\tau_{13}^{i}}{\delta x_1}\right] - \bar{\epsilon}_1^{(3)} + \frac{H_3^2}{4}F_{55}^{(3)}\frac{\delta\tau_{13}^{i}}{\delta x_1}\right] - \frac{H_3}{2}\frac{\delta\tau_{13}^{i}}{\delta x_1} = 0$$

$$\frac{A_{44}^{(3)}}{H_3}\left[\bar{\epsilon}_2^{(2)} - \frac{H_2^2}{4}F_{44}^{(2)}\left[\frac{\delta\tau_{23}^{th}}{\delta x_2} + \frac{\delta\tau_{23}^{i}}{\delta x_2}\right] - \bar{\epsilon}_2^{(3)} + \frac{H_3^2}{4}F_{44}^{(3)}\frac{\delta\tau_{23}^{i}}{\delta x_2}\right] - \frac{H_3}{2}\frac{\delta\tau_{23}^{i}}{\delta x_2} = 0 \qquad \text{(A.25)}$$

When a crack occurs in a given ply group, it can no longer carry a load at that point. The other laminate ply groups must carry the load at the crack locations. Thus, we can give the boundary conditions on the crack faces:

Ply group 1 or top layer: At $x_2 = \pm \frac{L_t}{2}$, $n_2^{(1)} = 0$

Ply group 2 or middle layer: At $x_1 = \pm \frac{L_m}{2}$, $n_1^{(2)} = 0$ (A.26)

Ply group 1 or top layer: At $x_2 = \pm \frac{L_b}{2}$, $n_2^{(3)} = 0$

In other words,

$$\begin{aligned} n_2^{(2)} + n_2^{(3)} &= N_2 \text{ at } x_2 = \pm \frac{L_t}{2} \\ n_2^{(1)} + n_2^{(2)} &= N_2 \text{ at } x_2' = \pm \frac{L_b}{2} \\ n_1^{(1)} + n_1^{(3)} &= N_1 \text{ at } x_1 = \pm \frac{L_m}{2} \end{aligned} \tag{A.27}$$

which implies that

$$\begin{aligned} \Delta n_2^{(2)} + \Delta n_2^{(3)} &= n_2^{(1)} \text{ at } x_2 = \pm \frac{L_t}{2} \\ \Delta n_2^{(1)} + \Delta n_2^{(2)} &= n_2^{(3)} \text{ at } x_2' = \pm \frac{L_b}{2} \\ \Delta n_1^{(1)} + \Delta n_1^{(3)} &= n_1^{(2)} \text{ at } x_1 = \pm \frac{L_m}{2} \end{aligned} \tag{A.28}$$

Now, before cracking, a force balance on the 1z plane gives:

$$N_{2i} = n_{2i}^{(1)} + n_{2i}^{(2)} + n_{2i}^{(3)}$$

and on the 2z plane, (A.29)

$$N_{1i} = n_{1i}^{(1)} + n_{1i}^{(2)} + n_{1i}^{(3)}$$

After cracking,

$$N_{2f} = n_{2f}^{(1)} + n_{2f}^{(2)} + n_{2f}^{(3)}$$

and (A.30)

$$N_{1f} = n_{1f}^{(1)} + n_{1f}^{(2)} + n_{1f}^{(3)}$$

Before cracking occurs, equation (A.2) can be written as:

$$\{n\}^{(k)} = [A]^{(k)}\{\hat{\epsilon}\} - \{n^t\}^{(k)} \tag{A.31}$$

so, the initial integrated force resultants can be expressed as:

$$\{N\}_i = [A]^{(1)}\{\hat{\epsilon}\} - \{n^t\}^{(1)} + [A]^{(2)}\{\hat{\epsilon}\} - \{n^t\}^{(2)} + [A]^{(3)}\{\hat{\epsilon}\} - \{n^t\}^{(3)} \tag{A.32}$$

After cracking, using equation (A.8), the final integrated force resultants are:

$$\{N\}_f=[A]^{(1)}\{\hat{\epsilon}\} - \{n^t\}^{(1)} + \{\Delta n\}^{(1)} + [A]^{(2)}\{\hat{\epsilon}\} - \{n^t\}^{(2)} + \{\Delta n\}^{(2)} + \{n\}_f{}^{(3)} \tag{A.33}$$

Combining equations (A.32) and (A.33),

$$\{\Delta n\}^{(1)} + \{\Delta n\}^{(2)} = [A]^{(3)}\,[\{\hat{\epsilon}\} - \{\bar{\epsilon}\}^{(3)}] \tag{A.34}$$

$$\{\Delta n\}^{(2)} + \{\Delta n\}^{(3)} = [A]^{(1)}\,[\{\hat{\epsilon}\} - \{\bar{\epsilon}\}^{(1)}] \tag{A.35}$$

$$\{\Delta n\}^{(1)} + \{\Delta n\}^{(3)} = [A]^{(2)}\,[\{\hat{\epsilon}\} - \{\bar{\epsilon}\}^{(2)}] \tag{A.36}$$

Relations (A.34) through (A.36) can be summarized.

$$\{\bar{\epsilon}\}^{(k)} = \{\hat{\epsilon}\} + [F]^{(k)}\,\{\Delta n\}^{(k)} \tag{A.37}$$

where $[F]=[A]^{-1}$. This leads to the relations,

$$\begin{aligned}
\{\bar{\epsilon}\}^{(2)} - \{\bar{\epsilon}\}^{(3)} &= [F]^{(2)}\{\Delta n\}^{(2)} - [F]^{(3)}\,\{\Delta n\}^{(3)} \\
\{\bar{\epsilon}\}^{(1)} - \{\bar{\epsilon}\}^{(2)} &= [F]^{(1)}\{\Delta n\}^{(1)} - [F]^{(2)}\,\{\Delta n\}^{(2)} \\
\{\bar{\epsilon}\}^{(1)} - \{\bar{\epsilon}\}^{(3)} &= [F]^{(1)}\{\Delta n\}^{(1)} - [F]^{(3)}\,\{\Delta n\}^{(3)}
\end{aligned} \tag{A.38}$$

Finally, by substituting equation (A.38) and the equilibrium relations, equations (A.10-A.12), into equations (A.23-A.25), one obtains the governing equations for matrix cracking:

$$\frac{1}{H_1}\begin{bmatrix} A_{55} & 0 \\ 0 & A_{44} \end{bmatrix}^{(1)} \left(\begin{bmatrix} F_{11} & F_{12} \\ F_{12} & F_{22} \end{bmatrix}^{(1)} \begin{Bmatrix} \Delta n_1 \\ \Delta n_2 \end{Bmatrix}^{(1)} - \begin{bmatrix} F_{11} & F_{12} \\ F_{12} & F_{22} \end{bmatrix}^{(2)} \begin{Bmatrix} \Delta n_1 \\ \Delta n_2 \end{Bmatrix}^{(2)} \right.$$

$$\left. - \frac{H_2{}^2}{4}\begin{bmatrix} F_{55} & 0 \\ 0 & F_{44} \end{bmatrix}^{(2)} \begin{Bmatrix} 2\dfrac{\delta^2 \Delta n_1{}^{(1)}}{\delta x_1{}^2} + \dfrac{\delta^2 \Delta n_1{}^{(2)}}{\delta x_1{}^2} \\ 2\dfrac{\delta^2 \Delta n_2{}^{(1)}}{\delta x_2{}^2} + \dfrac{\delta^2 \Delta n_2{}^{(2)}}{\delta x_2{}^2} \end{Bmatrix} \right) - \frac{H_1}{4} \begin{Bmatrix} \dfrac{\delta^2 \Delta n_1{}^{(1)}}{\delta x_1{}^2} \\ \dfrac{\delta^2 \Delta n_2{}^{(1)}}{\delta x_2{}^2} \end{Bmatrix} = \begin{Bmatrix} 0 \\ 0 \end{Bmatrix} \tag{A.39}$$

$$\frac{1}{H_2}\begin{bmatrix} A_{55} & 0 \\ 0 & A_{44} \end{bmatrix}^{(2)} \left(\begin{bmatrix} F_{11} & F_{12} \\ F_{12} & F_{22} \end{bmatrix}^{(1)} \begin{Bmatrix} \Delta n_1 \\ \Delta n_2 \end{Bmatrix}^{(1)} - \begin{bmatrix} F_{11} & F_{12} \\ F_{12} & F_{22} \end{bmatrix}^{(2)} \begin{Bmatrix} \Delta n_1 \\ \Delta n_2 \end{Bmatrix}^{(2)} \right.$$

$$\left. - \frac{H_1^2}{4} \begin{bmatrix} F_{55} & 0 \\ 0 & F_{44} \end{bmatrix}^{(1)} \begin{Bmatrix} \dfrac{\delta^2 \Delta n_1^{(1)}}{\delta x_1^2} \\ \dfrac{\delta^2 \Delta n_2^{(1)}}{\delta x_2^2} \end{Bmatrix} \right) - \frac{H_2}{4} \begin{Bmatrix} 2\dfrac{\delta^2 \Delta n_1^{(1)}}{\delta x_1^2} + \dfrac{\delta^2 \Delta n_1^{(2)}}{\delta x_1^2} \\ 2\dfrac{\delta^2 \Delta n_2^{(1)}}{\delta x_2^2} + \dfrac{\delta^2 \Delta n_2^{(2)}}{\delta x_2^2} \end{Bmatrix} = \begin{Bmatrix} 0 \\ 0 \end{Bmatrix} \tag{A.40}$$

$$\frac{1}{H_3}\begin{bmatrix} A_{55} & 0 \\ 0 & A_{44} \end{bmatrix}^{(3)} \left(\begin{bmatrix} F_{11} & F_{12} \\ F_{12} & F_{22} \end{bmatrix}^{(2)} \begin{Bmatrix} \Delta n_1 \\ \Delta n_2 \end{Bmatrix}^{(2)} - \begin{bmatrix} F_{11} & F_{12} \\ F_{12} & F_{22} \end{bmatrix}^{(3)} \begin{Bmatrix} \Delta n_1 \\ \Delta n_2 \end{Bmatrix}^{(3)} \right.$$

$$\left. - \frac{H_2^2}{4} \begin{bmatrix} F_{55} & 0 \\ 0 & F_{44} \end{bmatrix}^{(2)} \begin{Bmatrix} \dfrac{\delta^2 \Delta n_1^{(1)}}{\delta x_1^2} - \dfrac{\delta^2 \Delta n_1^{(3)}}{\delta x_1^2} \\ \dfrac{\delta^2 \Delta n_2^{(1)}}{\delta x_2^2} - \dfrac{\delta^2 \Delta n_2^{(3)}}{\delta x_2^2} \end{Bmatrix} \right) - \frac{H_3}{4} \begin{Bmatrix} -\dfrac{\delta^2 \Delta n_1^{(3)}}{\delta x_1^2} \\ -\dfrac{\delta^2 \Delta n_2^{(3)}}{\delta x_2^2} \end{Bmatrix} = \begin{Bmatrix} 0 \\ 0 \end{Bmatrix} \tag{A.41}$$

APPENDIX B

SOLUTION OF THE GOVERNING EQUATIONS FOR THE FINAL MODEL

The governing equations found in Appendix A are:

$$\frac{1}{H_1}\cdot\begin{pmatrix}A_{55} & 0\\ 0 & A_{44}\end{pmatrix}^{(1)}\cdot\left[\begin{pmatrix}F_{11} & F_{12}\\ F_{12} & F_{22}\end{pmatrix}^{(1)}\cdot\begin{pmatrix}\Delta n_1\\ \Delta n_2\end{pmatrix}^{(1)}-\begin{pmatrix}F_{11} & F_{12}\\ F_{12} & F_{22}\end{pmatrix}^{(2)}\cdot\begin{pmatrix}\Delta n_1\\ \Delta n_2\end{pmatrix}^{(2)}\cdots\right]\cdots=\begin{pmatrix}0\\ 0\end{pmatrix}$$

$$+\frac{H_2^{\,2}}{-4}\cdot\begin{pmatrix}F_{55} & 0\\ 0 & F_{44}\end{pmatrix}^{(2)}\cdot\begin{bmatrix}2\cdot\left[\frac{d}{dx_1}\left[\frac{d}{dx_1}\Delta n_1^{(1)}\right]\right]+\frac{d}{dx_1}\left[\frac{d}{dx_1}n_1^{(2)}\right]\\ 2\cdot\left[\frac{d}{dx_2}\left[\frac{d}{dx_2}\Delta n_2^{(1)}\right]\right]+\frac{d}{dx_2}\left[\frac{d}{dx_2}n_2^{(2)}\right]\end{bmatrix}\qquad\text{(B.1)}$$

$$+\frac{-H_1}{4}\cdot\begin{bmatrix}\left[\frac{d}{dx_1}\left[\frac{d}{dx_1}\Delta n_1^{(1)}\right]\right]\\ \left[\left[\frac{d}{dx_2}\left[\frac{d}{dx_2}\Delta n_2^{(1)}\right]\right]\right]\end{bmatrix}$$

$$\frac{1}{H_2}\cdot\begin{pmatrix}A_{55} & 0\\ 0 & A_{44}\end{pmatrix}^{(2)}\cdot\left[\begin{pmatrix}F_{11} & F_{12}\\ F_{12} & F_{22}\end{pmatrix}^{(1)}\cdot\begin{pmatrix}\Delta n_1\\ \Delta n_2\end{pmatrix}^{(1)}-\begin{pmatrix}F_{11} & F_{12}\\ F_{12} & F_{22}\end{pmatrix}^{(2)}\cdot\begin{pmatrix}\Delta n_1\\ \Delta n_2\end{pmatrix}^{(2)}\cdots\right]\cdots=\begin{pmatrix}0\\ 0\end{pmatrix}$$

$$+\frac{H_1^{\,2}}{-4}\cdot\begin{pmatrix}F_{55} & 0\\ 0 & F_{44}\end{pmatrix}^{(1)}\cdot\begin{bmatrix}\left[\frac{d}{dx_1}\left[\frac{d}{dx_1}\Delta n_1^{(1)}\right]\right]\\ \left[\left[\frac{d}{dx_2}\left[\frac{d}{dx_2}\Delta n_2^{(1)}\right]\right]\right]\end{bmatrix}\qquad\text{(B.2)}$$

$$+\frac{-H_2}{4}\cdot\begin{bmatrix}\left[\frac{d}{dx_1}\frac{d}{dx_1}\Delta n_1^{(1)}\right]\cdot 2+\frac{d}{dx_1}\left[\frac{d}{dx_1}\Delta n_1^{(2)}\right]\\ \left[\frac{d}{dx_2}\left[\frac{d}{dx_2}\Delta n_2^{(1)}\right]\right]\cdot 2+\frac{d}{dx_2}\left[\frac{d}{dx_2}\Delta n_2^{(2)}\right]\end{bmatrix}$$

$$\frac{1}{H_3}\cdot\begin{pmatrix} A_{55} & 0 \\ 0 & A_{44}\end{pmatrix}^{(3)}\cdot\left[\begin{pmatrix} F_{11} & F_{12} \\ F_{12} & F_{22}\end{pmatrix}^{(2)}\cdot\begin{pmatrix}\Delta n_1 \\ \Delta n_2\end{pmatrix}^{(2)} - \begin{pmatrix} F_{11} & F_{12} \\ F_{12} & F_{22}\end{pmatrix}^{(3)}\cdot\begin{pmatrix}\Delta n_1 \\ \Delta n_2\end{pmatrix}^{(3)} \ldots\right] \ldots = \begin{pmatrix}0\\0\end{pmatrix}$$

$$+\frac{H_2{}^2}{-4}\cdot\begin{pmatrix} F_{55} & 0 \\ 0 & F_{44}\end{pmatrix}^{(2)}\cdot\begin{bmatrix}\frac{d}{dx_1}\left[\frac{d}{dx_1}\Delta n_1{}^{(1)}\right] - \frac{d}{dx_1}\left[\frac{d}{dx_1}\Delta n_1{}^{(3)}\right] \\ \frac{d}{dx_2}\left[\frac{d}{dx_2}\Delta n_2{}^{(1)}\right] - \frac{d}{dx_2}\left[\frac{d}{dx_2}\Delta n_2{}^{(3)}\right]\end{bmatrix}\Bigg] \qquad \text{(B.3)}$$

$$+\frac{H_3}{4}\cdot\left[\begin{bmatrix}\frac{d}{dx_1}\left[\frac{d}{dx_1}\Delta n_1{}^{(3)}\right] \\ \left[\frac{d}{dx_2}\left[\frac{d}{dx_2}\Delta n_2{}^{(3)}\right]\right]\end{bmatrix}\right]$$

The assumed forms of the change in load terms (nmi, nti, nbi) are deduced from the initial model and are given by:

$$\Delta n_1{}^{(1)} = A\cdot\frac{\cosh\left(\lambda m\cdot x_1\right)}{\cosh\left(\lambda m\cdot\frac{Lm}{2}\right)} + B\cdot\frac{\cosh\left(\lambda t\cdot x_2\right)}{\cosh\left(\lambda t\cdot\frac{Lt}{2}\right)} + C\cdot\frac{\cosh\left(\lambda b\cdot x_2\right)}{\cosh\left(\lambda b\cdot\frac{Lb}{2}\right)} \qquad \text{(B.4)}$$

$$\Delta n_2{}^{(1)} = D\cdot\frac{\cosh\left(\lambda t\cdot x_2\right)}{\cosh\left(\lambda t\cdot\frac{Lt}{2}\right)} + E\cdot\frac{\cosh\left(\lambda b\cdot x_2\right)}{\cosh\left(\lambda b\cdot\frac{Lb}{2}\right)} + F\cdot\frac{\cosh\left(\lambda m\cdot x_1\right)}{\cosh\left(\lambda m\cdot\frac{Lm}{2}\right)} \qquad \text{(B.5)}$$

$$\Delta n_1{}^{(2)} = G\cdot\frac{\cosh\left(\lambda m\cdot x_1\right)}{\cosh\left(\lambda m\cdot\frac{Lm}{2}\right)} + H\cdot\frac{\cosh\left(\lambda t\cdot x_2\right)}{\cosh\left(\lambda t\cdot\frac{Lt}{2}\right)} + I\cdot\frac{\cosh\left(\lambda b\cdot x_2\right)}{\cosh\left(\lambda b\cdot\frac{Lb}{2}\right)} \qquad \text{(B.6)}$$

$$\Delta n_2{}^{(2)} = J\cdot\frac{\cosh\left(\lambda t\cdot x_2\right)}{\cosh\left(\lambda t\cdot\frac{Lt}{2}\right)} + K\cdot\frac{\cosh\left(\lambda b\cdot x_2\right)}{\cosh\left(\lambda b\cdot\frac{Lb}{2}\right)} + L\cdot\frac{\cosh\left(\lambda m\cdot x_1\right)}{\cosh\left(\lambda m\cdot\frac{Lm}{2}\right)} \qquad \text{(B.7)}$$

$$\Delta n_1(3) = M\cdot\frac{\cosh\left(\lambda m\cdot x_1\right)}{\cosh\left(\lambda m\cdot\frac{Lm}{2}\right)} + N\cdot\frac{\cosh\left(\lambda t\cdot x_2\right)}{\cosh\left(\lambda t\cdot\frac{Lt}{2}\right)} + O\cdot\frac{\cosh\left(\lambda b\cdot x_2\right)}{\cosh\left(\lambda b\cdot\frac{Lb}{2}\right)} \qquad \text{(B.8)}$$

$$\Delta n_2{}^{(3)} = P\cdot\frac{\cosh\left(\lambda t\cdot x_2\right)}{\cosh\left(\lambda t\cdot\frac{Lt}{2}\right)} + Q\cdot\frac{\cosh\left(\lambda b\cdot x_2\right)}{\cosh\left(\lambda b\cdot\frac{Lb}{2}\right)} + R\cdot\frac{\cosh\left(\lambda m\cdot x_1\right)}{\cosh\left(\lambda m\cdot\frac{Lm}{2}\right)} \qquad \text{(B.9)}$$

where the Li are the distances between the cracks in the top, middle, and bottom layers, respectively.
The λi act as the shear lag parameters discussed earlier for the top, middle, and bottom layers, respectively.

For all x.1 and all x.2, , the total load carried by the laminate must equal the applied load; therefore,

$\Delta n_1^{(1)} + \Delta n_1^{(2)} + \Delta n_1^{(3)} = 0$ and $\Delta n_2^{(1)} + \Delta n_2^{(2)} + \Delta n_2^{(3)} = 0$

for all x_1 and x_2.

Thus,

$-I - C = O$ $-H - B = N$ $-G - A = M$ $-L - F = R$ $-E - K = Q$ $-J - D = P$

and

$$n_1^{(3)} = (-G - A)\cdot\frac{\cosh\left(\lambda m\cdot x_1\right)}{\cosh\left(\frac{1}{2}\cdot\lambda m\cdot Lm\right)} + (-H - B)\cdot\frac{\cosh\left(\lambda t\cdot x_2\right)}{\cosh\left(\frac{1}{2}\cdot\lambda t\cdot Lt\right)} + (-I - C)\cdot\frac{\cosh\left(\lambda b\cdot x_2\right)}{\cosh\left(\frac{1}{2}\cdot\lambda b\cdot Lb\right)} \qquad (B.10)$$

$$n_2^{(3)} = (-E - K)\cdot\frac{\cosh\left(\lambda b\cdot x_2\right)}{\cosh\left(\frac{1}{2}\cdot\lambda b\cdot Lb\right)} + (-J - D)\cdot\frac{\cosh\left(\lambda t\cdot x_2\right)}{\cosh\left(\frac{1}{2}\cdot\lambda t\cdot Lt\right)} + (-L - F)\cdot\frac{\cosh\left(\lambda m\cdot x_1\right)}{\cosh\left(\frac{1}{2}\cdot\lambda m\cdot Lm\right)} \qquad (B.11)$$

Substituting into the governing equations:

$$\frac{\left[-F_{12}^{(1)}\cdot E + F_{11}^{(2)}\cdot I + F_{12}^{(2)}\cdot K\right]}{F_{11}^{(1)}} = C \qquad (B.12) \qquad \frac{-\left[F_{12}^{(1)}\cdot D - F_{11}^{(2)}\cdot H - F_{12}^{(2)}\cdot J\right]}{F_{11}^{(1)}} = B \qquad (B.13)$$

$$\frac{2\cdot\sqrt{A_{55}^{(1)}}}{\sqrt{2\cdot A_{55}^{(1)}\cdot H_2^{\,2}\cdot F_{55}^{(2)}\cdot A + A_{55}^{(1)}\cdot H_2^{\,2}\cdot F_{55}^{(2)}\cdot G + H_1^{\,2}\cdot A}}\cdot\sqrt{\begin{matrix}-F_{11}^{(2)}\cdot G + F_{11}^{(1)}\cdot A\ldots \\ +F\cdot F_{12}^{(1)} - L\cdot F_{12}^{(2)}\end{matrix}} = \lambda m \qquad (B.14)$$

$$4\cdot\frac{A_{55}^{(1)}}{\left[2\cdot A_{55}^{(1)}\cdot H_2^{\,2}\cdot F_{55}^{(2)}\cdot A + A_{55}^{(1)}\cdot H_2^{\,2}\cdot F_{55}^{(2)}\cdot G + H_1^{\,2}\cdot A\right]}\cdot\begin{bmatrix}-F_{11}^{(2)}\cdot G + F_{11}^{(1)}\cdot A\ldots \\ +F\cdot F_{12}^{(1)} - F_{12}^{(2)}\cdot L\end{bmatrix} = \lambda m^2$$

Second equation

$$\frac{-\left[F_{22}^{(1)}\cdot F - F_{12}^{(2)}\cdot G - F_{22}^{(2)}\cdot L\right]}{F_{12}^{(1)}} = A \qquad (B.15)$$

$$\frac{2\cdot\sqrt{A_{44}^{(1)}}}{\sqrt{H_1^{2}\cdot E + A_{44}^{(1)}\cdot H_2^{2}\cdot F_{44}^{(2)}\cdot K + 2\cdot A_{44}^{(1)}\cdot H_2^{2}\cdot F_{44}^{(2)}\cdot E}}\cdot\sqrt{\begin{matrix}F_{22}^{(1)}\cdot E - F_{12}^{(2)}\cdot I \ldots \\ +\left(-F_{22}\right)^{(2)}\cdot K + C\cdot F_{12}^{(1)}\end{matrix}} = \lambda b \qquad \text{(B.16)}$$

$$\frac{4}{\left[H_1^{2}\cdot E + A_{44}^{(1)}\cdot H_2^{2}\cdot F_{44}^{(2)}\cdot K + 2\cdot A_{44}^{(1)}\cdot H_2^{2}\cdot F_{44}^{(2)}\cdot E\right]}\cdot A_{44}^{(1)}\cdot\left[\begin{matrix}F_{22}^{(1)}\cdot E - F_{12}^{(2)}\cdot I \ldots \\ +\left(-F_{22}\right)^{(2)}\cdot K + C\cdot F_{12}^{(1)}\end{matrix}\right] = \lambda b^{2}$$

$$\frac{2\cdot\sqrt{A_{44}^{(1)}}}{\sqrt{H_1^{2}\cdot D + 2\cdot A_{44}^{(1)}\cdot H_2^{2}\cdot F_{44}^{(2)}\cdot D + A_{44}^{(1)}\cdot H_2^{2}\cdot F_{44}^{(2)}\cdot J}}\cdot\sqrt{\begin{matrix}-F_{12}^{(2)}\cdot H - F_{22}^{(2)}\cdot J \ldots \\ +F_{22}^{(1)}\cdot D + F_{12}^{(1)}\cdot B\end{matrix}} = \lambda t \qquad \text{(B.17)}$$

$$-4\cdot\left[\begin{matrix}F_{12}^{(2)}\cdot H + F_{22}^{(2)}\cdot J \ldots \\ +\left(-F_{22}\right)^{(1)}\cdot D - F_{12}^{(1)}\cdot B\end{matrix}\right]\cdot\frac{A_{44}^{(1)}}{\left[H_1^{2}\cdot D + 2\cdot A_{44}^{(1)}\cdot H_2^{2}\cdot F_{44}^{(2)}\cdot D + A_{44}^{(1)}\cdot H_2^{2}\cdot F_{44}^{(2)}\cdot J\right]} = \lambda t^{2}$$

The third and fourth governing equations are the same as the first two.

Fifth equation

$$\frac{-\left[F_{12}^{(2)}\cdot K + F_{11}^{(2)}\cdot I + F_{11}^{(3)}\cdot I + F_{12}^{(3)}\cdot(E+K)\right]}{F_{11}} = C \qquad \text{(B.18)}$$

$$4\cdot A_{55}^{(3)}\cdot\frac{\left[F_{11}^{(2)}\cdot G + F_{12}^{(2)}\cdot L + F_{11}^{(3)}\cdot(G+A) + F_{12}^{(3)}\cdot(L+F)\right]}{\left[2\cdot A_{55}\cdot H_2^{2}\cdot F_{55}^{(2)}\cdot A + A_{55}\cdot H_2^{2}\cdot F_{55}^{(2)}\cdot G + H_3^{2}\cdot(G+A)\right]} = \lambda m^{2} \qquad \text{(B.19)}$$

$$\frac{-\left[F_{11}^{(2)}\cdot H + F_{12}^{(2)}\cdot J + F_{11}^{(3)}\cdot H + F_{12}^{(3)}\cdot(J+D)\right]}{F_{11}^{(3)}} = B \qquad \text{(B.20)}$$

Sixth equation

$$\frac{-\left[F_{12}^{(2)}\cdot G + F_{22}^{(2)}\cdot L + F_{22}^{(3)}\cdot(L+F) + F_{12}^{(3)}\cdot G\right]}{F_{12}^{(3)}} = A \qquad \text{(B.21)}$$

$$4 \cdot A_{44}^{(3)} \cdot \frac{\left[F_{22}^{(2)} \cdot K + F_{12}^{(2)} \cdot I + F_{22}^{(3)} \cdot (E+K) + F_{12}^{(3)} \cdot (I+C)\right]}{\left[2 \cdot A_{44}^{(3)} \cdot H_2^{\,2} \cdot F_{44}^{(2)} \cdot E + A_{44}^{(3)} \cdot H_2^{\,2} \cdot F_{44}^{(2)} \cdot K + H_3^{\,2} \cdot (E+K)\right]} = \lambda b^2 \qquad \text{(B.22)}$$

$$4 \cdot A_{44}^{(3)} \cdot \frac{\left[F_{22}^{(3)} \cdot (J+D) + F_{12}^{(3)} \cdot (H+B) + F_{12}^{(2)} \cdot H + F_{22}^{(2)} \cdot J\right]}{\left[2 \cdot A_{44}^{(3)} \cdot H_2^{\,2} \cdot F_{44}^{(2)} \cdot D + A_{44}^{(3)} \cdot H_2^{\,2} \cdot F_{44}^{(2)} \cdot J + H_3^{\,2} \cdot (J+D)\right]} = \lambda t^2 \qquad \text{(B.23)}$$

Now we can combine these expressions with those given above in order to find more of the constants, noting that, for example, $F_{11}F_{12}=F_{12}F_{11}$ for a crossply laminate of the type [90n/0m/90p]s only.

Summarizing the constants found,

$$a \cdot K = I \qquad \text{(B.23)}$$

$$a = \frac{\left[F_{12}^{(2)} \cdot F_{11}^{(3)} + F_{12}^{(2)} \cdot F_{11}^{(1)} + F_{12}^{(3)} \cdot F_{11}^{(1)}\right]}{\left[-F_{11}^{(2)} \cdot F_{11}^{(3)} - F_{11}^{(2)} \cdot F_{11}^{(1)} - F_{11}^{(1)} \cdot F_{11}^{(3)}\right]}$$

$$a \cdot J = H \qquad \text{(B.24)}$$

where

$$b = \frac{\left[F_{22}^{(2)} \cdot F_{12}^{(3)} + F_{22}^{(2)} \cdot F_{12}^{(1)} + F_{22}^{(3)} \cdot F_{12}^{(1)}\right]}{\left[-F_{12}^{(2)} \cdot F_{12}^{(3)} - F_{12}^{(2)} \cdot F_{12}^{(1)} - F_{12}^{(1)} \cdot F_{12}^{(3)}\right]}$$

$$b \cdot L = G \qquad \text{(B.25)}$$

$$\frac{\left[F_{11}^{(2)} \cdot a + F_{12}^{(2)}\right]}{F_{11}^{(1)}} \cdot K - F_{12}^{(1)} \cdot \frac{E}{F_{11}^{(1)}} = C \quad \text{or} \quad c \cdot K - F_{12}^{(1)} \cdot \frac{E}{F_{11}^{(1)}} = C \qquad \text{(B.26)}$$

$$\frac{\left[F_{11}^{(2)} \cdot a + F_{12}^{(2)}\right]}{F_{11}^{(1)}} \cdot J - F_{12}^{(1)} \cdot \frac{D}{F_{11}^{(1)}} = B \quad \text{or} \quad c \cdot J - F_{12}^{(1)} \cdot \frac{D}{F_{11}^{(1)}} = B \qquad \text{(B.27)}$$

$$\frac{\left[F_{12}^{(2)} \cdot b + F_{22}^{(2)}\right]}{F_{12}^{(1)}} \cdot L - F_{22}^{(1)} \cdot \frac{F}{F_{12}^{(1)}} = A \quad \text{or} \quad d \cdot L - F_{22}^{(1)} \cdot \frac{F}{F_{12}^{(1)}} = A \qquad \text{(B.28)}$$

where

$$c = \frac{\left[F_{11}^{(2)} \cdot a + F_{12}^{(2)}\right]}{F_{11}^{(1)}}$$

$$d = \frac{\left[F_{12}^{(2)} \cdot b + F_{22}^{(2)}\right]}{F_{12}^{(1)}}$$

$$\begin{aligned} e = & -(b+d)\cdot\left[-d\cdot F_{11}^{(1)} + F_{11}^{(2)}\cdot b + F_{12}^{(2)}\right]\cdot A_{55}^{(1)}\cdot H_3^{\,2} \ldots \\ & +(-b-2\cdot d)\cdot\left[\begin{matrix}(b+d)\cdot F_{11}^{(3)} + 2\cdot F_{11}^{(2)}\cdot b - d\cdot F_{11}^{(1)} \ldots \\ +2\cdot F_{12}^{(2)} + F_{12}^{(3)}\end{matrix}\right]\cdot A_{55}^{(3)}\cdot H_2^{\,2}\cdot A_{55}^{(1)}\cdot F_{55}^{(2)} \ldots \\ & +-d\cdot\left[(b+d)\cdot F_{11}^{(3)} + F_{12}^{(2)} + F_{11}^{(2)}\cdot b + F_{12}^{(3)}\right]\cdot A_{55}^{(3)}\cdot H_1^{\,2} \end{aligned}$$

$$\begin{aligned} f = & \left[F_{12}^{(1)}\cdot b + F_{22}^{(2)} + F_{12}^{(2)}\cdot b + \left[(-b-2\cdot d)\cdot F_{11}^{(1)} + F_{11}^{(2)}\cdot b + F_{12}^{(2)}\right]\cdot\frac{F_{22}^{(1)}}{F_{12}^{(1)}}\right]\cdot A_{55}^{(1)}\cdot H_3^{\,2} \ldots \\ & +\left[-F_{12}^{(3)}\cdot d + \left[(2\cdot d+b)\cdot F_{11}^{(3)} + F_{12}^{(2)} + F_{11}^{(2)}\cdot b + F_{12}^{(3)}\right]\cdot\frac{F_{22}^{(1)}}{F_{12}^{(1)}}\right]\cdot A_{55}^{(3)}\cdot H_1^{\,2} \ldots \\ & +\left[\begin{matrix}(2\cdot d+b)\cdot F_{12}^{(1)} + (-b-2\cdot d)\cdot F_{12}^{(3)} \ldots \\ +\left[\begin{matrix}4\cdot F_{11}^{(2)}\cdot b + (3\cdot b+4\cdot d)\cdot F_{11}^{(3)} \ldots \\ +2\cdot F_{12}^{(3)} + (-4\cdot d-b)\cdot F_{11}^{(1)} + 4\cdot F_{12}^{(2)}\end{matrix}\right]\cdot\frac{F_{22}^{(1)}}{F_{12}^{(1)}}\end{matrix}\right]\cdot A_{55}^{(1)}\cdot F_{55}^{(2)}\cdot H_2^{\,2}\cdot A_{55}^{(3)} \end{aligned}$$

$$\begin{aligned} g = & 2\cdot\left[\left[\frac{\left[-F_{11}^{(3)} + F_{11}^{(1)}\right]}{F_{12}^{(1)}}\cdot F_{22}^{(1)} + \left[-F_{12}^{(1)} + F_{12}^{(3)}\right]\right]\cdot H_2^{\,2}\cdot F_{55}^{(2)}\cdot A_{55}^{(1)}\cdot A_{55}^{(3)}\cdot\frac{F_{22}^{(1)}}{F_{12}^{(1)}} \ldots \right. \\ & +\left[\frac{\left(-F_{11}\right)^{(3)}}{F_{12}^{(1)}}\cdot H_1^{\,2}\cdot F_{22}^{(1)} + F_{12}^{(3)}\cdot H_1^{\,2}\right]\cdot A_{55}^{(3)}\cdot\frac{F_{22}^{(1)}}{F_{12}^{(1)}} \ldots \\ & \left.+\left[F_{11}^{(1)}\cdot\frac{F_{22}^{(1)}}{F_{12}^{(1)}} - F_{12}^{(1)}\right]\cdot A_{55}^{(1)}\cdot H_3^{\,2}\cdot\frac{F_{22}^{(1)}}{F_{12}^{(1)}}\right. \end{aligned}$$

$$\begin{aligned} h = & \left[-2\cdot F_{22}^{(2)} + F_{12}^{(1)}\cdot c - F_{22}^{(3)} - F_{12}^{(3)}\cdot c - a\cdot\left[2\cdot F_{12}^{(2)} + F_{12}^{(3)}\right]\right]\cdot A_{44}^{(1)}\cdot A_{44}^{(3)}\cdot H_2^{\,2}\cdot F_{44}^{(2)} \ldots \\ & +\left[F_{12}^{(1)}\cdot c - F_{22}^{(2)} - a\cdot F_{12}^{(2)}\right]\cdot A_{44}^{(1)}\cdot H_3^{\,2} \end{aligned}$$

$$p=\left[\begin{array}{l}-4\cdot F_{22}^{(2)}+2\cdot F_{12}^{(1)}\cdot c+F_{22}^{(1)}-2\cdot F_{12}^{(3)}\cdot c-3\cdot F_{22}^{(3)}\ldots\\ +-a\cdot\left[4\cdot F_{12}^{(2)}+2\cdot F_{12}^{(3)}\right]+\dfrac{\left[F_{12}^{(3)}-F_{12}^{(1)}\right]\cdot F_{12}^{(1)}}{F_{11}^{(1)}}\end{array}\right]\cdot A_{44}^{(1)}\cdot A_{44}^{(3)}\cdot H_2^{\,2}\cdot F_{44}^{(2)}\ldots$$
$$+\left[\left[-F_{22}^{(2)}-F_{12}^{(3)}\cdot c-F_{22}^{(3)}\right]\cdot H_1^{\,2}-a\cdot\left[F_{12}^{(3)}+F_{12}^{(2)}\right]\cdot H_1^{\,2}\right]\cdot A_{44}^{(3)}\ldots$$
$$+\left[\left[F_{12}^{(1)}\cdot c-F_{22}^{(2)}+F_{22}^{(1)}-\frac{\left[F_{12}^{(1)}\right]^2}{F_{11}^{(1)}}\right]\cdot H_3^{\,2}-a\cdot F_{12}^{(3)}\cdot H_3^{\,2}\right]\cdot A_{44}^{(1)}$$

$$q=\left[F_{22}^{(1)}-\frac{\left[F_{12}^{(1)}\right]^2}{F_{11}^{(1)}}\right]\cdot A_{44}^{(1)}\cdot H_3^{\,2}\ldots$$
$$+\left[\left[F_{22}^{(1)}-F_{22}^{(3)}\right]\cdot 2+\frac{\left[2\cdot F_{12}^{(3)}-2\cdot F_{12}^{(1)}\right]\cdot F_{12}^{(1)}}{F_{11}^{(1)}}\right]\cdot A_{44}^{(1)}\cdot A_{44}^{(3)}\cdot H_2^{\,2}\cdot F_{44}^{(2)}\ldots$$
$$+\left[-F_{22}^{(3)}+F_{12}\cdot\frac{F_{12}^{(1)}}{F_{11}^{(1)}}\right]\cdot A_{44}^{(3)}\cdot H_1^{\,2}$$

In addition,

$e\cdot L^2+f\cdot F\cdot L+g\cdot F^2=0$ $\qquad$ $q\cdot E^2+p\cdot K\cdot E+h\cdot K^2=0$ $\qquad$ $h\cdot J^2+p\cdot D\cdot J+q\cdot D^2=0$

so

$$\begin{bmatrix}\frac{1}{(2\cdot g)}\cdot\left(-f\cdot L+L\cdot\sqrt{f^2-4\cdot g\cdot e}\right)\\ \frac{1}{(2\cdot g)}\cdot\left(-f\cdot L-L\cdot\sqrt{f^2-4\cdot g\cdot e}\right)\end{bmatrix}=F \qquad \text{(B.29)}$$

$$\begin{bmatrix}\frac{1}{(2\cdot q)}\cdot\left(-p\cdot K+K\cdot\sqrt{p^2-4\cdot q\cdot h}\right)\\ \frac{1}{(2\cdot q)}\cdot\left(-p\cdot K-K\cdot\sqrt{p^2-4\cdot q\cdot h}\right)\end{bmatrix}=E \qquad \text{(B.30)}$$

$$\begin{bmatrix}\frac{1}{(2\cdot q)}\cdot\left(-p\cdot J+J\cdot\sqrt{p^2-4\cdot q\cdot h}\right)\\ \frac{1}{(2\cdot q)}\cdot\left(-p\cdot J-J\cdot\sqrt{p^2-4\cdot q\cdot h}\right)\end{bmatrix}=D \qquad \text{(B.31)}$$

Summarizing the constants found,

$$A=\left[d-F_{22}^{(1)}\cdot\frac{t}{F_{12}^{(1)}}\right]\cdot L \qquad B=ra\cdot J \qquad C=rb\cdot K \qquad D=sa\cdot J \qquad E=sb\cdot K \qquad (B.32)$$

$$F=t\cdot L \qquad G=b\cdot L \qquad H=a\cdot J \qquad I=a\cdot K$$

where

$$sa=\begin{bmatrix}\frac{1}{(2\cdot q)}\cdot\left(-p+\sqrt{p^2-4\cdot q\cdot h}\right)\\ \frac{1}{(2\cdot q)}\cdot\left(-p-\sqrt{p^2-4\cdot q\cdot h}\right)\end{bmatrix} \qquad sb=\begin{bmatrix}\frac{1}{(2\cdot q)}\cdot\left(-p+\sqrt{p^2-4\cdot q\cdot h}\right)\\ \frac{1}{(2\cdot q)}\cdot\left(-p-\sqrt{p^2-4\cdot q\cdot h}\right)\end{bmatrix} \qquad t=\begin{bmatrix}\frac{1}{(2\cdot g)}\cdot\left(-f+\sqrt{f^2-4\cdot g\cdot e}\right)\\ \frac{1}{(2\cdot g)}\cdot\left(-f-\sqrt{f^2-4\cdot g\cdot e}\right)\end{bmatrix}$$

$$ra=\left[c-\frac{F_{12}^{(1)}}{F_{11}^{(1)}}\cdot sa\right] \qquad rb=\left[c-\frac{F_{12}^{(1)}}{F_{11}^{(1)}}\cdot sb\right]$$

We don't know apriori which values the above parameters will take for a given laminate. It turns out that, indeed, they must be different for different laminates. For the laminates discussed in this work,

$$t=\frac{1}{(2\cdot g)}\cdot\left(-f+\sqrt{f^2-4\cdot g\cdot e}\right)$$

and the values taken by sa and sb have opposite signs preceding the square root term for each laminate.

Thus, for the $[90/0/90_3]_s$ laminate,

$$sa=\frac{1}{(2\cdot q)}\cdot\left(-p-\sqrt{p^2-4\cdot q\cdot h}\right) \quad \text{and} \quad sb=\frac{1}{(2\cdot q)}\cdot\left(-p+\sqrt{p^2-4\cdot q\cdot h}\right)$$

and for the $[90_2/0_2/90]_s$ laminate,

$$sa=\frac{1}{(2\cdot q)}\cdot\left(-p+\sqrt{p^2-4\cdot q\cdot h}\right) \quad \text{and} \quad sb=\frac{1}{(2\cdot q)}\cdot\left(-p-\sqrt{p^2-4\cdot q\cdot h}\right)$$

Now the boundary conditions must be satisfied. They are:

$$\Delta n_1^{(1)}+\Delta n_1^{(3)}=N_{1i}^{(2)} \quad \text{at} \quad x_1=\frac{Lm}{2} \qquad (B.33)$$

$$\Delta n_2^{(3)}+\Delta n_2^{(2)}=N_{2i}^{(1)} \quad \text{at} \quad x_2=\frac{Lt}{2} \qquad (B.34)$$

$$\Delta n_2^{(1)}+\Delta n_2^{(2)}=N_{2i}^{(3)} \quad \text{at} \quad x_2=\frac{Lb}{2} \qquad (B.35)$$

where $N_{1i}^{(2)}$, $N_{2i}^{(1)}$, and $N_{2i}^{(3)}$ are the initial loads taken by the three layers in the 1 and 2 directions. They are found from the constitutive relations given in Appendix A. These cannot be satisfied everywhere, so each disturbance to the change in load in each layer is averaged in order to get an average solution to the boundary conditions.

$$\left(-2\cdot\frac{\tanh\left(\lambda t\cdot\frac{Lt}{2}\right)}{Lt}\cdot H - 1\cdot G - 2\cdot\frac{\tanh\left(\lambda b\cdot\frac{Lb}{2}\right)}{Lb}\cdot I\right) = N_{1i}^{(2)} \tag{B.36}$$

$$-D\cdot\frac{\cosh\left(\lambda t\cdot\frac{Lt}{2}\right)}{\cosh\left(\frac{1}{2}\cdot\lambda t\cdot Lt\right)} - E\cdot\frac{2\cdot\tanh\left(\lambda b\cdot\frac{Lb}{2}\right)}{Lb} - \frac{F\cdot 2\cdot\tanh\left(\lambda m\cdot\frac{Lm}{2}\right)}{Lm} = N_{2i}^{(1)} \tag{B.37}$$

$$D\cdot\frac{2\cdot\tanh\left(\lambda t\cdot\frac{Lt}{2}\right)}{Lt} + E\cdot\frac{\cosh\left(\lambda b\cdot\frac{Lb}{2}\right)}{\cosh\left(\frac{1}{2}\cdot\lambda b\cdot Lb\right)} + \frac{2\cdot\tanh\left(\lambda m\cdot\frac{Lm}{2}\right)}{Lm}\cdot F \ldots = N_{2i}^{(3)} \tag{B.38}$$

$$+J\cdot\frac{2\cdot\tanh\left(\lambda t\cdot\frac{Lt}{2}\right)}{Lt} + K\cdot\frac{\cosh\left(\lambda b\cdot\frac{Lb}{2}\right)}{\cosh\left(\frac{1}{2}\cdot\lambda b\cdot Lb\right)} + L\cdot\frac{2\cdot\tanh\left(\lambda m\cdot\frac{Lm}{2}\right)}{Lm}$$

Solving the first BC (equation 33) for L,

$$L = \frac{\left[-2\cdot\frac{\tanh\left(\frac{1}{2}\cdot\lambda t\cdot Lt\right)}{Lt}\cdot a\cdot J - 2\cdot\frac{\tanh\left(\frac{1}{2}\cdot\lambda b\cdot Lb\right)}{Lb}\cdot a\cdot K - N_{1i}^{(2)}\right]}{b}$$

Substituting for L in the third BC (equation 35) and solving for K

$$K = \frac{\left[N_{2i}^{(3)} + 2\cdot\frac{(t+1)}{b}\cdot N_{1i}^{(2)}\cdot\frac{\tanh\left(\frac{1}{2}\cdot\lambda m\cdot Lm\right)}{Lm}\right]}{\left[1 + sb - 4\cdot a\cdot\frac{(t+1)}{(b\cdot Lb)}\cdot\tanh\left(\frac{1}{2}\cdot\lambda b\cdot Lb\right)\cdot\frac{\tanh\left(\frac{1}{2}\cdot\lambda m\cdot Lm\right)}{Lm}\right]} \ldots + \frac{\left[2\cdot\left[2\cdot a\cdot\frac{(t+1)}{(b\cdot Lm)}\right]\cdot\tanh\left(\frac{1}{2}\cdot\lambda m\cdot Lm\right) + 2\cdot(-sa-1)\right]}{\left[1 + sb - 4\cdot a\cdot\frac{(t+1)}{(b\cdot Lb)}\cdot\tanh\left(\frac{1}{2}\cdot\lambda b\cdot Lb\right)\cdot\frac{\tanh\left(\frac{1}{2}\cdot\lambda m\cdot Lm\right)}{Lm}\right]}\cdot\tanh\left(\frac{1}{2}\cdot\lambda t\cdot Lt\right)\cdot\frac{J}{Lt} \tag{B.39}$$

Substituting for L and K in the second BC (equation 34) (B.40)

$$J = \frac{N_{2i}^{(1)}\cdot\left(cc - ee\cdot\frac{\tanh\left(\frac{1}{2}\cdot\lambda b\cdot Lb\right)}{Lb}\cdot\frac{\tanh\left(\frac{1}{2}\cdot\lambda m\cdot Lm\right)}{Lm}\right) - \left[\begin{array}{l}-2\cdot sb \ldots \\ +ff\cdot\frac{\tanh\left(\frac{1}{2}\cdot\lambda m\cdot Lm\right)}{Lm}\end{array}\right]\cdot\frac{\tanh\left(\frac{1}{2}\cdot\lambda b\cdot Lb\right)}{Lb}\cdot N_{2i}^{(3)} \ldots + \left[\begin{array}{l}\left(bb + aa\cdot\frac{\tanh\left(\frac{1}{2}\cdot\lambda m\cdot Lm\right)}{Lm}\right)\cdot\frac{\tanh\left(\frac{1}{2}\cdot\lambda b\cdot Lb\right)}{(Lb)} \ldots \\ +dd\cdot\left(cc - ee\cdot\frac{\tanh\left(\frac{1}{2}\cdot\lambda b\cdot Lb\right)}{Lb}\cdot\frac{\tanh\left(\frac{1}{2}\cdot\lambda m\cdot Lm\right)}{Lm}\right)\end{array}\right]\left[\begin{array}{l}-1\cdot\frac{\tanh\left(\frac{1}{2}\cdot\lambda m\cdot Lm\right)}{Lm}\cdot N_{1i}^{(2)}\end{array}\right]}{\left[\begin{array}{l}-sa\cdot\left(cc - ee\cdot\frac{\tanh\left(\frac{1}{2}\cdot\lambda b\cdot Lb\right)}{Lb}\cdot\frac{\tanh\left(\frac{1}{2}\cdot\lambda m\cdot Lm\right)}{Lm}\right) \ldots \\ +\left[\begin{array}{l}\left[2\cdot\frac{gg}{(Lb\cdot Lm)}\cdot\tanh\left(\frac{1}{2}\cdot\lambda m\cdot Lm\right) \ldots\right]\cdot\tanh\left(\frac{1}{2}\cdot\lambda b\cdot Lb\right)\cdot\left(ee\cdot\frac{\tanh\left(\frac{1}{2}\cdot\lambda m\cdot Lm\right)}{Lm} - 2\cdot hh\right) \ldots\end{array}\right]\cdot\frac{\tanh\left(\frac{1}{2}\cdot\lambda t\cdot Lt\right)}{Lt} \\ \left[\begin{array}{l}+-2\cdot\frac{sb}{Lb} \\ +ff\cdot\frac{\tanh\left(\frac{1}{2}\cdot\lambda m\cdot Lm\right)}{Lm}\cdot\left(cc - ee\cdot\frac{\tanh\left(\frac{1}{2}\cdot\lambda b\cdot Lb\right)}{Lb}\cdot\frac{\tanh\left(\frac{1}{2}\cdot\lambda m\cdot Lm\right)}{Lm}\right)\end{array}\right]\end{array}\right]}$$

where

$$aa=4\cdot dd\cdot(t+1)\cdot\frac{a}{b} \qquad bb=-4\cdot sb\cdot\frac{t+1}{b} \qquad cc=1+sb \qquad dd=2\cdot\frac{t}{b}$$

$$ee=4\cdot a\cdot\frac{(t+1)}{b} \qquad ff=2\cdot a\cdot dd \qquad gg=dd\cdot a \qquad hh=sa+1$$

and the other constants are given in terms of J, K, and L above. With the crack density terms,

$$J=\frac{\begin{bmatrix} N_{2i}^{(1)}\cdot\left[cc-ee\cdot\left(\tanh\left(\frac{1}{2}\cdot\lambda b\cdot Lb\right)\cdot\beta b\right)\cdot\tanh\left(\frac{1}{2}\cdot\lambda m\cdot Lm\right)\cdot\beta m\right]\ \ldots \\ +\left(-2\cdot sb+ff\cdot\tanh\left(\frac{1}{2}\cdot\lambda m\cdot Lm\right)\cdot\beta m\right)\cdot-1\cdot\tanh\left(\frac{1}{2}\cdot\lambda b\cdot Lb\right)\cdot\beta b\cdot N_{2i}^{(3)}\ \ldots \\ +\begin{bmatrix}\left(bb+aa\cdot\tanh\left(\frac{1}{2}\cdot\lambda m\cdot Lm\right)\cdot\beta m\right)\cdot\tanh\left(\frac{1}{2}\cdot\lambda b\cdot Lb\right)\cdot\beta b\ \ldots \\ +dd\cdot\left(cc-ee\cdot\tanh\left(\frac{1}{2}\cdot\lambda b\cdot Lb\right)\cdot\tanh\left(\frac{1}{2}\cdot\lambda m\cdot Lm\right)\cdot\beta b\cdot\beta m\right)\end{bmatrix}\cdot-1\cdot\tanh\left(\frac{1}{2}\cdot\lambda m\cdot Lm\right)\cdot\beta m\cdot N_{1i}^{(2)}\end{bmatrix}}{\begin{bmatrix}-sa\cdot\left(cc-ee\cdot\tanh\left(\frac{1}{2}\cdot\lambda b\cdot Lb\right)\cdot\tanh\left(\frac{1}{2}\cdot\lambda m\cdot Lm\right)\cdot\beta b\cdot\beta m\right)\ \ldots \\ +\begin{bmatrix}\left(\begin{matrix}2\cdot gg\cdot\tanh\left(\frac{1}{2}\cdot\lambda m\cdot Lm\right)\cdot\beta m\ \ldots \\ +-2\cdot sb\end{matrix}\right)\cdot\tanh\left(\frac{1}{2}\cdot\lambda b\cdot Lb\right)\cdot\beta b\cdot\left(\begin{matrix}ee\cdot\tanh\left(\frac{1}{2}\cdot\lambda m\cdot Lm\right)\cdot\beta m\ \ldots \\ +-2\cdot hh\end{matrix}\right)\ \ldots\end{bmatrix}\cdot\tanh\left(\frac{1}{2}\cdot\lambda t\cdot Lt\right)\cdot\beta t \\ \begin{bmatrix}+ff\cdot\tanh\left(\frac{1}{2}\cdot\lambda m\cdot Lm\right)\cdot\beta m\cdot\left(cc-ee\cdot\tanh\left(\frac{1}{2}\cdot\lambda b\cdot Lb\right)\cdot\tanh\left(\frac{1}{2}\cdot\lambda m\cdot Lm\right)\cdot\beta m\cdot\beta b\right)\end{bmatrix}\end{bmatrix}}$$

where $\beta i=\frac{1}{Li}$

$$K=\frac{\left[N_{2i}^{(3)}+2\cdot\frac{(t+1)}{b}\cdot N_{1i}^{(2)}\cdot\tanh\left(\frac{1}{2}\cdot\lambda m\cdot Lm\right)\cdot\beta m\right]}{\left[1+sb-4\cdot a\cdot\frac{(t+1)}{(b)}\cdot\tanh\left(\frac{1}{2}\cdot\lambda b\cdot Lb\right)\cdot\tanh\left(\frac{1}{2}\cdot\lambda m\cdot Lm\right)\cdot\beta m\cdot\beta b\right]}\ \ldots$$
$$+\frac{\left[4\cdot a\cdot\frac{(t+1)}{(b)}\cdot\tanh\left(\frac{1}{2}\cdot\lambda m\cdot Lm\right)\cdot\beta m+2\cdot(-sa-1)\right]}{\left[1+sb-4\cdot a\cdot\frac{(t+1)}{(b)}\cdot\tanh\left(\frac{1}{2}\cdot\lambda b\cdot Lb\right)\cdot\tanh\left(\frac{1}{2}\cdot\lambda m\cdot Lm\right)\cdot\beta m\cdot\beta b\right]}\cdot\tanh\left(\frac{1}{2}\cdot\lambda t\cdot Lt\right)\cdot\beta t\cdot J$$

$$L=\frac{\left[-2\cdot\tanh\left(\frac{1}{2}\cdot\lambda t\cdot Lt\right)\cdot\beta t\cdot a\cdot J-2\cdot\tanh\left(\frac{1}{2}\cdot\lambda b\cdot Lb\right)\cdot\beta b\cdot a\cdot K-N_{1i}^{(2)}\right]}{b}$$

The constants can be found for the case of initial cracking. In order to simplify for the case of zero cracks, all the tanh terms are approximately equal to one for Li large.

$$J := \frac{N_{2i}^{(1)} \cdot (cc - ee \cdot \beta b \cdot \beta m) - (-2 \cdot sb + ff \cdot \beta m) \cdot \beta b \cdot N_{2i}^{(3)} \ldots + ((bb + aa \cdot \beta m) \cdot \beta b + dd \cdot (cc - ee \cdot \beta b \cdot \beta m)) \cdot -1 \cdot \beta m \cdot N_{1i}^{(2)}}{(-sa \cdot (cc - ee \cdot \beta b \cdot \beta m) + ((2 \cdot gg \cdot \beta m - 2 \cdot sb) \cdot \beta b \cdot (ee \cdot \beta m - 2 \cdot hh) + ff \cdot \beta m \cdot (cc - ee \cdot \beta m \cdot \beta b)) \cdot \beta t)}$$

$$K := \frac{\left[N_{2i}^{(3)} + 2 \cdot \frac{(t+1)}{b} \cdot N_{1i}^{(2)} \cdot \beta m\right]}{\left[1 + sb - 4 \cdot a \cdot \frac{(t+1)}{(b)} \cdot \beta m \cdot \beta b\right]} + \frac{4 \cdot a \cdot \frac{(t+1)}{(b)} \cdot \beta m + 2 \cdot (-sa - 1)}{1 + sb - 4 \cdot a \cdot \frac{(t+1)}{(b)} \cdot \beta m \cdot \beta b} \cdot \beta t \cdot J$$

$$L := \frac{\left[-2 \cdot \beta t \cdot a \cdot J - 2 \cdot \beta b \cdot a \cdot K - N_{1i}^{(2)}\right]}{b}$$

Then the crack density terms are set equal to zero, and

$$J := \frac{-N_{2i}^{(1)}}{sa} \tag{B.41}$$

$$K := \frac{N_{2i}^{(3)}}{1 + sb} \tag{B.42}$$

$$L := \frac{-N_{1i}^{(2)}}{b} \tag{B.43}$$

APPENDIX C

DETERMINATION OF STRAIN ENERGY RELEASED DUE TO CRACKING

For a given crack density, the change in work due to external applied loads is equal to the work needed for the previous crack density minus the work needed to achieve the current crack density. The applied loading is the same. The external work for state j is thus,

$$\Delta W_{extj} = 2 \cdot N_1 \cdot F_{11}^{(3)} \cdot \Delta n_1^{(3)} + F_{12}^{(3)} \cdot \Delta n_2^{(3)} + 2 \cdot N_2 \cdot \left[F_{12}^{(2)} \cdot \Delta n_1^{(2)} + F_{22}^{(2)} \cdot \Delta n_2^{(2)} \right] \cdot Area \qquad (C.1)$$

where N_1 and N_2 are applied loads in the 1 and 2 directions. As stated in Appendix A, the coordinate system is referenced to the 90 degree layer. A factor of 2 is used because N_1 and N_2 are half laminate loads.

$$Area = L_m \cdot L_i \qquad (C.2)$$

where Li=Lb or Lt depending upon which lamina is cracked at the current state, or, if the middle lamina is cracked, i refers to the ply group previously cracked.

The in-plane strain energy for ply group k is given by:

$$\Delta W_{intipj}^{(k)} = \frac{1}{2} \cdot \begin{pmatrix} \Delta n_1 & \Delta n_2 \end{pmatrix}^{(k)} \cdot \left[\begin{pmatrix} F_{11} & F_{12} \\ F_{12} & F_{22} \end{pmatrix}^{(k)} \cdot \begin{pmatrix} \Delta n_1 \\ \Delta n_2 \end{pmatrix}^{(k)} + 2 \cdot \begin{pmatrix} \varepsilon_1 \\ \varepsilon_2 \end{pmatrix} - 2 \cdot \begin{pmatrix} F_{11} & F_{12} \\ F_{12} & F_{22} \end{pmatrix}^{(k)} \cdot \begin{pmatrix} n_1^t \\ n_2^t \end{pmatrix}^{(k)} \right] \qquad (C.3)$$

where ε_1 and ε_2 are the strains in the laminate at the time of cracking. They are given with a caret over them in Appendix A. The change in load terms are defined for crack state j.
The change in load terms are actually area averages. They are integrated over area and divided by area.

For example,

$$\Delta n_1 = \frac{\int_{-\frac{A}{2}}^{\frac{A}{2}} \Delta n_1 \, dA}{A} \qquad (C.4)$$

and

$$\Delta n_1^2 = \frac{\int_{-\frac{A}{2}}^{\frac{A}{2}} \Delta n_1^2 \, dA}{A} \qquad (C.5)$$

This operation is straightforward for the Δn_1 terms but not for the Δn_1^2 terms. Both are described more fully below.

For the change in load in the top layer,

$$\Delta n_1^{(1)} = A\cdot 2\cdot\frac{\tanh\left(\lambda m\cdot\frac{Lm}{2}\right)}{\lambda m\cdot Lm} + B\cdot 2\cdot\frac{\tanh\left(\lambda t\cdot\frac{Lt}{2}\right)}{\lambda t\cdot Lt} + C\cdot 2\cdot\frac{\tanh\left(\lambda b\cdot\frac{Lb}{2}\right)}{\lambda b\cdot Lb}$$

$$\Delta n_2^{(1)} = D\cdot 2\cdot\frac{\tanh\left(\lambda t\cdot\frac{Lt}{2}\right)}{\lambda t\cdot Lt} + E\cdot 2\cdot\frac{\tanh\left(\lambda b\cdot\frac{Lb}{2}\right)}{\lambda b\cdot Lb} + F\cdot 2\cdot\frac{\tanh\left(\lambda m\cdot\frac{Lm}{2}\right)}{\lambda m\cdot Lm} \qquad (C.6)$$

For the change in load in the middle layer,

$$\Delta n_1^{(2)} = G\cdot 2\cdot\frac{\tanh\left(\lambda m\cdot\frac{Lm}{2}\right)}{\lambda m\cdot Lm} + H\cdot 2\cdot\frac{\tanh\left(\lambda t\cdot\frac{Lt}{2}\right)}{\lambda t\cdot Lt} + I\cdot 2\cdot\frac{\tanh\left(\lambda b\cdot\frac{Lb}{2}\right)}{\lambda b\cdot Lb}$$

$$\Delta n_2^{(2)} = J\cdot 2\cdot\frac{\tanh\left(\lambda t\cdot\frac{Lt}{2}\right)}{\lambda t\cdot Lt} + K\cdot 2\cdot\frac{\tanh\left(\lambda b\cdot\frac{Lb}{2}\right)}{\lambda b\cdot Lb} + L\cdot 2\cdot\frac{\tanh\left(\lambda m\cdot\frac{Lm}{2}\right)}{\lambda m\cdot Lm} \qquad (C.7)$$

For the change in load in the bottom layer,

$$\Delta n_1^{(3)} = (-G-A)\cdot 2\cdot\frac{\tanh\left(\lambda m\cdot\frac{Lm}{2}\right)}{\lambda m\cdot Lm} + (-H-B)\cdot 2\cdot\frac{\tanh\left(\lambda t\cdot\frac{Lt}{2}\right)}{\lambda t\cdot Lt} + (-I-C)\cdot 2\cdot\frac{\tanh\left(\lambda b\cdot\frac{Lb}{2}\right)}{\lambda b\cdot Lb}$$

$$\Delta n_2^{(3)} = (-E-K)\cdot 2\cdot\frac{\tanh\left(\lambda b\cdot\frac{Lb}{2}\right)}{\lambda b\cdot Lb} + (-J-D)\cdot 2\cdot\frac{\tanh\left(\lambda t\cdot\frac{Lt}{2}\right)}{\lambda t\cdot Lt} + (-L-F)\cdot 2\cdot\frac{\tanh\left(\lambda m\cdot\frac{Lm}{2}\right)}{\lambda m\cdot Lm} \qquad (C.8)$$

These terms have the same form regardless of where cracking has occurred. For example, cracking in the top lamina group only means that the effects of the middle and bottom are averaged, while the top layer term is integrated between cracks.
For the Δn terms this is the same as averaging all three terms, but for the Δn^2 terms the effect is different. For the example of cracking in the top lamina group, before integration,

$$\Delta n_1^{(1)} = \frac{A\cdot 2\cdot\tanh\left(\lambda m\cdot\frac{Lm}{2}\right)}{\lambda m\cdot Lm} + B\cdot\frac{\cosh(\lambda t\cdot x2)}{\cosh\left(\lambda t\cdot\frac{Lt}{2}\right)} + \frac{C\cdot 2\cdot\tanh\left(\lambda b\cdot\frac{Lb}{2}\right)}{\lambda b\cdot Lb} \qquad (C.9)$$

so,

$$\left[\Delta n_1^{(1)}\right]^2 = 4\cdot A^2\cdot\frac{\tanh\left(\frac{1}{2}\cdot\lambda m\cdot Lm\right)^2}{\left(\lambda m^2\cdot Lm^2\right)} + 4\cdot A\cdot\frac{\tanh\left(\frac{1}{2}\cdot\lambda m\cdot Lm\right)}{(\lambda m\cdot Lm)}\cdot B\cdot\frac{\cosh(\lambda t\cdot x2)}{\cosh\left(\frac{1}{2}\cdot\lambda t\cdot Lt\right)} \ldots$$
$$+ 8\cdot A\cdot\frac{\tanh\left(\frac{1}{2}\cdot\lambda m\cdot Lm\right)}{(\lambda m\cdot Lm)}\cdot C\cdot\frac{\tanh\left(\frac{1}{2}\cdot\lambda b\cdot Lb\right)}{(\lambda b\cdot Lb)} \ldots$$
$$+ B^2\cdot\frac{\cosh(\lambda t\cdot x2)^2}{\cosh\left(\frac{1}{2}\cdot\lambda t\cdot Lt\right)^2} + 4\cdot B\cdot\frac{\cosh(\lambda t\cdot x2)}{\cosh\left(\frac{1}{2}\cdot\lambda t\cdot Lt\right)}\cdot C\cdot\frac{\tanh\left(\frac{1}{2}\cdot\lambda b\cdot Lb\right)}{(\lambda b\cdot Lb)} + 4\cdot C^2\cdot\frac{\tanh\left(\frac{1}{2}\cdot\lambda b\cdot Lb\right)^2}{\left(\lambda b^2\cdot Lb^2\right)} \tag{C.10}$$

$$\int_{-\frac{Lt}{2}}^{\frac{Lt}{2}}\left[n_1^{(1)}\right]^2 dx2 = \left[\frac{\tanh\left(\frac{1}{2}\cdot\lambda t\cdot Lt\right)}{\lambda t} + \frac{1}{2}\cdot\frac{Lt}{\cosh\left(\frac{1}{2}\cdot\lambda t\cdot Lt\right)^2}\right]\cdot B^2 \ldots$$
$$+ 8\cdot\left(\frac{1}{\lambda b\cdot Lb}\cdot C\cdot\tanh\left(\frac{1}{2}\cdot\lambda b\cdot Lb\right) + \frac{1}{\lambda m\cdot Lm}\cdot A\cdot\tanh\left(\frac{1}{2}\cdot\lambda m\cdot Lm\right)\right)\cdot\frac{\tanh\left(\frac{1}{2}\cdot\lambda t\cdot Lt\right)}{\lambda t}\cdot B \ldots$$
$$+ 4\cdot Lt\cdot\frac{\left(\tanh\left(\frac{1}{2}\cdot\lambda b\cdot Lb\right)\cdot\lambda m\cdot Lm\cdot C + A\cdot\tanh\left(\frac{1}{2}\cdot\lambda m\cdot Lm\right)\cdot\lambda b\cdot Lb\right)^2}{\left[(\lambda b\cdot Lb)^2\cdot(\lambda m\cdot Lm)^2\right]} \tag{C.11}$$

The other terms are given by essentially the same expression, but with the constants switched appropriately. For $\Delta n_1^{(1)}\cdot\Delta n_2^{(1)}$, for example, B^2 becomes $B\cdot D$, A^2 becomes $A\cdot F$, and C^2 becomes $C\cdot E$. In addition, $A\cdot B$ becomes $A\cdot D$, $A\cdot C$ becomes $A\cdot E$ and $B\cdot C$ becomes $B\cdot E$. Shown explicitly, using equation C.9 and equation C.12 shown below,

$$\Delta n_2^{(1)} = D\cdot\frac{\cosh(\lambda t\cdot x2)}{\cosh\left(\lambda t\cdot\frac{Lt}{2}\right)} + E\cdot 2\cdot\frac{\tanh\left(\lambda b\cdot\frac{Lb}{2}\right)}{\lambda b\cdot Lb} + F\cdot 2\cdot\frac{\tanh\left(\lambda m\cdot\frac{Lm}{2}\right)}{\lambda m\cdot Lm} \tag{C.12}$$

the result is:

$$\int_{-\frac{Lt}{2}}^{\frac{Lt}{2}} \Delta n_1^{(1)} \cdot \Delta n_2^{(1)}\, dx2 = B \cdot D \cdot \left[\frac{\tanh\left(\frac{1}{2}\cdot\lambda t \cdot Lt\right)}{\lambda t} + \frac{1}{2}\cdot\frac{Lt}{\cosh\left(\frac{1}{2}\cdot\lambda t\cdot Lt\right)^2} \right] \ldots \tag{C.13}$$

$$+ \left[\begin{array}{l} (A\cdot D + B\cdot F)\cdot\dfrac{\tanh\left(\frac{1}{2}\cdot\lambda m\cdot Lm\right)}{(\lambda m\cdot Lm)} \ldots \\ +(C\cdot D + B\cdot E)\cdot\dfrac{\tanh\left(\frac{1}{2}\cdot\lambda b\cdot Lb\right)}{(\lambda b\cdot Lb)} \end{array} \right] \cdot \frac{\tanh\left(\lambda t\cdot\frac{Lt}{2}\right)}{\lambda t} \cdot 4 \ldots$$

$$+ \left[\begin{array}{l} A\cdot F\cdot\dfrac{\tanh\left(\frac{1}{2}\cdot\lambda m\cdot Lm\right)^2}{\left(\lambda m^2\cdot Lm^2\right)} \ldots \\ +(C\cdot F + A\cdot E)\cdot\dfrac{\tanh\left(\frac{1}{2}\cdot\lambda b\cdot Lb\right)}{\lambda b\cdot Lb}\cdot\dfrac{\tanh\left(\frac{1}{2}\cdot\lambda m\cdot Lm\right)}{\lambda m\cdot Lm} \ldots \\ +C\cdot E\cdot\dfrac{\tanh\left(\frac{1}{2}\cdot\lambda b\cdot Lb\right)^2}{\left(\lambda b^2\cdot Lb^2\right)} \end{array} \right] \cdot 4\cdot Lt$$

Similarly, cracking in the middle lamina group means

$$n_1^{(1)} = \frac{A\cdot\cosh(\lambda m\cdot x1)}{\cosh\left(\lambda m\cdot\frac{Lm}{2}\right)} + B\cdot 2\cdot\frac{\tanh\left(\lambda t\cdot\frac{Lt}{2}\right)}{\lambda t\cdot Lt} + \frac{C\cdot 2\cdot\tanh\left(\lambda b\cdot\frac{Lb}{2}\right)}{\lambda b\cdot Lb} \tag{C.14}$$

so

$$\left[n_1^{(1)}\right]^2 = A^2\cdot\frac{\cosh(\lambda m\cdot x1)^2}{\cosh\left(\frac{1}{2}\cdot\lambda m\cdot Lm\right)^2} + 4\cdot A\cdot\frac{\cosh(\lambda m\cdot x1)}{\cosh\left(\frac{1}{2}\cdot\lambda m\cdot Lm\right)}\cdot B\cdot\frac{\tanh\left(\frac{1}{2}\cdot\lambda t\cdot Lt\right)}{(\lambda t\cdot Lt)} \ldots \tag{C.15}$$

$$+ 4\cdot A\cdot\frac{\cosh(\lambda m\cdot x1)}{\cosh\left(\frac{1}{2}\cdot\lambda m\cdot Lm\right)}\cdot C\cdot\frac{\tanh\left(\frac{1}{2}\cdot\lambda b\cdot Lb\right)}{(\lambda b\cdot Lb)} \ldots$$

$$+ 4\cdot B^2\cdot\frac{\tanh\left(\frac{1}{2}\cdot\lambda t\cdot Lt\right)^2}{\left(\lambda t^2\cdot Lt^2\right)} + 8\cdot B\cdot\frac{\tanh\left(\frac{1}{2}\cdot\lambda t\cdot Lt\right)}{(\lambda t\cdot Lt)}\cdot C\cdot\frac{\tanh\left(\frac{1}{2}\cdot\lambda b\cdot Lb\right)}{(\lambda b\cdot Lb)} + 4\cdot C^2\cdot\frac{\tanh\left(\frac{1}{2}\cdot\lambda b\cdot Lb\right)^2}{\left(\lambda b^2\cdot Lb^2\right)}$$

and

$$\int_{-\frac{Lm}{2}}^{\frac{Lm}{2}} nt1^2\,dx1 = A^2\cdot\left[\frac{\tanh\left(\frac{1}{2}\cdot\lambda m\cdot Lm\right)}{\lambda m}+\frac{Lm}{2\cdot\cosh\left(\frac{1}{2}\cdot\lambda m\cdot Lm\right)^2}\right]\ldots \tag{C.16}$$
$$+\frac{\tanh\left(\frac{1}{2}\cdot\lambda m\cdot Lm\right)}{\lambda m}\cdot\left[\frac{\tanh\left(\frac{1}{2}\cdot\lambda b\cdot Lb\right)}{(\lambda b\cdot Lb)}\cdot C+\frac{\tanh\left(\frac{1}{2}\cdot\lambda t\cdot Lt\right)}{(\lambda t\cdot Lt)}\cdot B\right]\cdot 8\cdot A\ldots$$
$$+4\cdot Lm\cdot\frac{\left(C\cdot\tanh\left(\frac{1}{2}\cdot\lambda b\cdot Lb\right)\cdot\lambda t\cdot Lt+\tanh\left(\frac{1}{2}\cdot\lambda t\cdot Lt\right)\cdot B\cdot\lambda b\cdot Lb\right)^2}{\left[(\lambda t\cdot Lt)^2\cdot(\lambda b\cdot Lb)^2\right]}$$

For example, for initial cracking in the top laminate layer,

$$\Delta W_{ext} = 2\cdot N_1\cdot\left[F_{11}^{(3)}\cdot 2\cdot\frac{H+B}{\lambda t}+F_{12}^{(3)}\cdot 2\cdot\frac{J+D}{\lambda t}\right]+2\cdot N_2\cdot\left[F_{12}^{(2)}\cdot 2\cdot\frac{H}{\lambda t}+F_{22}^{(2)}\cdot 2\cdot\frac{J}{\lambda t}\right] \tag{C.17}$$

$$\Delta W_{int} = F_{11}^{(1)}\cdot\frac{B^2}{\lambda t}+2\cdot F_{12}^{(1)}\cdot\frac{B\cdot D}{\lambda t}+4\cdot\frac{B}{\lambda t}\cdot\left[\varepsilon_1-F_{11}^{(1)}\cdot n_1^{t(1)}-F_{12}^{(1)}\cdot n_2^{t(1)}\right]\ldots \tag{C.18}$$
$$+F_{22}^{(1)}\cdot\frac{D^2}{\lambda t}+4\cdot\frac{D}{\lambda t}\cdot\left[\varepsilon_2-F_{12}^{(1)}\cdot n_1^{t(1)}-F_{22}^{(1)}\cdot n_2^{t(1)}\right]\ldots$$
$$+F_{11}^{(2)}\cdot\frac{H^2}{\lambda t}+2\cdot F_{12}^{(2)}\cdot\frac{H\cdot D}{\lambda t}+4\cdot\frac{H}{\lambda t}\cdot\left[\varepsilon_1-F_{11}^{(2)}\cdot n_1^{t(2)}-F_{12}^{(2)}\cdot n_2^{t(2)}\right]\ldots$$
$$+F_{22}^{(2)}\cdot\frac{J^2}{\lambda t}+4\cdot\frac{J}{\lambda t}\cdot\left[\varepsilon_2-F_{12}^{(2)}\cdot n_1^{t(2)}-F_{22}^{(2)}\cdot n_2^{t(2)}\right]\ldots$$
$$+F_{11}^{(3)}\cdot\frac{(B+H)^2}{\lambda t}+2\cdot F_{12}^{(3)}\cdot\frac{(B+H)\cdot(D+J)}{\lambda t}\ldots$$
$$+4\cdot\frac{(B+H)}{\lambda t}\cdot\left[-\varepsilon_1+F_{11}^{(3)}\cdot n_1^{t(3)}+F_{12}^{(3)}\cdot n_2^{t(3)}\right]+F_{22}^{(3)}\cdot\frac{(D+J)^2}{\lambda t}\ldots$$
$$+4\cdot\frac{(D+J)}{\lambda t}\cdot\left[-\varepsilon_2+F_{12}^{(3)}\cdot n_1^{t(3)}+F_{22}^{(3)}\cdot n_2^{t(3)}\right]$$

Of course, the expressions for subsequent cracking are substantially more complicated.

The transverse shear terms must also be found for each ply group k and are given by:

$$dWts^{(k)} = \frac{1}{2}\cdot\frac{H_k^{\,2}}{4}\cdot\left(F_{44}\cdot\tau_{23}^{\,2} + 2\cdot F_{45}\cdot\tau_{13}\cdot\tau_{23} + F_{55}\cdot\tau_{13}^{\,2}\right)^{(k)}\cdot dArea \tag{C.19}$$

where

$$\tau_{23}^{(k)} = \frac{\delta\Delta n_2^{(k)}}{\delta x_2} \qquad \text{and} \qquad \tau_{13}^{(k)} = \frac{\delta\Delta n_1^{(k)}}{\delta x_1} \tag{C.20}$$

Again, an averaging scheme is used. For the first ply group,

$$\tau_{13}^{(1)} = A\cdot\lambda m\cdot\frac{\sinh\left(\lambda m\cdot x_1\right)}{\cosh\left(\lambda m\cdot\frac{Lm}{2}\right)} \tag{C.21}$$

$$\tau_{23}^{(1)} = D\cdot\lambda t\cdot\frac{\sinh\left(\lambda t\cdot x_2\right)}{\cosh\left(\lambda t\cdot\frac{Lt}{2}\right)} + E\cdot\lambda b\cdot\frac{\sinh\left(\lambda b\cdot x_2\right)}{\sinh\left(\lambda b\cdot\frac{Lb}{2}\right)} \tag{C.22}$$

$$\left[\tau_{13}^{(1)}\right]^2 = A^2\cdot\lambda m^2\cdot\frac{\sinh\left(\lambda m\cdot x_1\right)^2}{\cosh\left(\lambda m\cdot\frac{Lm}{2}\right)^2} \tag{C.23}$$

$$\left[\tau_{23}^{(1)}\right]^2 = D^2\cdot\lambda t^2\cdot\frac{\sinh\left(\lambda t\cdot x_2\right)^2}{\cosh\left(\lambda t\cdot\frac{Lt}{2}\right)^2} + E^2\cdot\lambda b^2\cdot\frac{\sinh\left(\lambda b\cdot x_2\right)^2}{\sinh\left(\lambda b\cdot\frac{Lb}{2}\right)^2} + D\cdot\lambda t\cdot\frac{\sinh\left(\lambda t\cdot x_2\right)}{\cosh\left(\lambda t\cdot\frac{Lt}{2}\right)}\cdot E\cdot\lambda b\cdot\frac{\sinh\left(\lambda b\cdot x_2\right)}{\sinh\left(\lambda b\cdot\frac{Lb}{2}\right)} \tag{C.24}$$

For cracking in the top layer only, the effects of the middle and bottom layers are averaged. Thus, when the derivatives are taken of the $\Delta n_i^{(k)}$ terms, the middle and bottom layer terms are constant. The interlaminar shear terms are:

$$\tau_{13}^{(1)} = 0 \qquad \left[\tau_{13}^{(1)}\right]^2 = 0 \tag{C.25}$$

$$\tau_{23}^{(1)} = D \cdot \lambda t \cdot \frac{\sinh\left(\lambda t \cdot x_2\right)}{\cosh\left(\lambda t \cdot \frac{Lt}{2}\right)} \qquad \left[\tau_{23}^{(1)}\right]^2 = D^2 \cdot \lambda t^2 \cdot \frac{\sinh\left(\lambda t \cdot x_2\right)^2}{\cosh\left(\lambda t \cdot \frac{Lt}{2}\right)^2} \tag{C.26}$$

$$\tau_{23}^{(1)} = \int_{-\frac{Lt}{2}}^{\frac{Lt}{2}} \frac{B \cdot \lambda t}{Lt} \cdot \frac{\sinh\left(\lambda t \cdot x_2\right)}{\cosh\left(\lambda t \cdot \frac{Lt}{2}\right)} dx_2 \qquad \text{so} \qquad \tau_{23}^{(1)} = 0 \tag{C.27}$$

$$\left[\tau_{23}^{(1)}\right]^2 = \int_{-\frac{Lt}{2}}^{\frac{Lt}{2}} D^2 \cdot \lambda t^2 \cdot \frac{\sinh\left(\lambda t \cdot x_2\right)^2}{\cosh\left(\lambda t \cdot \frac{Lt}{2}\right)^2} dx_2 \tag{C.28}$$

so

$$\left[\tau_{23}^{(1)}\right]^2 = \frac{D^2 \cdot \lambda t^2}{Lt} \cdot \left[\frac{\tanh\left(\lambda t \cdot \frac{Lt}{2}\right)}{\lambda t} - \frac{Lt}{2 \cdot \cosh\left(\lambda t \cdot \frac{Lt}{2}\right)^2}\right] \tag{C.29}$$

Then,

$$\begin{aligned} \Delta W_{ts} = \frac{1}{8} \cdot H_1^2 \cdot \left[F_{44}^{(1)} \cdot \left[\tau_{23}^{(1)}\right]^2 + F_{55}^{(1)} \cdot \left[\tau_{55}^{(1)}\right]^2\right] \ldots \\ + \frac{1}{8} \cdot H_2^2 \cdot \left[F_{44}^{(2)} \cdot \left[\tau_{23}^{(2)}\right]^2 + F_{55}^{(2)} \cdot \left[\tau_{55}^{(2)}\right]^2\right] \ldots \\ + \frac{1}{8} \cdot H_3^2 \cdot \left[F_{44}^{(3)} \cdot \left[\tau_{23}^{(3)}\right]^2 + F_{55}^{(3)} \cdot \left[\tau_{55}^{(3)}\right]^2\right] \end{aligned} \tag{C.30}$$

Note that if a crack has previously formed in the middle ply group, the 13 shear stress may not be zero. In this case the appropriate value is the previous value for each lamina group.

Finally, for the above example of the first crack occuring in the top ply group,

$$\Delta Wts = \frac{1}{4}\cdot H_1^{\,2}\cdot\left[F_{44}^{(1)}\cdot D^2\cdot \lambda t\right] + \frac{1}{4}\cdot H_2^{\,2}\cdot\left[F_{44}^{(2)}\cdot J^2\cdot \lambda t\right] + \frac{1}{4}\cdot H_3^{\,2}\cdot\left[F_{44}^{(3)}\cdot (D+J)^2\cdot \lambda t\right] \qquad (C.31)$$

VITA

Jane Lynette Daugherty Runkle was born May 29, 1963 in Park Ridge, Illinois. She earned her Bachelor's Degree in Engineering from Purdue University on May 19, 1985. At the same time, she was commissioned an officer in the United States Air Force and was stationed at Los Angeles Air Force Base. While in the Air Force Space Division Office for Manned Spaceflight, she managed contractor efforts on the Space Assembly, Maintenance, and Servicing Study and on the Spacecraft Partitioning and Interface Standards Study. She then joined the Medium Launch Vehicle System Program Office, where she managed the development, qualification and acceptance of solid rocket motor and ordnance systems for the McDonnell Douglas Delta II launch vehicle. Jane earned her M.S. in Engineering Science from Louisiana State University in May of 1991.